

RESONANCE AND NON-RESONANCE RAMAN STUDIES
OF BIOLOGICAL MOLECULES

A THESIS

Presented to

The Faculty of the Division of Graduate Studies

by

Robert Cheng Chi Chang

In Partial Fulfillment
of the Requirements for the Degree
Doctor of Philosophy
in the School of Chemistry

Georgia Institute of Technology

August, 1976

RESONANCE AND NON-RESONANCE RAMAN STUDIES
OF BIOLOGICAL MOLECULES

Approved:

Nai-Teng Yu, Chairman
R 11 11 1 1+

RONALD H. FELTON *D.*

Raymond F. Borkman

Date approved by Chairman: Aug. 20, 1976

ACKNOWLEDGMENTS

First of all, I wish to express my sincere appreciation to my thesis advisor, Dr. Nai-Teng Yu, for his support and advice during the course of this research. I would like to thank my reading committee for their valuable suggestions and serving as members of my reading committee, especially Dr. Ronald H. Felton for his advice in resonance Raman works.

Also, special thanks are given to Dr. John F. R. Kuck, Jr. for his discussion and generous supply of lenses, and to Dr. Emily J. East for her help in lens protein research and reading and correcting the English of the manuscript.

I am greatly indebted to my wife, Yi-Huei, for her patience, support and encouragement during the course of this work.

TABLE OF CONTENTS

	Page
ACKNOWLEDGMENTS.	ii
LIST OF TABLES	v
LIST OF ILLUSTRATIONS.	vi
SUMMARY.	ix
Chapter	
I. A BRIEF REVIEW ON PRINCIPLES AND TECHNIQUES OF RAMAN SPECTROSCOPY.	1
1. Introduction.	1
2. Theories of Raman Scattering.	5
I. Classical Theory of Raman and Rayleigh Effect	
II. Quantum Theory of Raman Effect	
(i) Non-resonance Raman Effect	
(ii) Resonance Raman Effect	
(iii) Application of Resonance Raman to Metalloporphyrins and Related Systems	
3. Experimental Techniques	19
I. Raman Scattering Apparatus	
II. Sample Handling Techniques	
4. Interpretations of Protein Raman Spectra.	23
I. Dependence of Amide Modes on Conformation	
II. Raman Spectra of Poly-L-lysine and Glucagon as Model Systems	
(i) Poly-L-lysine	
(ii) Glucagon	
III. Tyrosine Doublet at 850 and 830 cm^{-1}	
IV. Dependence of $\nu(\text{S-S})$ on Local Geometry	
II. NON-RESONANCE RAMAN STUDIES OF HUMAN AND ANIMAL LENSES.	33
1. Introduction.	33
2. Materials and Methods	35
3. Results and Discussion.	39
I. Structural and Conformational Implications of Raman Spectrum of Intact Human Lens	
II. Protein Fractions of Rat Lens and Their Raman Spectroscopic Studies	
III. Prevalence of α -Helical Form in Chick and Pigeon Lens Proteins	

TABLE OF CONTENTS

Chapter	Page
IV. Heterogeneous Nature of Chicken Lens	
V. Comparison of δ -Crystallin Conformation in Intact Lens and in Isolated State	
VI. Effect of Heat Denaturation on the Conformation of δ -Crystallin	
VII. Distribution of Glycogen and Proteins in Pigeon Lens	
VIII. Direct Evidence for the Existence of α -Helical δ -Crystallin in Reptilian Lenses	
IX. Polarized Raman Studies of Chick Lens	
X. Effects of Aging and UV Irradiation on Sulfhydryl Groups of Intact Rat and Mouse Lenses	
III. RESONANCE RAMAN SPECTROSCOPIC STUDIES OF METALLOPORPHYRINS AND HEMEPROTEINS.	78
1. Introduction.	78
2. Materials and Methods	79
3. Results and Discussion.	81
I. Structure Sensitive Vibrational Bands of Resonance Raman Spectra of Metallo-octaethylporphyrins	
II. An Anomalous Polarized Line in Resonance Raman Spectra of Metalloporphyrins and Hemeproteins as a Structural Probe of Metal Displacement	
III. Dispersion of Depolarization Ratio	
IV. Excitation Profiles of Nickel(II)etio-porphyrin I	
Appendices	
I. METALLOPORPHYRIN EXCITED ELECTRONIC STATES.	114
II. PRESERVATION OF LENS PROTEINS	117
III. RESONANCE RAMAN SPECTRA AND EXCITATION PROFILES OF NICKEL(II)ETIOPORPHYRIN I.	121
IV. VISIBLE ABSORPTION SPECTRA AND DEPOLARIZATION RATIOS OF DEUTERATED NICKEL(II)MESOPORPHYRIN IX DIMETHYL ESTER AND NICKEL(II)PROTOPORPHYRIN IX DIMETHYL ESTER.	123
BIBLIOGRAPHY	124
VITA	135

LIST OF TABLES

Table	Page
1. Raman Frequencies (cm^{-1}) and Tentative Assignments for Intact Human Lens (300-1800 cm^{-1})	41
2. Correlation Between Protein Backbone Conformation and Amides I and III Frequencies (cm^{-1}).	43
3. Resonance Raman Frequencies (cm^{-1}) and Polarizations for NiOEP	85
4. Resonance Raman Frequencies (cm^{-1}) and Polarizations for FeOEPCl	89
5. Important Internal Coordinates Contributing to the Potential Energy of Normal Modes above 1500 cm^{-1} in NiOEP (D_{4h}).	91
6. Correlation of the Anomalously Polarized Frequency (cm^{-1}) with Ct-N Distance (\AA)	97

LIST OF ILLUSTRATIONS

Figure	Page
1. Energy Level Diagram for the Raman Effect	6
2. Laser Raman Scattering Apparatus.	20
3. Raman Spectra of (top) α -Helical Poly-L-lysine, 3% in H ₂ O, pH 11.8, T = 4°C, and (bottom) β -Sheet Poly-L-lysine, 3% in H ₂ O, pH 11.8, T = 52°C	28
4. Raman Spectra of Glucagon in Various States of Aggregation (a) Spectrum of crystallin glucagon (powder form), (b) Spectrum of freshly prepared aqueous glucagon and (c) Spectrum of gels formed from (b) on standing (~ 40 hrs at 26°C)	30
5. Correlation Between the C-C-S-S-C-C Geometry and $\nu(S-S)$ Frequency.	32
6. Structure of Human Lens	34
7. Raman Spectrum of the Cortex of Intact Human Lens	40
8. Separation of the Water-soluble Rat Lens Proteins by Gel Chromatography on Sephadex G-200 Column.	45
9. Raman Spectra of α -, β -, and γ -Crystallin and Albuminoid in Lyophilized Powder.	46
10. Comparisons of the Raman Spectra of Monkey (~ 3 years old), Chick (~ 10 days), and Pigeon (~ 8 weeks)	50
11. Raman Spectrum of Glycogen (solid, liver glycogen from Pfanstiehl Laboratory)	51
12. Raman Spectra of Old Hen Lens (~ 10 years old) as a Function of Location	54
13. Separation of δ -Crystallin of One Day Old Chick Lens Proteins by Gel Chromatography on Sephadex G-200 Column.	56
14. Raman Spectra of Isolated δ -Crystallin in pH 7.0 H ₂ O Solution and in Lyophilized Powder.	57

LIST OF ILLUSTRATIONS (Continued)

Figure	Page
15. Circular Dichroism Curve of Isolated δ -Crystallin in H ₂ O (pH 7.0) Solution (2 mg/ml) in the 200-260 nm Region	59
16. Raman Spectra of Native and Heat-denatured δ -Crystallin.	62
17. Raman Spectra of Adult Pigeon Lens as a Function of Location	63
18. Raman Spectrum of the Annular Pad of an Adult Pigeon.	65
19. Raman Spectra of Intact Lizard and Snake Lenses	66
20. Raman Spectra of Intact Snapping Turtle and Caiman Lenses	68
21. Three Scattering Geometries for Oriented Polypeptides	69
22. Raman Spectra of Intact Chick Lens in the Amide I Region.	71
23. Schematic Arrangement of Polarized Raman Studies of Chick Lens	72
24. Raman Spectra of Intact Rat Lens (nucleus) as a Function of Age in the S-H and S-S Vibrational Regions	74
25. Raman Spectra of Intact Rat Lens (cortex) as a Function of Age in the S-H and S-S Vibrational Regions	75
26. SH Contents of Both Normal and UV Irradiated Mouse Lenses as a Function of Age: Nucleus and Cortex.	77
27. Resonance Raman Spectra of Crystalline and Solution Samples of Ni(II)OEP-meso-h ₄	82
28. Resonance Raman Spectra of Crystalline and Solution Samples of Ni(II)OEP-meso-d ₄	83
29. Labeling Scheme for the Porphinato Moiety and Structure of Porphyrins	92

LIST OF ILLUSTRATIONS (Concluded)

Figure	Page
30. Resonance Raman Spectra of Cu(II)OEP: (a) Sample supplied by Dr. D. Dolphin; (b) Sample obtained from CH ₂ Cl ₂ -hexane solution; (c) CH ₂ Cl ₂ solution sample of ² (a) and (b).	94
31. Resonance Raman Spectra of Ni(II)OEP-meso-d ₄ in CS ₂ Solution.	101
32. Resonance Raman Spectra of Ni(II)Etio-meso-d ₄ in CS ₂ Solution.	102
33. Resonance Raman Spectra of Ni(II)MesoDME-meso-d ₄ in CS ₂ Solution.	103
34. Resonance Raman Spectra of Ni(II)ProtoDME-meso-d ₄ in CS ₂ Solution.	104
35. Excitation Profiles and Absorption Spectrum of Ni(II)Etio-meso-h ₄ and -d ₄ in CDCl ₃	107
36. The Effect of Jahn-Teller Instability on a Potential Energy Curve.	111
37. Absorption Spectrum of a Typical Metalloporphyrin: Cu(II)OEP in Hexane at Room Temperature	115
38. Raman Spectra of the Nucleus of Rabbit Lens in Both Intact and Lyophilized States	118
39. Resonance Raman Spectra and Excitation Profiles of Ni(II)Etio	121
40. Excitation Profiles of Ni(II)Etio in CDCl ₃	122
41. Visible Absorption Spectrum and Depolarization Ratios (1211 cm ⁻¹) of Ni(II)ProtoDME-meso-d ₄ (top), Visible Absorption Spectrum and Depolarization Ratios (1207 cm ⁻¹) of Ni(II)MesoDME-meso-d ₄ (bottom)	123

SUMMARY

This research deals with structural studies of ocular lens proteins and metalloporphyrins by laser Raman scattering techniques.

Non-resonance Raman studies of intact lenses (human, monkey, rat, chicken, pigeon, mouse, and reptiles) and certain isolated crystallins have been made. It is found that α -, β -, and γ -crystallin isolated or in intact mammalian lenses have predominantly anti-parallel β -pleated sheet structure, while δ -crystallin in bird lenses exists in situ and after chromatography chiefly in the α -helical conformation.

Upon heat denaturation, δ -crystallin is changed from a protein with largely α -helical structure to a protein with largely β -pleated sheet structure.

From polarized studies of intact chick lens, it is revealed that δ -crystallin is quite possibly a globular protein.

Raman spectral features also show that glycogen is present throughout the adult pigeon lens with the highest concentration in the nucleus; however, it is absent in chicken lens and in pigeon annular pad.

One of the aging parameters, oxidation of sulfhydryl groups, in mouse lens is accelerated by exposure of lenses to long-wave UV irradiation.

Comparison of resonance Raman spectra of D_{4h} and D_{2d} molecular forms of nickel(II)octaethylporphyrin-meso- h_4 and $-d_4$ indicates that high frequency bands are structure-sensitive. Spectra of Cu(II)OEP imply

the existence of two molecular forms in this compound.

Based on resonance Raman studies of a series of metalloporphyrins of known structure, an important correlation is found between the position of the anomalously polarized line ($1550-1610\text{ cm}^{-1}$) and the distance from the center of the porphyrin ring to the pyrrole nitrogen. A decrease in this distance corresponds to an increase in the Raman frequency. The significance of this correlation is that it can be used for quantitative assessment of the out-of-plane displacement of the metal in heme proteins.

The variation of depolarization ratio for an inversely polarized band can be interpreted in terms of lowering of the symmetry of metalloporphyrins from D_{4h} . The rigorous symmetry of nickel(II)protoporphyrin-IX-dimethyl-ester-meso- d_4 is proposed as C_s because of the effect of peripheral substituents.

Detailed excitation profiles in the Q band region of nickel(II)-etioporphyrin-I have been obtained. Theoretical interpretation of the observed profiles for b_{1g} and b_{2g} modes requires the presence of the Jahn-Teller effect in the doubly degenerate electronic states.

CHAPTER I

A BRIEF REVIEW ON PRINCIPLES AND TECHNIQUES OF RAMAN SPECTROSCOPY

1. Introduction

When electromagnetic radiation irradiates a molecule, the energy may be transmitted, absorbed, or scattered. The Raman effect is one member of the various light scattering phenomena.

The naming of the Raman effect honors Sir C. V. Raman, who first discovered it experimentally in 1928 in the course of extended research on molecular light scattering. It should be noted that the effect had been predicted by Smekal in 1923 and therefore this effect is also referred to as the Smekal-Raman effect.

In the Raman effect, photons of the exciting radiation interact with molecules of the sample being irradiated. The energies of the scattered photons are either increased or decreased relative to the exciting photons by quantized increments which correspond to the energy differences in the vibrational and rotational energy levels of the molecule. These scattered lines, called Raman lines, are characteristic of the vibrational or rotational modes of the substance and are therefore a "fingerprint" of that substance.

It has been shown that the infrared absorption also depends on these same vibrational and rotational energy levels. While infrared and Raman spectra have this similarity, they are not exactly the same

since the selection rules and relative band intensities differ in many cases. The infrared absorption arises when the vibrational or rotational motion produces a change in the permanent dipole moment while Raman scattering occurs when the vibrational or rotational motion produces an induced dipole moment or change in the polarizability of the molecule. For example when a molecule has a center of symmetry, all vibrations which are symmetrical with respect to the center are infrared inactive. An example of such a molecule is carbon dioxide. The symmetrical stretching vibration gives rise to a band in the Raman spectrum. Thus Raman and infrared spectra can provide complementary information for each other.

It should be noted that the wave numbers derived from the Raman spectra are the differences between incident and scattered frequencies. The positions of the Raman bands do not depend on the frequency of the exciting radiation. In resonance Raman scattering, the incident photon energy enters the electronic transition region and the relative intensity of the Raman lines in a spectrum depends strongly on the exciting wavelength.

The study of molecular vibrational frequencies, available from Raman and infrared spectra, has played an important role in the structural studies of small molecules, and has great potential for biological materials as well. Vibrational frequencies are sensitive to geometric and bonding arrangements of localized groups of atoms in a molecule, and reflect intermolecular interactions as well. These features also affect the Raman and infrared intensities. Therefore the structural information content of Raman and infrared spectra is very high. However,

infrared spectroscopy encounters the difficulty that water, the nearly universal biological medium, effectively absorbs infrared radiation over much of the vibrational frequency range. Raman spectroscopy is not subject to this limitation, since water is a poor Raman scatterer.

The early work in Raman spectroscopy using mercury arc sources required time consuming photographic detection with low signal to noise ratio. With modern laser sources, high quality Raman spectra are obtained photoelectrically in minutes. Also classical Raman spectroscopy required large samples while modern laser Raman spectroscopy requires only a small amount of sample. In addition, lasers make possible systematic studies of the resonance Raman effect. When the excitation wavelength falls into an electronic absorption band of the sample, then certain Raman bands can be greatly enhanced. This resonance Raman effect is due to a coupling of electronic and vibrational transitions, and the vibrational modes which are subject to Raman enhancement are localized on the biological chromophore. Consequently the resonance Raman effect can be used as a structural probe to study the structural features of a chromophore at high dilution in solution or in a biological matrix. The other advantages of laser Raman spectroscopy for biological applications are (1) small sample sizes, (2) high dilution for resonance Raman studies of chromophores, (3) the Raman effect of water does not interfere with that of the sample, (4) not restricted to a particular form of the sample, (5) wide wavenumber range available, (6) large differences in scattering intensity among various functional groups.

The most serious practical obstacle of Raman spectroscopy is the interference from fluorescence. Raman scattering is inherently a much

less efficient process than fluorescence, and only a small amount of fluorescence is sufficient to obscure the Raman signals. In general fluorescence can arise from impurities in the sample or may be intrinsic to the molecule under study. In the former event, Raman signals can be improved by purifying the sample or by prolonging laser irradiation to burn out the impurities (Lord and Yu, 1970a,b). In the latter event, purification and prolonged laser irradiation are of no use. This circumstance is encountered particularly in resonance Raman studies, when the molecule is excited in an electronic absorption band. Addition of an external quenching agent such as iodide ion to the sample has been used to suppress the intrinsic fluorescence (Friedman and Hochstrasser, 1975b). Some other techniques, for example placing a rotating polarizer before the polarization scrambler, have been developed to suppress the intrinsic fluorescence (Arguello, et al., 1974).

Recently, a new Raman technique which is called "Coherent Anti-Stokes Raman Spectroscopy" has been developed with a great potential to overcome many of the problems, especially the intrinsic fluorescence obstacle (Begley, et al., 1974a,b), of conventional Raman spectroscopy. This is the technique of three wave mixing and it was discovered over a decade ago. However, because of the lack of tunable laser sources, further development has been rather slow. Coherent anti-Stokes Raman spectroscopy has been applied to the analysis of gases, liquid samples, and to the measurement of nonlinear properties of materials. For certain studies, coherent anti-Stokes Raman spectroscopy seems very successful.

2. Theories of Raman Scattering

I. Classical Theory of Raman and Rayleigh Effect

The Raman effect is concerned with the phenomenon of a change of frequency when light is scattered by molecules, but the Rayleigh effect is concerned with the scattered light without change of light frequency. If the frequency of the incident light is ν_o and that of a component of the scattered light is ν_r , then the frequency shift $\nu_o - \nu_r = \nu_m$ may be either positive or negative in sign, and its magnitude is referred to as a Raman frequency.

In Figure 1, the lines designated $V=0$ and $V=1$ represent the vibrational energy levels of the molecule. When a photon interacts with a molecule in the ground state ($V=0$), the molecule is excited momentarily to a virtual state which is not a stable energy level at room temperature for the molecule. Since the molecule cannot remain in this virtual state, it may scatter a photon and return to the ground state. The scattered photon has therefore the same energy content and frequency as the incident exciting photon, and gives rise to Rayleigh scattering. If the molecule does not return to the ground state and only returns to an excited vibrational state such as $V=1$, the energy of the scattered photon is equal to the energy of the exciting photon minus the energy difference between the $V=1$ and $V=0$ levels. The scattered photon has therefore a lower energy content and frequency than that of the incident photon, and gives rise to Stokes line. Also, there is a possibility that the molecule in an excited level is excited to a virtual state by interaction with the exciting photon. The molecule may then scatter a photon and then return to the ground state. The energy of the scattered photon is equal to the energy of the

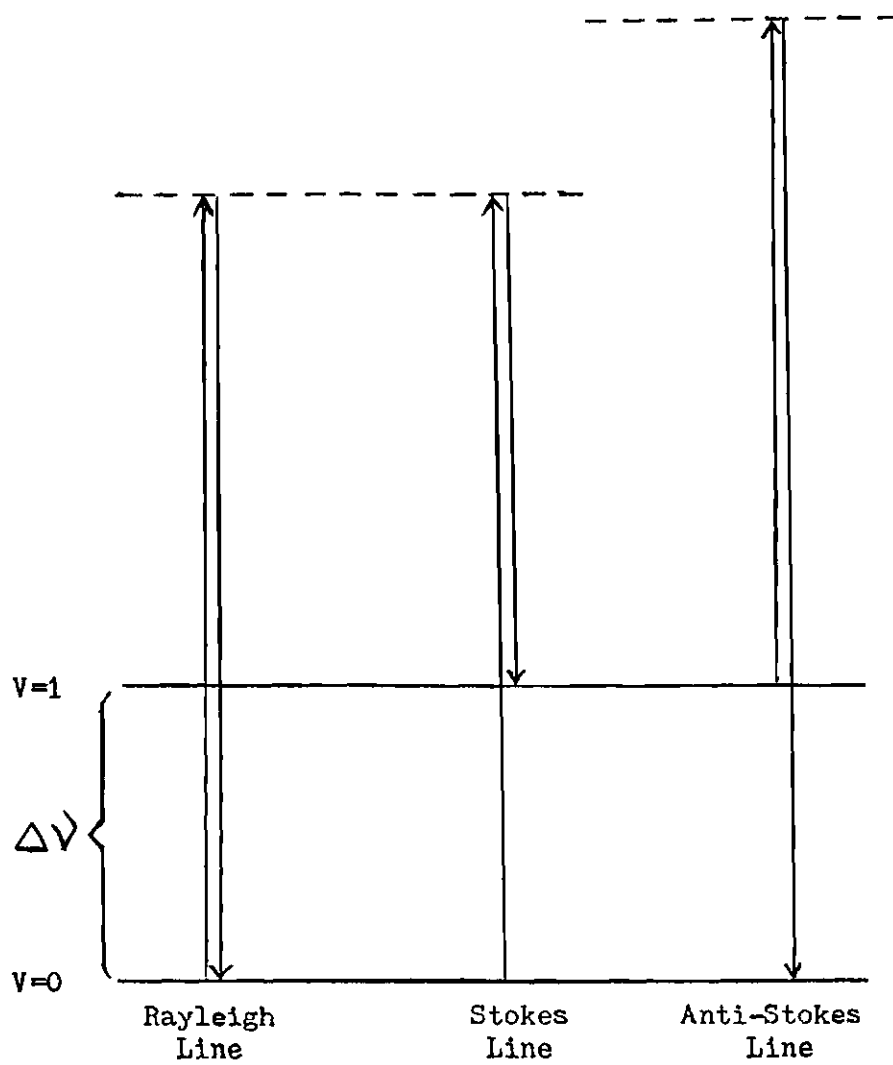


Figure 1. Energy Level Diagram for the Raman Effect

exciting photon plus the energy difference between the initial and final states. The scattered photon has therefore a higher energy content and frequency than that of the incident photon, and gives rise to anti-Stokes line. At room temperature most of the molecules are in the ground state rather than in an excited state, consequently, the anti-Stokes lines are of much lower intensity than the Stokes lines.

A simple classical treatment of Raman effect and Rayleigh effect is in terms of the dipole moments induced by the electric field of the radiation; thus

$$\vec{\mu} = \alpha \vec{E}_0 \cos 2\pi \nu_0 t \quad (1)$$

where $\vec{\mu}$ is the induced dipole moment, α is the molecular polarizability, \vec{E}_0 is the electric field, and ν_0 is the frequency of the incident photon. The polarizability α has tensor property and is a function of the vibration, so that for a given normal mode of frequency, ν_m

$$\alpha = \alpha_0 + \alpha_1 \cos 2\pi \nu_m t \quad (2)$$

Substituting Equation (2) into Equation (1)

$$\begin{aligned} \vec{\mu} &= \alpha_0 \vec{E}_0 \cos 2\pi \nu_0 t + \alpha_1 \vec{E}_0 (\cos 2\pi \nu_0 t) (\cos 2\pi \nu_m t) \\ &= \alpha_0 \vec{E}_0 \cos 2\pi \nu_0 t + \frac{1}{2} \alpha_1 \vec{E}_0 [\cos 2\pi (\nu_0 - \nu_m) t + \cos 2\pi (\nu_0 + \nu_m) t] \end{aligned} \quad (3)$$

By classical electromagnetic theory, an oscillating dipole radiates power at a rate given by

$$I = \frac{16\pi^4 \nu_0^4}{3c^3} |\vec{\mu}|^2 \quad (4)$$

Substituting Equation (3) into Equation (4)

$$I = \frac{16\pi^4 \nu_0^4}{3c^3} [\alpha_0^2 E_0^2 \cos^2 2\pi \nu_0 t + \alpha_1^2 E_0^2 \cos^2 2\pi (\nu_0 + \nu_m) t + \alpha_1^2 E_0^2 \cos^2 2\pi (\nu_0 - \nu_m) t + \text{etc.}] \quad (5)$$

Equation (5) correctly predicts the major qualitative features of the Raman effect. The first term corresponds to scattering without change of frequency, i.e., Rayleigh scattering; its intensity depends only on the molecular polarizability and so this phenomenon will be expected to arise with all substances. The second and third terms correspond to scattering with change of frequency, i.e., Raman scattering; the high frequency term is called the anti-Stokes line and the low frequency term, the Stokes line.

In the usual laser scattering experiment, the incident light is plane polarized light polarized perpendicular to the scattering plane. The scattered light intensity is measured at right angle to the incident light. The scattered light intensity can be analyzed into components which are perpendicular and parallel to the incident polarization. The ratio of these components, called the depolarization ratio ρ_1 , can be expressed in terms of invariants of the scattering tensor.

$$\rho_1 = \frac{I_{\perp}}{I_{\parallel}} = \frac{3G^s + 5G^a}{10G^o + 4G^s} \quad (6)$$

where

$$\begin{aligned}
 G^o &= \frac{1}{3} (\alpha_{xx} + \alpha_{yy} + \alpha_{zz})^2 \\
 G^s &= \frac{1}{3} [(\alpha_{xx} - \alpha_{yy})^2 + (\alpha_{xx} - \alpha_{zz})^2 + (\alpha_{yy} - \alpha_{zz})^2] \\
 &\quad + \frac{1}{2} [(\alpha_{xy} + \alpha_{yx})^2 + (\alpha_{xz} + \alpha_{zx})^2 + (\alpha_{yz} + \alpha_{zy})^2] \\
 G^a &= \frac{1}{2} [(\alpha_{xy} - \alpha_{yx})^2 + (\alpha_{xz} - \alpha_{zx})^2 + (\alpha_{yz} - \alpha_{zy})^2] \tag{7}
 \end{aligned}$$

G^o is the isotropic component, G^s is the anisotropic component, and G^a is the antisymmetric component.

Far from resonance G^a vanishes for a symmetric scattering tensor. According to Equation (6), the value of depolarization ratio is equal to or less than $3/4$ in C_{4v} , D_{2d} , D_4 , or D_{4h} symmetry groups. For non-totally symmetric vibrations, $G^o=0$ and the depolarization ratio is $3/4$, for totally symmetric vibrations, $0 < \rho_1 < 3/4$.

Near resonance the scattering tensor is not symmetric and G^a will contribute an antisymmetric component, vibrations of b_1 or b_2 symmetry will have $\rho_1 = 3/4$, while vibrations of a_2 symmetry which are characterized by $G^a \neq 0$, $G^s = G^o = 0$ may even have an infinite depolarization ratio. This a_2 vibrational mode will not be present in the non-resonance Raman spectrum. For totally symmetric vibrations, the depolarization ratio is still between 0 and $3/4$.

Raman lines with $\rho_1 < 3/4$ are called polarized lines (p); with $\rho_1 = 3/4$, depolarized lines (dp); and $\rho_1 \rightarrow \infty$ inversely polarized lines (ip).

In a complicated molecule, it is quite possible that polarized or depolarized vibrations accidentally overlap with an inversely polarized

band and contribute some intensity to the perpendicular component of inversely polarized lines. These lines with $3/4 < \rho < \infty$ are called anomalously polarized lines by Spiro (Spiro and Strekas, 1972).

II. Quantum Theory of Raman Effect

It has been shown (Behringer, 1958) that when a freely orientable molecule, initially in a vibronic state m , is perturbed by plane-polarized incident light of frequency ν_0 and intensity I_0 and passes into a vibronic state n while scattering light of frequency $\nu_0 \pm \nu_{mn}$ ($\nu_{mn} = \nu_m - \nu_n$), the total intensity of scattered light (4π solid angle) is given by

$$I = \frac{2^7 \pi^5}{3^2 c^4} I_0 (\nu_0 \pm \nu_{mn})^4 \sum_{\rho, \sigma} \left| (\alpha_{\rho\sigma})_{mn} \right|^2 \quad (8)$$

where c is the light velocity and the sum goes over $\rho = x, y, z$ and $\sigma = x, y, z$ which independently refer to the molecule fixed coordinate system. According to the dispersion theory, the $\rho\sigma^{\text{th}}$ matrix element of the polarizability tensor for transition $m \rightarrow n$, $(\alpha_{\rho\sigma})_{mn}$, is given by (Tang and Albrecht, 1970)

$$(\alpha_{\rho\sigma})_{mn} = \sum_e \left[\frac{\langle m | R_\sigma | e \rangle \langle e | R_\rho | n \rangle}{E_e - E_m - h\nu_0} + \frac{\langle m | R_\rho | e \rangle \langle e | R_\sigma | n \rangle}{E_e - E_n + h\nu_0} \right] \quad (9)$$

where E_e is the energy of the exact molecular eigenstates $|e\rangle$, ν_0 is the frequency of the incident light, R_ρ is the ρ^{th} component of the electronic dipole moment operator, and the summation is over all molecular states except initial state m and final state n . From Equation (9) it is easy to understand that when the incident light frequency approaches a certain

vibronic transition frequency, i.e., $h\nu_0 \rightarrow E_e - E_n$, the first term in Equation (9) becomes dominant and leads to the well known phenomenon "resonance Raman scattering."

While some of the transition moments on Equation (9) are experimentally or theoretically determinable it will be very difficult to carry out the summation over all the molecular eigenstates. However, in order to treat Raman intensity as a problem of vibronic interactions, Albrecht (1961) first introduced the adiabatic approximation (Born-Oppenheimer Approximation) for all wave functions involved and then expanded the electronic parts by a first order Herzberg-Teller series.

For adiabatic approximation, Albrecht used

$$|m\rangle = |g\rangle|i\rangle \text{ or } \bar{\psi}_m(r,Q) = \theta_g(r,Q) \varphi_i^g(Q) \quad (10)$$

$$|n\rangle = |g\rangle|j\rangle \text{ or } \bar{\psi}_n(r,Q) = \theta_g(r,Q) \varphi_j^g(Q)$$

$$|e\rangle = |e\rangle|v\rangle \text{ or } \bar{\psi}_e(r,Q) = \theta_e(r,Q) \varphi_v^e(Q)$$

where θ_g and θ_e are the electronic ground state and excited state wavefunctions, respectively. $\varphi_{i,j}^g(Q)$ and $\varphi_v^e(Q)$ are the vibrational wavefunctions of the ground electronic state and excited state, respectively.

Substituting Equation (10) into Equation (9), the scattering tensor appears as

$$\begin{aligned} (\alpha_{\rho\sigma})_{gi,gj} = \sum_{e,v} & \left[\frac{\langle i | \langle g | R_\sigma | e \rangle | v \rangle \langle v | \langle e | R_\sigma | g \rangle | j \rangle}{E_{ev} - E_{gj} - h\nu_0} \right. \\ & \left. + \frac{\langle i | \langle g | R_\sigma | e \rangle | v \rangle \langle v | \langle e | R_\sigma | g \rangle | j \rangle}{E_{ev} - E_{gj} + h\nu_0} \right] \quad (11) \end{aligned}$$

By application of Herzberg-Teller expansion of the electronic wavefunctions for small coordinate displacement of the nucleus from its equilibrium position in the ground state through first order perturbation (Sharf, 1971), the electronic wavefunctions are

$$|e\rangle = |e^0\rangle + \sum_a \sum_{s \neq e} \frac{(h_a^0)_{es} \cdot Q_a}{E_e^0 - E_s^0} |s^0\rangle \quad (12)$$

and

$$|g\rangle = |g^0\rangle + \sum_a \sum_{t \neq g} \frac{(h_a^0)_{gt} \cdot Q_a}{E_g^0 - E_t^0} |t^0\rangle$$

where $(h_a^0) = \left(\frac{\partial H}{\partial Q_a} \right)$ is the vibronic coupling operator for normal mode a evaluated at $Q_a = 0$, $|e^0\rangle$ is the electronic wavefunction evaluated at $Q_a = 0$, s and t are excited states, and $(h_a^0)_{es} = \langle e^0 | \left(\frac{\partial H}{\partial Q_a} \right)_0 | s^0 \rangle$.

Substituting Equation (12) into Equation (11) yields

$$(\alpha_{\rho\sigma})_{gi,gj} = A' + B' \quad (13)$$

$$A' = \sum_e^i \sum_v \left[\frac{M_{ge}^\sigma M_{eg}^\rho}{E_{ev} - E_{gi} - h\nu_0} \right] \langle gi | ev \rangle \langle ev | gj \rangle$$

$$B' = \sum_e^i \sum_{vs \neq e} \sum_a \frac{(h_a^0)_{es}}{(E_e^0 - E_s^0)(E_{ev} - E_{gi} - h\nu_0)} \left[M_{ge}^\sigma M_{sg}^\rho \langle gi | ev \rangle \langle ev | Q_a | gj \rangle \right. \\ \left. + M_{gs}^\sigma M_{ge}^\rho \langle gi | Q_a | ev \rangle \langle ev | gj \rangle \right]$$

where $(M_{ge}^\sigma) = \langle g^0 | R_\sigma | e^0 \rangle$, the coupling between ground and excited electronic state is neglected and the terms with $(E_{ev} - E_{gi} + h\nu_0)^{-1}$ are also

discarded.

(i) Non-resonance Raman Effect. In the non-resonance Raman case ($E_{ev} - E_{gi} \gg h\nu_0$), the approximate sum rule first developed by Van Vleck (1929) leads to

$$\sum_{\nu} \langle gi | ev \rangle \langle ev | gj \rangle = \langle gi | gj \rangle = \delta_{ij} = \text{kroncker delta}$$

$$\sum_{\nu} \langle gi | ev \rangle \langle ev | Q_a | gj \rangle = \sum_{\nu} \langle gj | ev \rangle \langle ev | Q_a | gi \rangle = \langle gi | Q_a | gj \rangle \quad (14)$$

$$= \begin{cases} 0 & \text{if } V_a^j \neq V_a^i \pm 1 \\ \left[\frac{(V_a^i + 1)h}{8\pi^2 \mu \nu} \right]^{1/2} & \text{if } V_a^j = V_a^i + 1 \\ \left[\frac{V_a^i h}{8\pi^2 \mu \nu} \right]^{1/2} & \text{if } V_a^j = V_a^i - 1 \end{cases}$$

where the values for the nonvanishing integrals are taken for harmonic oscillator wave functions, V_a^i is the quantum number of normal mode a of the i^{th} vibrational state, μ is the reduced mass of the oscillator, and ν is the normal mode frequency.

Substituting Equation (14) into Equation (13) leads to

$$(\alpha_{\rho\sigma})_{gi,gj} = A'' + B'' \quad (15)$$

$$A'' = \sum_e' \left[\frac{M_{ge}^{\sigma} M_{eg}^{\rho}}{E_{ev} - E_{gi} - h\nu_0} \right] \langle gi | gj \rangle$$

$$B'' = \sum_e' \sum_{s \neq e} \sum_a \frac{(h_a)_{es}^{\circ}}{(E_e^{\circ} - E_s^{\circ})(E_{ev} - E_{gi} - h\nu_0)} (M_{ge}^{\sigma} M_{sg}^{\rho} + M_{gs}^{\sigma} M_{ge}^{\rho}) \langle gi | Q_a | gj \rangle$$

According to Equations (14) and (15) it is seen that A'' vanishes when $i \neq j$ and is therefore responsible for undisplaced Rayleigh scattering. At the same time the expression B'' is responsible for displaced scattering of fundamentals which are the major part of the Raman effect since it vanishes unless $v_a^j = v_a^i \pm 1$. Scattering of combinations and overtones is derived from terms of higher order.

The condition that $v_a^j = v_a^i \pm 1$ is necessary but not sufficient for B'' not to vanish. It is further required that neither $(h_a)_{es}^0$ nor appropriate components of M_{ge} and M_{gs} vanish. Thus the electronic states e and s must both be upper states in allowed electronic transitions. For a totally symmetric ground state this means that the symmetry species, Γ_s and Γ_e , of these electronic states must correspond separately to Γ_ρ , the species of at least one of the translations. At the same time the direct product $\Gamma_e \times \Gamma_{H'} \times \Gamma_s$ must contain the totally symmetric representation in order for $(h_a)_{es}^0$ not to vanish. Here $\Gamma_{H'}$ is the species symbol for the irreducible representation for which $(\frac{\partial H}{\partial Q_a})_0$ is a basis. Thus if Γ_a is the species symbol for the a^{th} normal mode and $\Gamma_e = \Gamma_\rho$ and $\Gamma_s = \Gamma_\rho$, the requirement is that $\Gamma_a \times \Gamma_\rho \times \Gamma_\rho$ contains the totally symmetric species. Thus Γ_a must correspond to at least one of the species contained in the direct product $\Gamma_\rho \times \Gamma_\rho$, (namely, Γ_{x^2} , Γ_{xy} , Γ_{xz} , Γ_{y^2} , Γ_{yz} , and Γ_{z^2}). These are the well known selection rules for non-resonance Raman effect:

"A mode of vibration can be active in Raman scattering if the irreducible representation to which it can be assigned contains x^2 , y^2 , z^2 , xy , xz , or yz ."

(ii) Resonance Raman Effect. When ν_0 approaches $E_{ev} - E_{gi}$, Equation (9) must be modified by a damping coefficient of the exact

molecular eigenstate $|e\rangle$ through an additional term in the frequency denominators. The modified Equation (9) by Behringer (1958) becomes

$$(\alpha_{\rho\sigma})_{mn} = \sum_e \left[\frac{\langle m | R_\sigma | e \rangle \langle e | R_\rho | n \rangle}{E_e - E_m - h\nu_0 - i\Gamma_e} + \frac{\langle m | R_\rho | e \rangle \langle e | R_\sigma | n \rangle}{E_e - E_m + h\nu_0 - i\Gamma_e} \right] \quad (16)$$

where Γ_e is the damping coefficient of the electronic state $|e\rangle$. By introducing the same treatment as Equations (10)-(12), Albrecht (1961) obtained the scattering tensor as

$$(\alpha_{\rho\sigma})_{gi,gj} = A + B \quad (17)$$

$$A = \sum_e \sum_v \frac{M_{ge}^\sigma M_{eg}^\rho}{E_{ev} - E_{gi} - h\nu_0 - i\Gamma_{ev}} \langle gi | ev \rangle \langle ev | gj \rangle$$

$$B = \sum_e \sum_v \sum_{s \neq e} \sum_a \frac{(h_a)_{es}^0}{(E_e^0 - E_s^0)(E_{ev} - E_{gi} - h\nu_0 - i\Gamma_{ev})}$$

$$\times [M_{ge}^\sigma M_{sg}^\rho \langle gi | ev \rangle \langle ev | Q_a | gj \rangle + M_{gs}^\sigma M_{ge}^\rho \langle gi | Q_a | ev \rangle \langle ev | gj \rangle]$$

Qualitative consideration of Equation (17) reveals that with $i \neq j$, $\langle gi | ev \rangle \langle ev | gj \rangle$ need not vanish; therefore, the A term can be responsible for Raman scattering and this is different from non-resonance Raman effect where the A term is responsible for Rayleigh scattering only. Further, the contribution from the A term to the Raman intensity depends in no way upon vibronic coupling of state e with other states. Similarly, Rayleigh intensity may derive in part from B term since neither $\langle gi | Q_a | ev \rangle \langle ev | gj \rangle$ nor $\langle gi | ev \rangle \langle ev | Q_a | gj \rangle$ need vanish when $i = j$.

Recently, Mingardi and Siebrand (1975) improved Albrecht's theory

by adding a non-adiabatic coupling term to the scattering tensor. In their expansion method, the scattering tensor at resonance can be simplified to

$$(\alpha_{\rho\sigma})_{gi,gj} = A + B + D \quad (18)$$

$$D = \sum_e \sum_v \sum_{s \neq e} \sum_x \sum_a \frac{(h_a)_e^0}{(E_e^0 - E_s^0)(E_{ev} - E_{gi} - h\nu_0 - i\Gamma_{ev})}$$

$$\times \left[M_{eg}^\sigma M_{gs}^\rho \langle gj|ev \rangle \langle ev|Q_a|sx \rangle \langle sx|gi \rangle (\delta_{v,x-1} - \delta_{v,x+1}) \right.$$

$$\times \frac{h\nu_s^a}{E_{ev} - E_{sx}} - M_{eg}^\rho M_{gs}^\sigma \langle gj|sx \rangle \langle sx|Q_a|ev \rangle \langle ev|gi \rangle$$

$$\left. \times (\delta_{x,v-1} - \delta_{x,v+1}) \frac{h\nu_e^a}{E_{ev} - E_{sx}} \right]$$

where $|sx\rangle$ is the vibrational wavefunction of the excited state s with x quanta of energy $h\nu_s^a$ in the normal mode a . The A and B terms correspond to the A and B terms of Albrecht (Equation (17)). The D term is the first-order nonadiabatic correction term.

(iii) Application of Resonance Raman to Metalloporphyrins and Related Systems. It has been demonstrated (Nafie, et al., 1973) that when the laser exciting frequency approaches the Q band, the vibrations effective in mixing B and Q states dominate the resonance Raman spectra in metalloporphyrins and related heme proteins. These vibrations are primarily the nontotally symmetric modes. However, when the exciting frequency approaches the B band, the totally symmetric modes become dominant in the

resonance Raman spectra.

Shelnutt, et al. (1976) have shown that for nontotally symmetric modes which mix B and Q states only B term in Equation (18) needs to be considered if the molecule retains at least C_{4v} symmetry in the excited state. The vibrational overlap factors determine which terms in the sum over v will be important. For the ground state and the excited state Q of metalloporphyrins, the potential surfaces are similar as evidenced by the near equality of the vibrational frequencies for the ground state and state Q, and only a small shift in the equilibrium positions for nontotally symmetric modes is expected. Therefore, in this case, the overlap factors in the B term will be large for $v = 0$ and 1 when $i = 0$, $j = 1$. The two terms yield equal maxima in the excitation profiles at the 0-1 and 0-0 frequencies of the state Q. The B term is of the form

$$I \sim |B|^2 \sim \left| \frac{1}{E_{Q0} - E_{g0} - h\nu_0 - i\Gamma_{Q0}} \pm \frac{1}{E_{Q1} - E_{g0} - h\nu_0 - i\Gamma_{Q1}} \right|^2 \quad (19)$$

where the plus sign (destructive) holds for a_{1g} , b_{1g} , and b_{2g} vibrations in a D_{4h} metalloporphyrin and minus sign (constructive) for a_{2g} modes. Constructive interference will place intensity in the excitation profile between the 0-0 and 0-1 frequencies (Friedman and Hochstrasser, 1975a).

For totally symmetric modes which derive intensity from the A term of Equation (18) and which are called Franck-Condon modes, the Franck-Condon overlaps, $\langle g_0 | e \nu \rangle$ or $\langle e \nu | g_1 \rangle$, again determine which of the terms in the sum over v are significant. The overlaps, $\langle g_0 | e \nu \rangle$ or $\langle g_1 | e 0 \rangle$ will be non-zero if the vibration is totally symmetric and there is either a change of frequency in the state e or a displacement of the equilibrium

internuclear separation in the excited state. In the case of metalloporphyrins, the excited state vibrational frequencies are assumed the same as for the ground state, and there is evidence in the related cobalamin complexes that nuclear equilibrium position of excited state potential surfaces are shifted slightly for most a_{1g} modes. Therefore, the $\langle g_0|e_0\rangle$, $\langle g_0|e_1\rangle$, $\langle g_1|e_0\rangle$, and $\langle g_1|e_1\rangle$ overlap factors are dominant. As a result, enhancement is primarily at the 0-0 and 0-1 frequencies. Since overlap factors over $v \cong 2$ are small, neglecting all but $v = 0$ and 1 terms, the A term is of the form

$$I \sim |A|^2 \sim \left| \frac{\langle g_1|e_1\rangle}{E_{Q1} - E_{g0} - h\nu_0 - i\Gamma_{Q1}} - \frac{\langle e_0|g_0\rangle}{E_{Q0} - E_{g0} - h\nu_0 - i\Gamma_{Q0}} \right|^2 \quad (20)$$

where the phase between 0-0 and 0-1 is constructive.

Since A term contribution of the scattered intensity depends on the square of the extinction coefficient, whereas the B term contribution depends linearly on the extinction coefficient, the A term contribution to the resonance Raman intensity is particularly sensitive to the intensity of the resonance electronic absorption. As a result, upon excitation into an intense absorption band such as the Soret band, strong enhancement of a_{1g} modes is expected for metalloporphyrins. Dominance of a_{1g} polarized vibrations has been demonstrated in the resonance Raman spectra of cytochrome oxidase and CrTPPCl, the former is excited by 363.8 nm laser line (Friedman and Hochstrasser, 1973) and the latter by 457.9 nm line.

3. Experimental Techniques

I. Raman Scattering Apparatus

The experimental apparatus in our laboratory is shown in Figure 2. It consists of (1) an excitation laser source, (2) a sample cell, (3) the optics for collecting the scattered light, (4) the double monochromator, (5) the detector, and (6) the photon counting electronics.

The exciting radiation sources are provided by a Coherent Radiation Model CR-5 argon ion laser, a Model 500K krypton ion laser, and an argon ion laser pumped Coherent Radiation Model 490 dye laser. The CR-3 Ar⁺ laser has an output of 1.0 watt (at 25 amperes) at 514.5 nm polarized vertically with respect to the laboratory. Later a CR-5 Ar⁺ laser replaces the CR-3 Ar⁺ laser and has an output of 1.0 watt (at 21 amperes) at 514.5 nm. The Kr⁺ laser has an output of 0.2 watt (at 30 amperes) at 530.9 nm. Sodium fluorescein in ethylene glycol is used as fluorescent dye for the dye laser. The output of the dye laser is about 0.2 watt at 550.0 nm in the presence of COT (cyclooctatetraene) when pumped by 4 watts (all lines) CR-5 Ar⁺ laser.

An interference filter is used to remove plasma emission lines and sometimes neutral density filters are used to reduce the incident laser power to avoid local heating and photodecomposition of samples. After passing through an interference and neutral filter, the monochromatic laser beam is focused and directed upward onto the sample with the scattering column aligned parallel to the vertical entrance of the double monochromator.

The scattered light is then collected at 90 degree scattering angle by an f/1.1 lens and imaged with a 3:1 magnification on the entrance slit

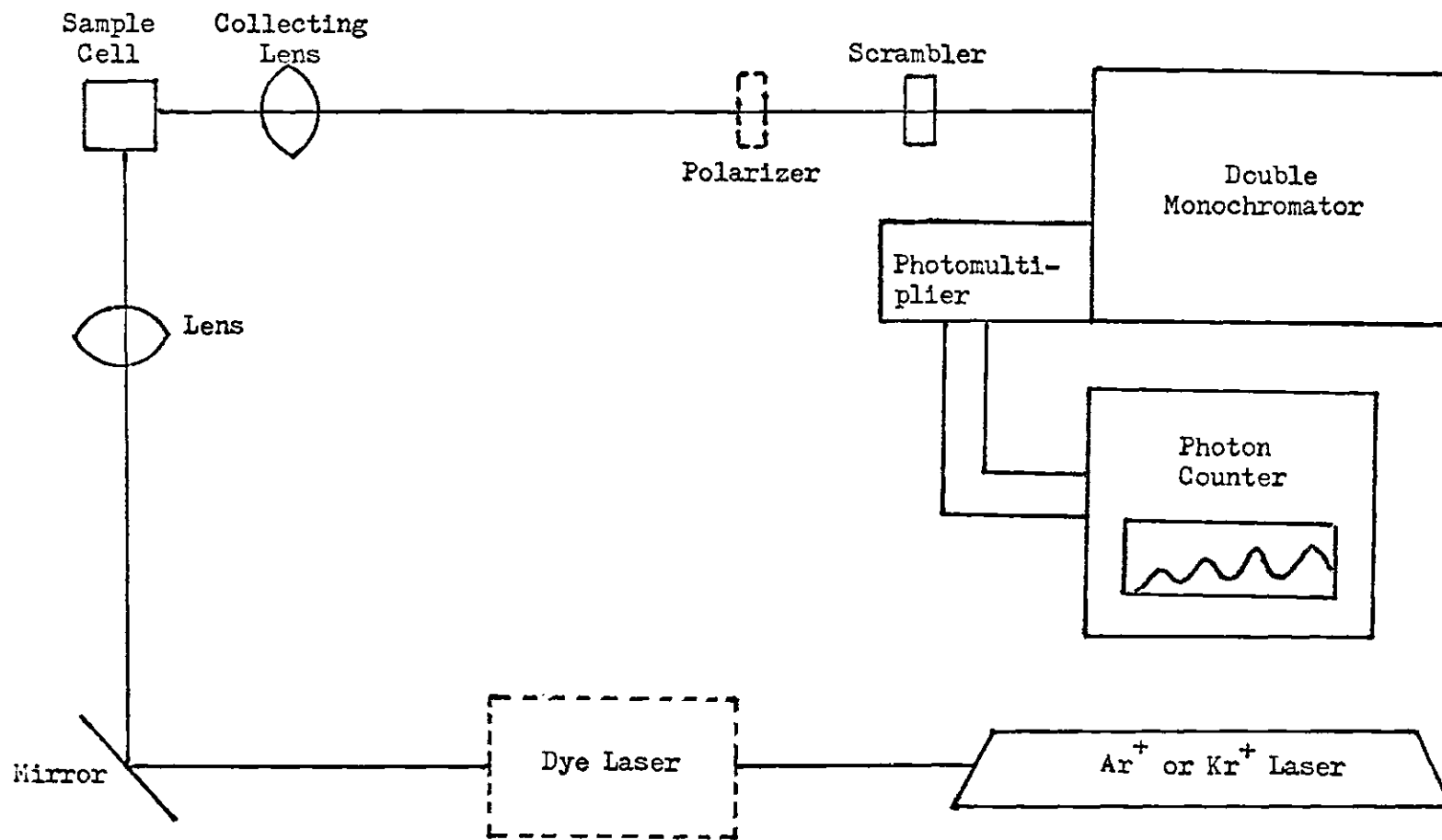


Figure 2. Laser Raman Scattering Apparatus

of a Spex 1401 double monochromator.

A polarization scrambler which is placed in front of the entrance slit provides randomly polarized light and thus insures that the response of the spectrometer and detector would be independent of the polarization of the scattered light.

For some resonance spectra the scattered light is analyzed into its parallel (I_{\parallel}) and perpendicular (I_{\perp}) components with respect to the polarization of the incident laser beam by a polarizer placed between the collecting lens and the polarization scrambler.

The spectrometer is Spex 1401 double monochromator. Two monochrometers are necessary to reduce the Rayleigh scattered component sufficiently to observe the Raman scattered component. The replica gratings have 1200 grooves/mm and are blazed at 500.0 nm. Typical entrance, intermediate, and exit slit widths are 250, 250, and 250 microns, and the entrance slit height is 10 mm.

The scattered light from the exit of the double monochromator is detected by an RCA C-31034 photomultiplier. By cooling to -20°C with a Products for Research (Model TE-104) thermoelectrically refrigerated chamber, the photomultiplier dark count is reduced from 120 counts per second at room temperature to about 10 counts per second. The photomultiplier is operated at -1680 volts. The pulses from phototube are counted by the Spex DC-1 photon counting electronics. The spectrum is recorded directly on the chart paper.

The wavenumber shifts of the Raman spectrometer are calibrated by using the spectrum of toluene as a standard (Aleksanyan and Sterin, 1957). The response of the Raman scattering apparatus is calibrated by a 45-watt

quartz-halogen tungsten coiled-coil filament lamp (Optronic Laboratories Model 245C L-124) as standard of spectral irradiance. The calibration curve is similar to that obtained by the theoretically calculated intensities of the rotational Raman lines of D_2 (Hamaguchi, et al., 1974).

II. Sample Handling Techniques

For non-resonance solution samples, the so-called axial/transverse and transverse/transverse methods are commonly employed. Since small glass capillary cells (0.5 - 1.0 mm bore) are used, the sample volume is now reduced to the range 5-20 μ l. In the axial/transverse method the laser beam enters along the axis of a capillary and the scattered light is collected at 90° to the capillary wall. The capillary with a fire-polished flat end is held vertically so that its axis is parallel with the entrance slit of the spectrometer. However, in the transverse/transverse arrangement the incident beam is perpendicular to the cell axis. Standard melting point capillary tubes of approximately 1.0 mm bore have been found to work satisfactorily. The end of the capillary tube may be sealed to prevent evaporation or air oxidation.

Solid samples (amorphous or crystalline) can be packed into a conical depression at the end of a 1/8 inch stainless steel rod, which is held horizontally. The laser beam is then directed upward and focused onto the sample at the grazing angle so that the scattering column is a strip on the power surface, 1/8 inch long and approximately 20 microns wide. When the control of relative humidity is required, the sample rod can be fastened inside a thermovac flask equipped with a rubber "O" ring and a vacuum tight stopcock. For intact lenses, the specimen is placed in a glass tube filled with the culture medium which keeps the organ in

the living state. The focused laser beam irradiated the lens at different positions in order to collect selectively the Raman light from different parts of the lens.

For resonance solution samples, in order to reduce the heating of strongly absorbing samples the sample cell is rotated at about 1000 rpm by a DC motor. Further cooling can be achieved by blowing cold nitrogen gas at the rotating cell. The cell is a quartz cell (3/4 inch diameter) and requires only about 0.2 ml of liquid sample. It is retained in an aluminum holder and is positioned so that the scattering column is in the solution approximately 0.15 mm from the cylindrical surface of the cell.

For colored solid samples (e.g., metalloporphyrins), KBr pellets (0.5 mg of porphyrin/200 mg of KBr) or crystalline powder affixed to transparent tape may be used to obtain spectra. To prevent photodecomposition, the pellet or tape is held in place on a rotating aluminum platform (3/4 inch diameter) by applying parafilm over the outer edge of the sample. The platform is oriented so that the incident beam and the surface of the pellet formed a 10-15° angle.

4. Interpretation of Protein Raman Spectra

I. Dependence of Amide Modes on Conformation

For Raman conformational analyses of polypeptide and protein spectra, it is important to elucidate the nature of the vibrations of the CONH group. It has been shown that there are nine frequencies associated with the peptide group motion of the model compound N-methylacetamide: 3280 (amide A), 3090 (amide B), 1653 (amide I), 1567 (amide II), 1299 (amide III), 627 (amide IV), 725 (amide V), 600 (amide VI), and 206 (amide VII)

(Miyazawa, et al., 1956, 1958). Among these modes, the amide I, II, and III are more useful in the conformational studies and have been extensively investigated by both infrared (Miyazawa and Blout, 1961) and Raman spectroscopy (Yu and Liu, 1972; Yu, et al., 1972). The amide I vibration is primarily C=O stretching (~ 70%) with some contributions due to the C-N stretching and the N-H in-plane bending. The amide II and III vibrations are both a mixture of the C-N stretching and N-H in-plane bending.

The factors which affect the amide I, II, and III frequencies in a polypeptide chain are: φ and ψ dihedral angles, H-bonding and interaction effects among peptide units. The effect of φ and ψ angles on amide I and III vibrations was recently studied by Hsu, et al. (in press) using N-acetyl-L-alanine-N-methylamide $\text{CH}_3\text{CONHCH}(\text{CH}_3)\text{CONHCH}_3$ as a model. The results of interest are that the amide I frequency distribution for α -helical conformations is very narrow, and that for extended conformations is only about 2 cm^{-1} . However, the difference between these two regions is 10.5 cm^{-1} ($1653.5 \rightarrow 1664 \text{ cm}^{-1}$). The linewidth associated with the unordered structure is expected to be larger than a regular structure because of a wider distribution in φ and ψ angles. In amide III region the normal vibration calculations indicate that the frequencies are more sensitive to small changes in φ and ψ . In the α -helical region a change of 10° in φ causes a shift of 11 cm^{-1} ; and a change of 6 cm^{-1} for a 10° variation of φ and ψ in the β region. This result indicates that amide III band is very sensitive to the conformation of the polypeptide chain.

The effect of H-bonding is to decrease the C=O stretching frequency but to increase the NH bending frequency. For N-methylacetamide the frequency shifts from gaseous phase (non H-bonded) to liquid phase (H-bonded)

are as follows: amide I ($1715 \rightarrow 1650 \text{ cm}^{-1}$), amide II ($1494 \rightarrow 1563 \text{ cm}^{-1}$), and amide III ($1263 \rightarrow 1300 \text{ cm}^{-1}$) (Shimanouchi, et al., 1974).

The vibration interactions among intra- and inter-chain peptide units were first considered by Miyazawa (1960). In his perturbation theory, a localized amide frequency is given by

$$\nu(\delta, \delta') = \nu_0 + \sum_s D_s \cos s\delta + D'_1 \cos \delta'$$

In this equation ν_0 is the unperturbed peptide group frequency. The second term arises from the intrachain interactions, and the coefficient D_s is determined by vibrational interactions between s^{th} neighbors in the chain, and δ is the intrachain phase difference. Similarly, the coefficient D'_1 is associated with the interchain hydrogen bonds, and δ' is the interchain phase difference.

If a polypeptide chain assumes the α -helical conformation, the interchain interactions may be neglected. Since the intrachain hydrogen bonds are formed between third neighbors, the D_3 term should be included in the expression

$$\nu(\delta) = \nu_0 + D_1 \cos \delta + D_3 \cos 3\delta$$

The polarized infrared spectra of an oriented film of high molecular weight α -helical poly- γ -benzyl-L-glutamate have been measured in the region $1800\text{-}1500 \text{ cm}^{-1}$. The parallel amide I band ($\delta = 0$) and the perpendicular amide I band ($\delta = 2\pi/3.6$) have been observed at 1650 and 1652 cm^{-1} , respectively. On the other hand, the parallel amide II band and the per-

pendicular amide II band are observed at 1516 and 1546 cm^{-1} , respectively.

Miyazawa's perturbation treatments of the amide I vibrations of β polypeptides are inconsistent with a detailed normal coordinate analysis of crystalline polyglycine I (Krimm and Abe, 1972). To achieve a more consistent understanding, Krimm and Abe (1972) modified the perturbation expression by adding the transition dipole coupling term D_{11} . The new equation is given by

$$\nu(\delta, \delta') = \nu_0 + D_1 \cos \delta + D_1' \cos \delta' + D_{11} \cos \delta \cos \delta'$$

For the antiparallel β -pleated sheet structure of polyglycine I, the following relations hold

$$\nu(0,0) = 1674 = \nu_0 + D_1' + D_{11}$$

$$\nu(0,\pi) = 1685 = \nu_0 - D_1' - D_{11}$$

$$\nu(\pi,0) = 1636 = \nu_0 + D_1' - D_{11}$$

$$\nu(\pi,\pi) = [1723] = \nu_0 - D_1' + D_{11}$$

The value of $\nu(\pi,\pi)$ is predicted on the basis of $\nu_0 = 1679.5$, $D_1' = -24.5$, and $D_{11} = 19 \text{ cm}^{-1}$, which are obtained by solving the first three equations. For poly-L-alanine in β -structure, whose observed frequencies are $\nu(0,0) = 1669$, $\nu(0,\pi) = 1695$, and $\nu(\pi,0) = 1630 \text{ cm}^{-1}$, the constants are $\nu_0 = 1682.0$, $D_1' = -32.5$, and $D_{11} = 19.5 \text{ cm}^{-1}$. The differences in the structure of these two β polypeptides are reflected in the similarity and differences between these parameters.

II. Raman Spectra of Poly-L-lysine and Glucagon as Model Systems

(i) Poly-L-lysine. The vibrations of a polypeptide backbone are not isolated from the motions of the side chain. To examine the effects of conformational changes on Raman spectra without uncertainties due to differences in side chains, one needs a model homopolypeptide which is capable of assuming a variety of conformations. Poly-L-lysine exists in aqueous solution as a random-coil at low pH, α -helix at high pH and low temperature, and the antiparallel β -pleated sheet structure at high pH and high temperature (Davidson and Fasman, 1967). Raman spectra have been reported for all three conformations in aqueous solution (Yu, Lip-pert, and Peticolas, 1973).

The conversion of α -helix to β -structure causes the following frequency shifts: $1645 \rightarrow 1670 \text{ cm}^{-1}$ (amide I), $1311 \rightarrow 1240 \text{ cm}^{-1}$ (amide III), and $945 \rightarrow 1002 \text{ cm}^{-1}$ (C-C stretching) (Figure 3). The amide I frequency at 1645 cm^{-1} is unusually low for α -helix since it is normally observed at $1650\text{-}1660 \text{ cm}^{-1}$. The amide III at 1311 cm^{-1} in α -helical poly-L-lysine is rather high in comparison with the other α -helical polypeptides ($1265\text{-}1300 \text{ cm}^{-1}$). It should be noted that the observed intensity at 1311 cm^{-1} is not completely due to the amide III mode, because the amide III intensity for α -helix is intrinsically weak. The CH_2 deformation also contributes to the intensity at 1311 cm^{-1} .

(ii) Glucagon. Glucagon is a polypeptide hormone of 29 amino acid residues whose sequence is known. It exists in $\sim 75\%$ α -helix in crystals, and a random coiled form in freshly prepared acidic solution. On standing at 26°C , this acidic solution is gradually converted into a gel, which is known to be predominantly antiparallel β -structure. Raman spectra in the

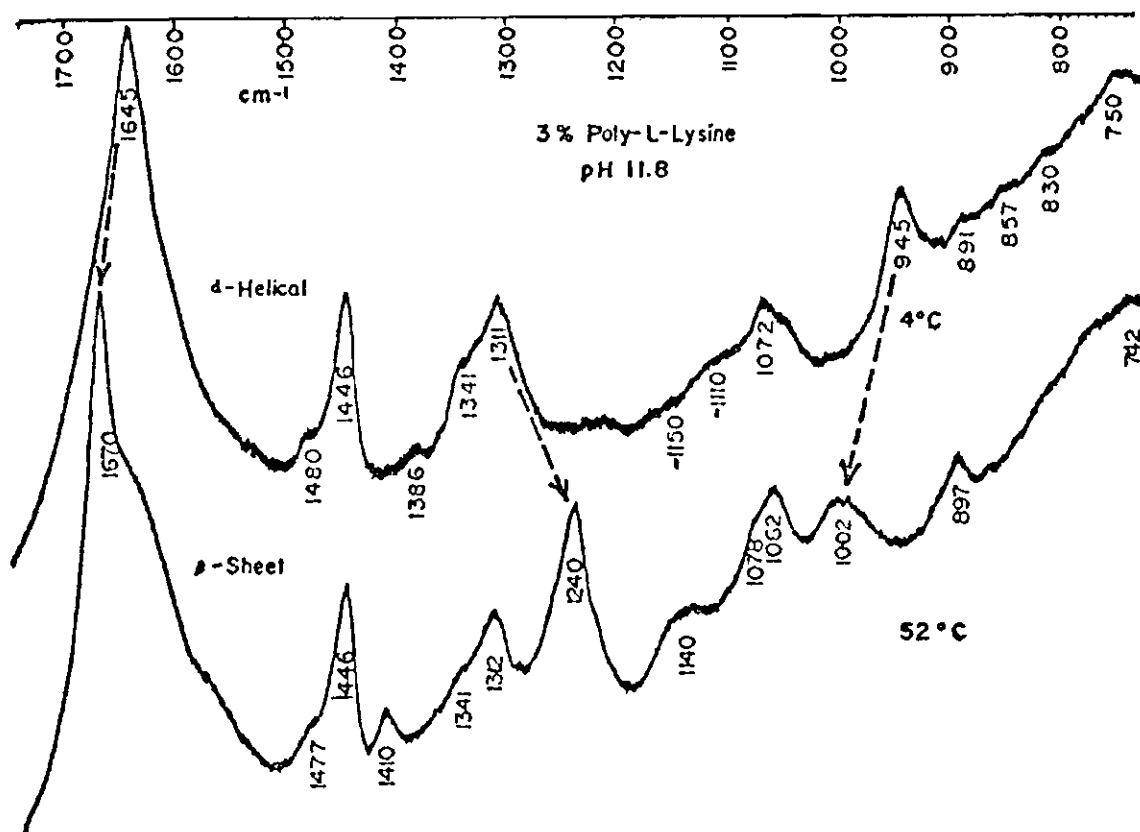


Figure 3. Raman Spectra of (top) α -Helical Poly-L-lysine, 3% in H_2O , pH 11.8, $T = 4^\circ C$, and (bottom) β -Sheet Poly-L-lysine, 3% in H_2O , pH 11.8, $T = 52^\circ C$ (reproduced from Yu, Lippert, and Peticolas, 1973)

1120-1700 cm^{-1} region of glucagon have been reported (Yu and Liu, 1972).

In Figure 4 are presented the Raman spectra of glucagon in crystals, freshly prepared aqueous solution (pH 2.25) and gels. In descending order, these spectra show a stepwise decrease in frequency of the amide III lines from 1266 (α -helix) to 1248 (random coil) and then to 1232 cm^{-1} (antiparallel β). These frequencies are very similar to those of α -helical poly-L-alanine, random-coiled poly-L-glutamic acid, and antiparallel β polyglycine I, respectively. In the 1630-1700 cm^{-1} region, the amide I line of crystalline glucagon is seen at 1658 cm^{-1} (α -helix). In Figure 4b the strong water line near 1640 cm^{-1} has obscured the amide I frequency of glucagon in freshly prepared aqueous solution. Upon gel formation, however, the amide line sharpens considerably and shows up in the spectrum as an intense sharp line at 1672 cm^{-1} (antiparallel β) on the sloping background of water.

III. Tyrosine Doublet at 850 and 830 cm^{-1}

Yu, Jo, and Liu (1972) first noticed a change in the intensity ratio of the tyrosine doublet at 830 and 850 cm^{-1} when ribonuclease (lyophilized powder) was dissolved in water. They suggested that this might be attributed to the change in the local environment of the three tyrosine having an abnormally high pK_a value. Subsequent studies (Yu and Jo, 1973; Yu, Jo, and O'Shea, 1973) on cobramine B and neurotoxin α indicated that the intensity ratio, $I(850)/I(830)$, depended on protein conformation and was possibly linked to the strong hydrogen bonds involving the phenolic hydroxyl groups in the "buried" environment not accessible to water.

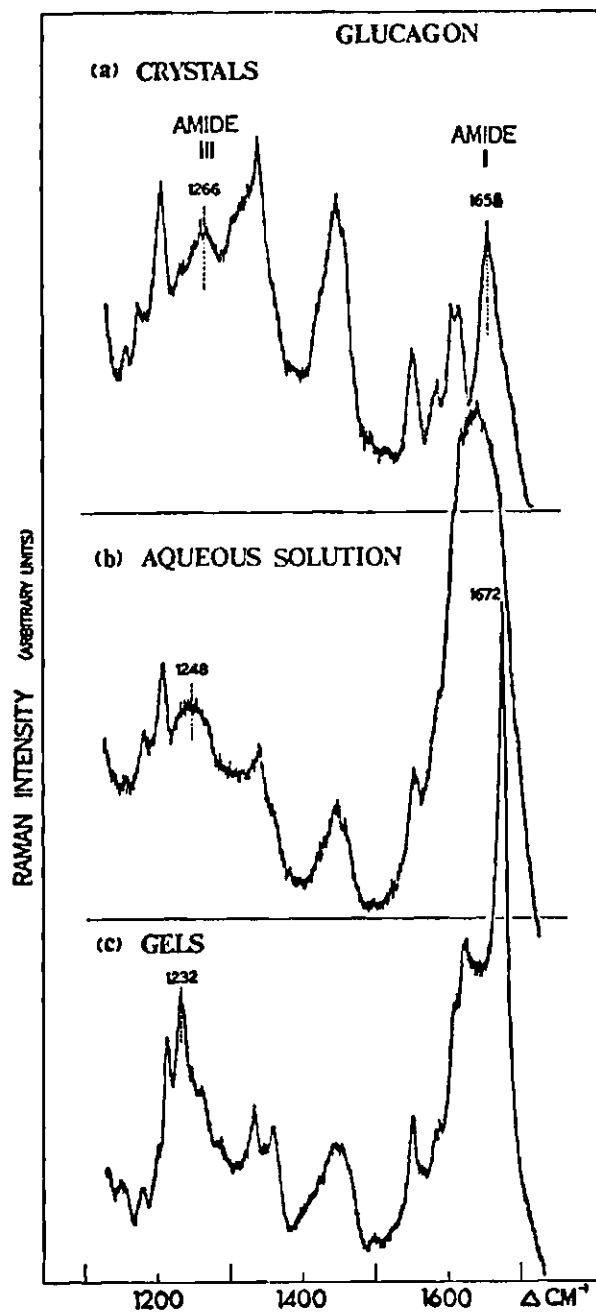


Figure 4. Raman Spectra of Glucagon in Various States of Aggregation
 (a) Spectrum of crystalline glucagon (powder form),
 (b) Spectrum of freshly prepared aqueous glucagon and
 (c) Spectrum of gels formed from (b) on standing (~ 40 hrs at 26°C) (reproduced from Yu and Liu, 1972)

Recently Siamwiza, et al. (1975) showed the doublet is due to Fermi resonance between the ring-breathing vibration and the overtone of an out-of-plane ring bending vibration of the para-substituted benzenes. Further examination of the effects of pH and solvents on the doublet and of the crystallographic data demonstrated that the intensity ratio of the two lines is determined by the nature of the hydrogen bonding of the phenolic hydroxyl group. When the hydroxyl group is strongly hydrogen bonded to a negative ion such as CO_2^- the intensity of the higher frequency is less than that of the lower frequency. The typical ratio is 3:10. The intensity of higher frequency is stronger if the hydrogen bonding is weak or an acidic external proton is bonded to the oxygen of the phenolic hydroxyl group. The intensity ratio in this case is 10:4.

IV. Dependence of $\nu(\text{S-S})$ on Local Geometry

Raman spectra of compounds containing disulfide bonds show well-defined lines in the $500\text{-}600\text{ cm}^{-1}$ region, which arise from S-S stretching mode. The behavior of these Raman lines as a function of structural parameters has been extensively investigated using model compounds (Sugeta, et al., 1972, 1973; Nogami, et al., 1975). They have shown that the S-S frequency did not depend on the CS-SC dihedral angles, but rather on the torsional angles about the C-S bonds in the C-C-S-S-C-C group. Assuming that the dihedral angle around the S-S bond is fixed at $\sim 90^\circ$ (gauche), the S-S frequency then depends on whether the two torsional angles about the C-S bonds are both gauche, one gauche and one trans, or both trans. The $\nu(\text{S-S})$ frequencies are 510 cm^{-1} (GGG), 525 cm^{-1} (GGT), and 540 cm^{-1} (TGT). A diagram showing this correlation is presented in Figure 5.

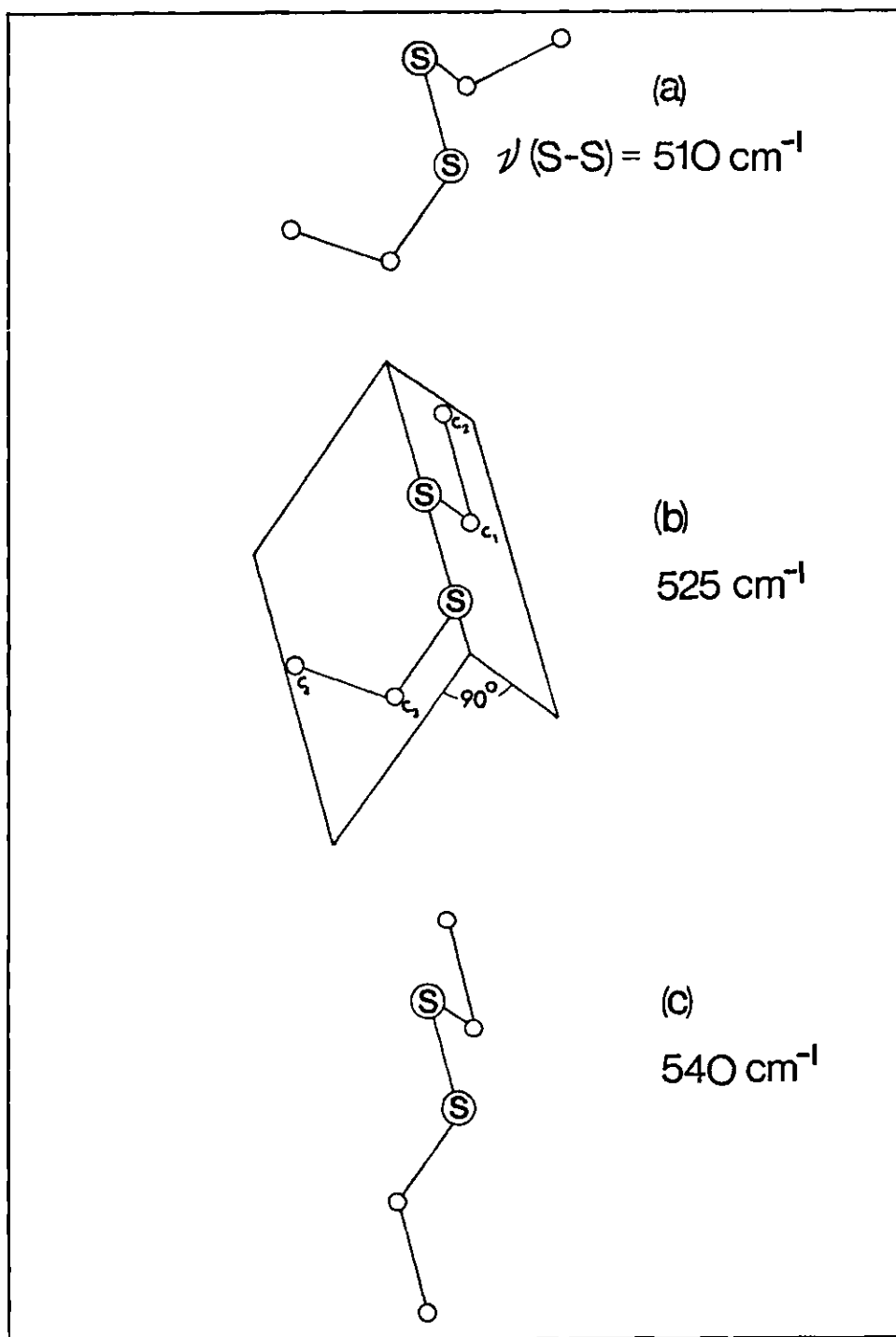


Figure 5. Correlation Between the C-C-S-S-C-C Geometry and $\nu(\text{S-S})$ Frequency

CHAPTER II

NON-RESONANCE RAMAN STUDIES OF HUMAN AND ANIMAL LENSES

1. Introduction

Every year the vision of well over a million people is clouded or occluded by cataract, a loss of transparency of the lens of the eye. To prevent this disease one must understand its causes; therefore, it requires a better understanding of the structure of the human lens, of its metabolic process and changes induced in it by increasing age and external influences.

Because of the high protein content and the transparency of the lens, Raman spectroscopy provides a powerful unique technique to study the structures of the intact lenses and the relationships to the transparency and cataractogenesis.

A great deal of research has been carried out on animal models because of the limited availability of normal human lenses and the difficulties of experimentation on humans. There are important differences between the human lens and the lens of the usual research animals (Kuck, 1974). Some of these differences may in themselves be significant clues to the causes of cataract in humans. Therefore it is important to establish the structural similarities and differences between the human and the animal lens so that it is possible to evaluate the applicability of the information obtained from the animal lens to human cataract.

Figure 6 shows the structure of the human lens. It is illustrated

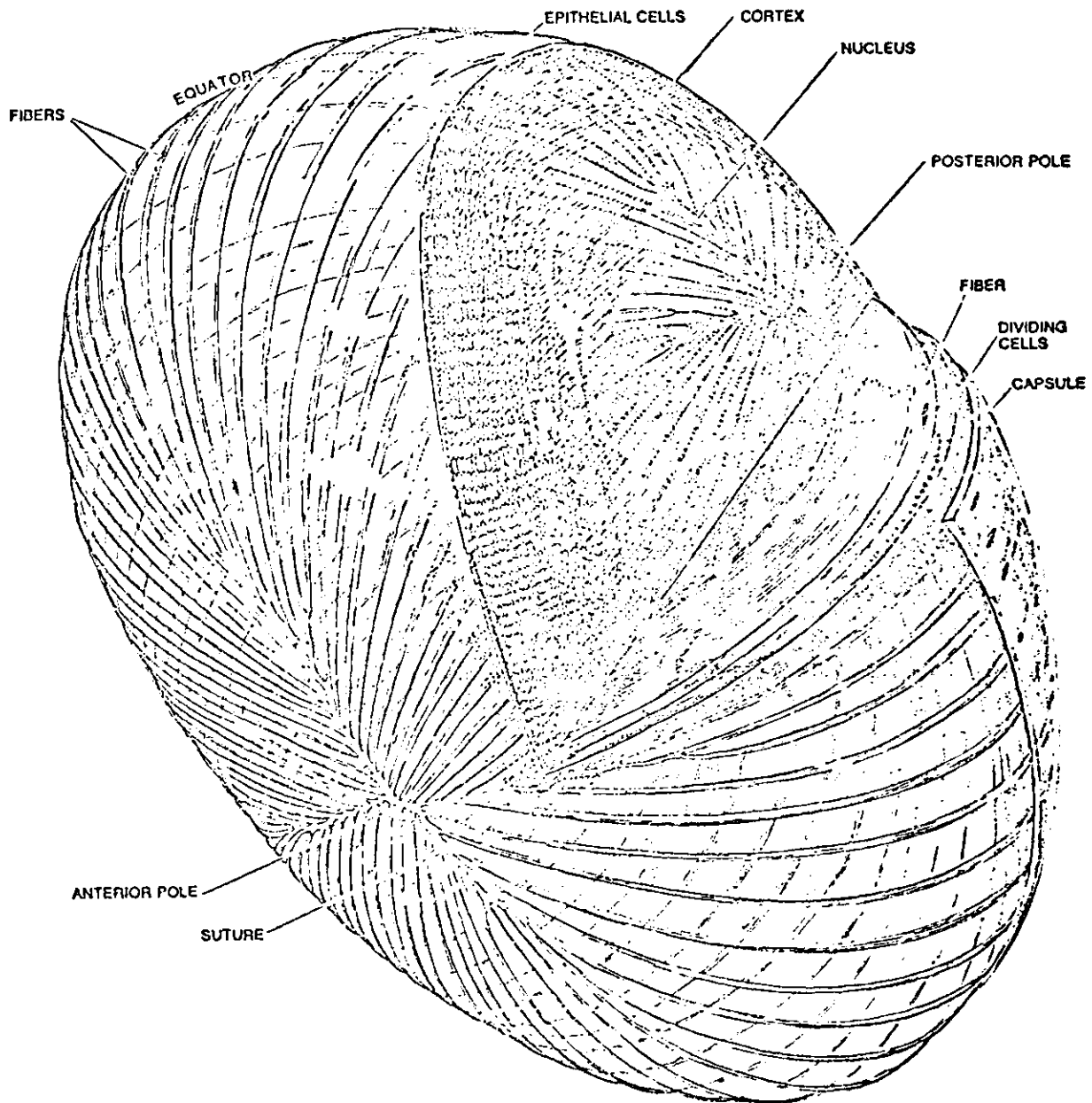


Figure 6. Structure of Human Lens (reproduced from van Heyningen, 1975)

diagrammatically with the capsule, outer covering, largely cut away to reveal the lens fibers. Growth of the lens originates with the division of the epithelial cells in a band near the equator. The new cells elongate to form fibers, up to a centimeter long and very thin, that wrap around the periphery of the lens and meet at the sutures. The outer fibers are nucleated and are roughly hexagonal in section; as these fibers are displaced inward toward the center by newer cortical fibers they change shape and lose their cell nuclei.

2. Materials and Methods

Lens Materials

All intact lenses were generously supplied by Dr. J. F. R. Kuck, Jr. of Emory University. The animals were decapitated in the laboratory, eyes enucleated at once and lenses prepared in a modified T-K medium (Thoft and Kinoshita, 1965; Kuck, East, and Yu, 1976).

Modified T-K Medium

The modified T-K medium was a mixture of several parts. Part I: MgSO_4 (55.6 mg/500 ml H_2O), Na_2HPO_2 (34.3 mg/500 ml), KH_2PO_2 (34.3 mg/500 ml), KCl (248.0 mg/500 ml), KHCO_3 (84.0 mg/500 ml), and NaHCO_3 (1.94 g/500 ml); Part II: NaCl (7.90 g/500 ml); Part III: CaCl_2 (1.7 g/100 ml). Equal volumes of I and II were mixed and 1% of III was added. In addition, 140 mg ABGG mixture per 100 ml solution was added. The ABGG mixture (antibiotic-glucose-glutamine) contained 4.0 g glucose, 63 mg penicillin G (K-salt), 63 mg streptomycin, and 0.45 g glutamine. The medium was saturated with 95% O_2 -5% CO_2 .

Isolation of Rat Lens Protein Fractions

The frozen rat lenses were generously supplied by Dr. J. F. Kuck, Jr. After the lenses were thawed, they were washed with distilled water and decapsulated and then the nuclear portions of the lens were crushed with a glass rod (10 ml of water/gram of lens). The stirring was continued overnight by a small magnetic stirring rod in a small vial on a magnetic stirrer. The insoluble proteins were removed by centrifugation at 12,000 rpm for 30 minutes and then were washed 5 times with ice-cold distilled water. After washing, the water insoluble proteins were lyophilized. The water soluble proteins were separated by the method of van Dam and Cate (1966). A 6 ml protein solution which contained approximately 0.4 g of protein was fractionated on a column (1.5 x 110 cm) of Sephadex G-200 equilibrated with 0.1M Tris buffer which contained 0.1M NaCl, 0.001M EDTA, and 0.001M 2-mercaptoethanol and adjusted to pH 9.0 with 6M HCl. The flow rate was 6 ml/hour and 2 ml fractions were collected. The transmittance at 280 nm was monitored with an LKB 8300 Uvicord II ultraviolet absorptionmeter equipped with a 3 mm path length cell and the flow rate was controlled by a peristaltic pump. The 10 ml central portions of α -, β -, and γ -crystallin were each dialyzed against distilled water 24 hours by changing water four times. After dialysis the protein solutions were adjusted to pH 7.3 and then lyophilized.

Purification of δ -Crystallin

Chick lens δ -crystallin was purified by a modification of the procedure of Watanabe and Kawakami (1973). The decapsulated lenses of one day old chick were dissolved in 1-2 ml of Tris buffer (same as above) per gram of lenses. The insoluble part of the lenses was removed by

centrifugation at 12,000 rpm for 30 minutes. The slightly opalescent solution was applied to a Sephadex G-200 column (1.5 x 110 cm) which was equilibrated with the same Tris buffer used for dissolving the lenses. The flow rate of the column was 7 ml/hr and the fraction size was 2 ml. The 10 ml central portion of the second peak, which contained δ -crystallin was dialyzed against distilled water, adjusted to pH 7.0 with 0.1M KOH and lyophilized.

Heat Denaturation of δ -Crystallin

A water solution of δ -crystallin (50 mg/ml, pH 7.0) was placed in a 100°C water bath. The protein solution became a gel as soon as it was placed in the bath. Water was placed on top of the gel, and the gel was maintained at 100°C for one hour. The gel was then cooled, broken into a suspension and lyophilized.

Raman Spectroscopic Methods

The laser Raman system and the sample handling techniques for obtaining the spectra of lyophilized powders, aqueous solutions and intact lens were similar to those described in Chapter I. All of the spectra were obtained with the 514.5 nm line excitation excepting the spectrum of lizard lens, which was recorded with the 647.1 nm line excitation of krypton ion laser.

Circular Dichroism (CD) Spectra of δ -Crystallin

The CD spectra of δ -crystallin solutions were obtained with a Jasco Model J-20 automatic recording spectropolarimeter. The δ -crystallin, which had been purified by gel filtration at pH 9.0, was studied in 0.01M sodium phosphate buffer, pH 7.0, at a concentration of 2 mg/ml in 0.05 mm cells. The protein concentration was determined by using $A_{280\text{nm}}^{1\%}$ of 4

(Piatigorsky, Zelenka, and Simpson, 1974) and by using the microbiuret method of Zalemhof and Chargaff (1966). The CD data are expressed in terms of mean residue ellipticity, $[\theta]$, using the mean residue weight of 110, calculated from the amino acid composition of δ -crystallin (Waley, 1969). The mean residue ellipticity of δ -crystallin at 208 nm was calculated to be -2.56×10^4 degrees cm^2 per decimole.

Estimation of Glycogen by Raman Spectroscopy

Lyophilized powders were prepared from 3 ml water solutions containing 5 mg of chick δ -crystallin and from 5 to 15 mg of glycogen (Pfanzstiehl Lab.). The Raman line at 481 cm^{-1} is due to glycogen with no contribution from protein residues, and the line at 1004 cm^{-1} is due to phenylalanine residues with no contribution from glycogen (Kuck, East, and Yu, 1976). The calibration curve can be expressed by the equation:

$$\frac{\text{wt. glycogen}}{\text{wt. } \delta\text{-crystallin}} = \frac{I_{481 \text{ cm}^{-1}}/I_{1004 \text{ cm}^{-1}}}{2.3} \quad (21)$$

To use Equation 21 to estimate the ratio of glycogen to δ -crystallin in the pigeon lens nucleus it was assumed that the concentration of α , β , and γ -crystallins in the pigeon lens nucleus are negligible (amide I line at 1656 cm^{-1}) and that pigeon lens δ -crystallin has the same mole percent Phe as chick lens δ -crystallin. Since the relative intensity of the 481 cm^{-1} line to the 1004 cm^{-1} line from the pigeon lens nucleus is 4.0, Raman spectra indicate that there is 1.7 times as much glycogen as δ -crystallin in the pigeon lens nucleus.

Long-wave UV Irradiation of Mouse Lens

Mice were irradiated in plastic cages ($14 \frac{7}{8} \times 12 \frac{7}{8} \times 6 \frac{5}{8}$

inches deep), divided into two compartments by a wire mesh separator running lengthwise. Each compartment had an F-15T8 BLB UV lamp (General Electric) projecting through it. The UV irradiation had a wavelength range from 310 to 410 nm with the intensity about 4 mW/cm^2 at surface of the lamp. The end of the lamp extended outside the cage wall through tight fitting holes bored in the plastic $2 \frac{1}{4}$ inches above the cage bottom and centered in the compartment. Thus the mice were within two inches of the lamp's surface except when they climbed on the separator. The cage top was a wire mesh fitted over the cage. Mice were placed in the cages after weaning at about one month of age; 10-12 of the same age occupied a compartment. Irradiation was continuous. Control (non-irradiated) mice were kept under regular colony conditions where ambient light levels were usually low.

3. Results and Discussion

I. Structural and Conformational Implications of Raman Spectrum of Intact Human Lens

The Raman spectrum of the cortex of a six months intact human lens is shown in Figure 7. The vibrational frequencies in wavenumber (cm^{-1}) ($300\text{-}1800 \text{ cm}^{-1}$) and tentative assignments are listed in Table 1.

It has been recognized for some time that the amide I region ($1630\text{-}1680 \text{ cm}^{-1}$) and amide III region ($1220\text{-}1300 \text{ cm}^{-1}$) in the Raman spectra of proteins are sensitive to the geometry of the peptide backbone groups of the protein and therefore are sensitive to the secondary structure of the protein (Chapter I).

Studies of the Raman spectra of synthetic polypeptide and proteins

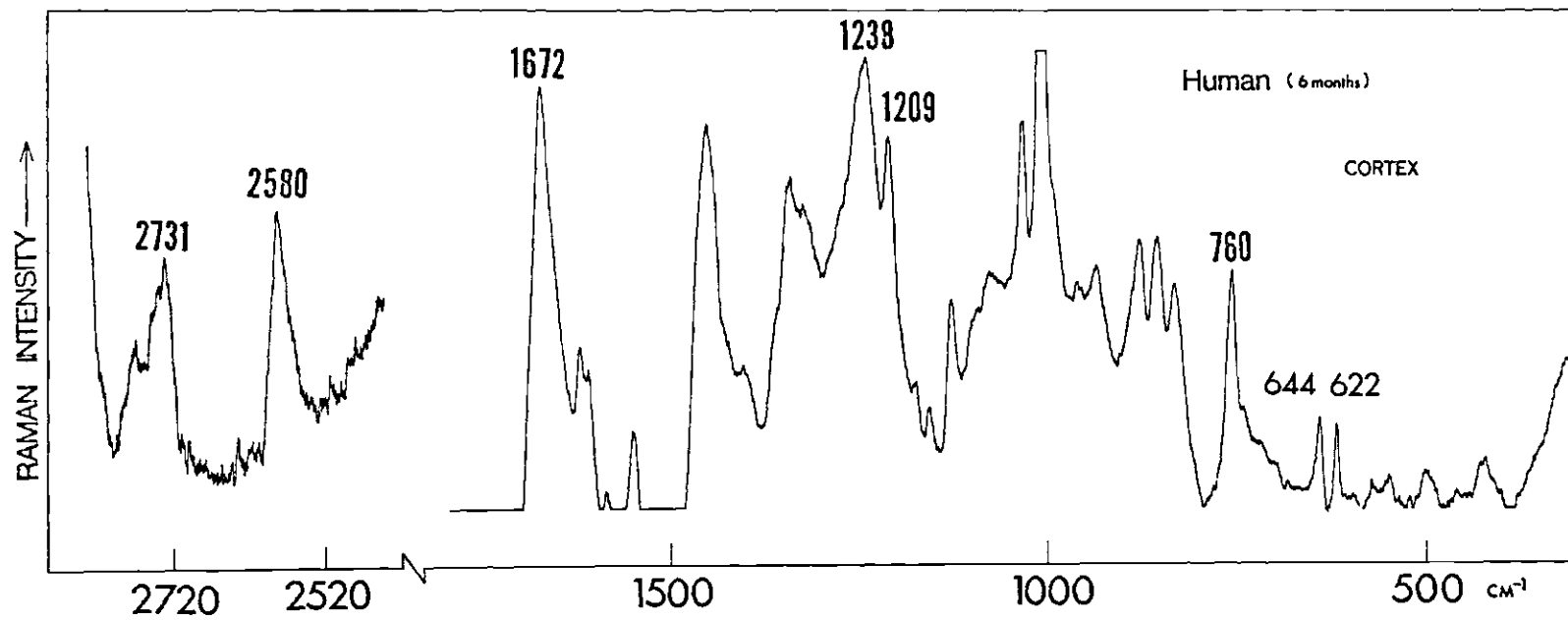


Figure 7. Raman Spectrum of the Cortex of Intact Human Lens

Table 1. Raman Frequencies (cm^{-1}) and Tentative Assignments for Intact Human Lens ($300\text{-}1800\text{ cm}^{-1}$)

Frequencies (cm^{-1})	Tentative Assignments	Frequencies (cm^{-1})	Tentative Assignments
426 (0.5)		1072 (1.5 b)	ν (C-N)
462 (0.1)		1100 (0.5 sh)	ν (C-N)
496 (0.7)		1127 (2.5 s)	ν (C-N)
552 (0.4)		1157 (1.0)	ν (C-N)
572 (0.5)	Trp	1178 (1.5)	Tyr & Phe
606 (0.1)		1209 (4.0 s)	Tyr
622 (1.4)	Phe	1238 (7.0)	Amide III
644 (1.5)	Tyr	1322 (2.0 sh)	δ (CH)
708 (0.3)	ν (C-S)	1340 (2.5 s)	Trp
726 (0.5)	ν (C-S)	1361 (1.2 sh)	Trp
746 (0.5 sh)		1400 (1.2)	$-\text{CO}_2^-$
760 (4.0 s)	Trp	1424 (1.5 sh)	δ (NH) of Trp
834 (2.8)	Tyr	1447 (9.0)	δ (CH_2)
856 (3.3)	Tyr	1494 (0.5 sh)	
880 (3.2)	Trp	1550 (2.7 s)	Trp
938 (2.0)	ν (C-C)	1578 (0.2 sh)	Trp
960 (1.8)	ν (C-C)	1585 (0.4)	Tyr & Phe
990 (2.5 sh)		1608 (2.3)	Phe
1005 (10.0 s)	Phe	1618 (2.3)	Tyr
1032 (4.0 s)	Phe	1672 (9.0)	Amide I

Abbreviations: s, sharp; sh, shoulder; b, bump

The values in parentheses are relative Raman intensity.

of known structure indicate that the α -helical form displays a strong amide I vibrational frequency at $1650 \pm 5 \text{ cm}^{-1}$ with relatively weak scattering in the amide III region, and that anti-parallel β -pleated sheet gives a strong and sharp amide I at $1670 \pm 2 \text{ cm}^{-1}$ with a strong amide III line at $1225\text{-}1240 \text{ cm}^{-1}$. The random coil form, on the other hand, shows a broad amide I band at about 1665 cm^{-1} with a medium intensity but broad amide III at about 1248 cm^{-1} . Table 2 shows the correlation between protein backbone conformation and amide I, amide III frequencies.

From Table 2 and the distinct amide I and amide III lines at 1672 and 1238 cm^{-1} of the spectrum of the intact human lens, it is suggested that the proteins in the cortex region exist mainly in anti-parallel β -pleated sheet structure. This does not exclude the possibility that a small amount of unordered structure may also be present.

It has been shown (Chapter I) that the intensity ratio of the tyrosine doublet at 834 and 856 cm^{-1} is determined by the nature of the hydrogen bonding of the phenolic hydroxyl groups in the tyrosine residues. If the hydrogen bonding is weak the higher frequency is stronger and the ratio is about 10:4. The peak intensity ratio, $I(856)/I(834)$, in intact human lens is about 10:8.5. This ratio suggests that the majority of the hydroxyl groups of the tyrosyl residues, whether "buried" or "exposed," form weak hydrogen bonds or serve as acceptors to other protons that are acidic donors.

Raman spectroscopy also can be used to investigate the oxidation state of cysteine residues in the intact state without the complication of possible air oxidation. The Raman spectrum of an intact human lens in

Table 2. Correlation Between Protein Backbone Conformation and Amides I and III Frequencies (cm^{-1})

Conformation	Amide I (cm^{-1})		Amide III (cm^{-1})	
	Raman	Infrared	Raman	Infrared
α -Helix	1660 ± 4	1657 s	> 1264	1262 s
β -Structure:				
Antiparallel	1673 ± 2	1685 m	1227-1240	1236 m
Parallel	1655*	1655*		
Random-Coil:				
Solvated	1655		1248 ± 4	
Non H-Bonded	1685		1235 ± 5	

*Theoretically predicted value. At present, there is no experimental evidence for it.

Abbreviations: s, strong; m, medium

the sulfhydryl group stretching region ($2500-2800\text{ cm}^{-1}$) is included in Figure 7.

The assignment of the observed 2580 cm^{-1} line to the sulfhydryl stretching mode is based on: (1) the stretching frequency of S-H is 2558 cm^{-1} for L-cysteine solid; (2) the stretching frequency of S-H is 2583 cm^{-1} for L-cysteine solution at pH 5.2; (3) the stretching frequency of S-D is 1875 cm^{-1} for L-cysteine solution at pD 5.2; (4) the stretching frequency of S-D is 1870 cm^{-1} for deuterated lens proteins. The S-H stretching frequency observed for the lens proteins is somewhat higher than that of hemoglobin in which it is observed near 2560 cm^{-1} by Fourier transform infrared spectroscopy (Bare *et al.*, 1974). Since the sulfhydryl vibration depends on the state of aggregation and is different for oxy- and deoxyhemoglobin, it may be considered as conformation dependent.

II. Protein Fractions of Rat Lens and Their Raman Spectroscopic Studies

The lens of most vertebrate eyes contains a high concentration of protein. For example, the adult rat lens has approximately 30% in the peripheral region and more than 70% in the central region. In general, vertebrate lens proteins are classified as water insoluble fraction and water soluble fraction, the water insoluble fraction is called albuminoid and water soluble fraction contains α -, β -, and γ -crystallin. Figure 8 shows a typical chromatogram of the separation of the water soluble rat lens proteins into α -, β -, and γ -crystallin by gel chromatography on Sephadex G-200 column.

Figure 9 shows the Raman spectra of α -, β -, γ -crystallin and albuminoid of rat lens in the region from 300 to 1700 cm^{-1} .

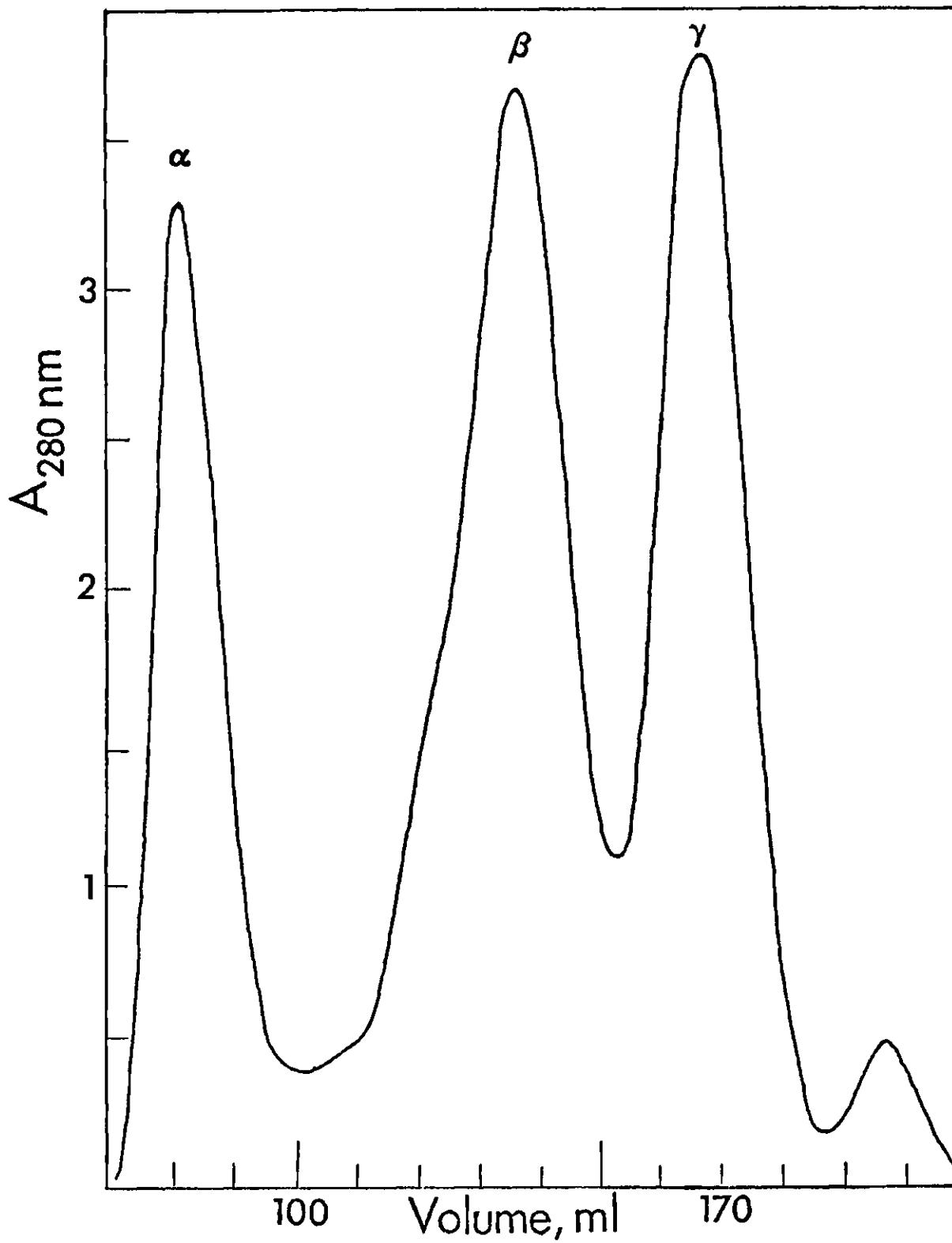


Figure 8. Separation of the Water-soluble Rat Lens Proteins by Gel Chromatography on Sephadex G-200 Column (The unlabeled fraction contains low molecular weight materials such as RNA, etc.)

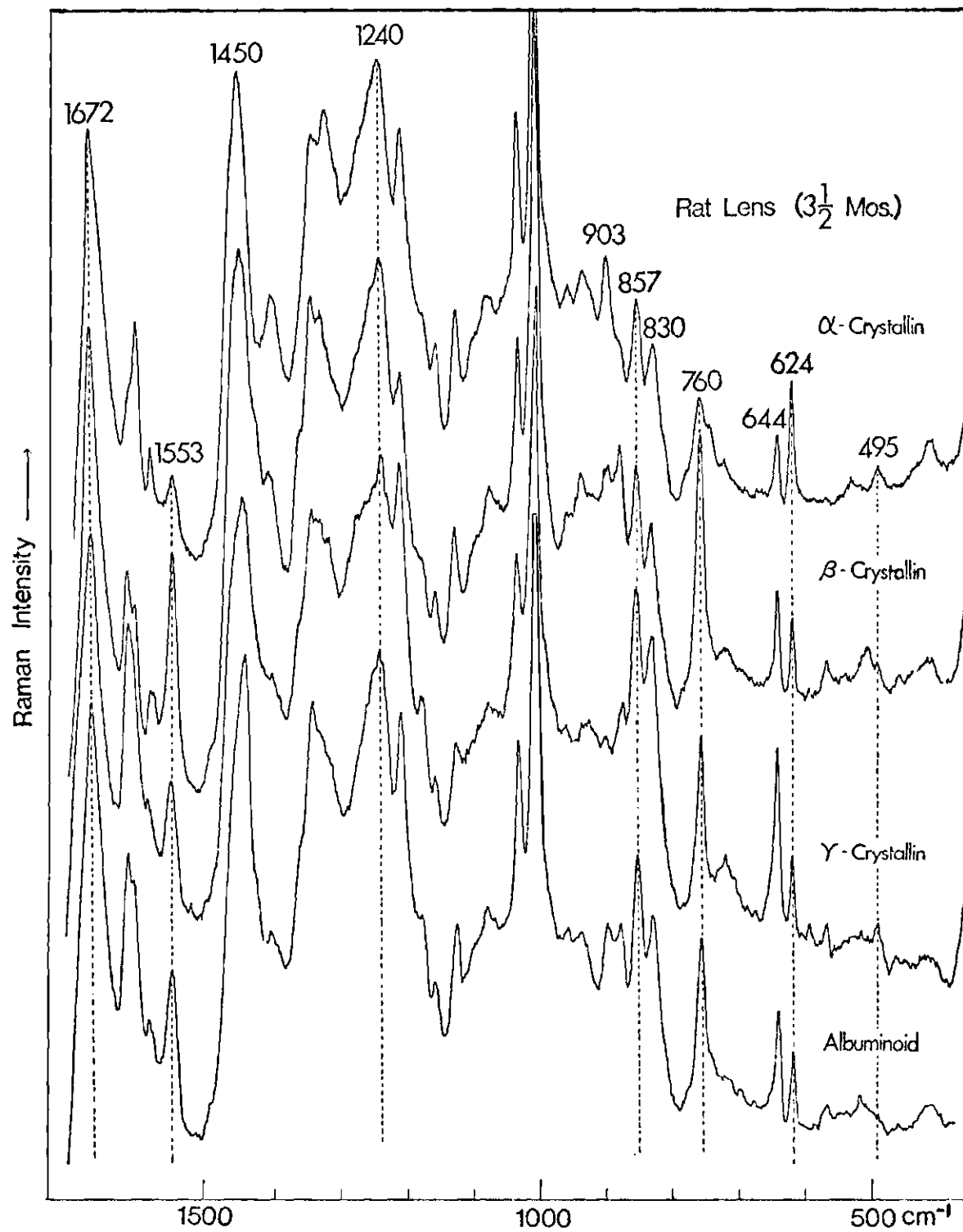


Figure 9. Raman Spectra of α -, β -, and γ -Crystallin and Albuminoid in Lyophilized Powder

The lines at 624 cm^{-1} due to phenylalanine and 644 cm^{-1} due to tyrosine show variation in relative intensity, indicating different phenylalanine to tyrosine ratios among these proteins. The peak intensity ratios, $I(624)/I(644)$, are approximated 1.9:1, 1:1.3, 1:2.3, and 1:1.5 for α -, β -, γ -crystallin and albuminoid, respectively. Early studies of albuminoid of rat lens indicated that albuminoid contained mainly γ -crystallin (Lerman, 1969) in good agreement with our Raman results. From the Raman intensity ratios $I(624)/I(644)$, it can be calculated that the albuminoid of rat lens is derived approximately from 84% of γ -crystallin, 16% of α -crystallin and only a trace of β -crystallin. This is completely different from bovine lens in which the albuminoid is mainly derived from α -crystallin (Yu and East, 1975).

Raman spectra of compounds containing disulfide bonds show well-defined lines in the $500\text{-}600\text{ cm}^{-1}$ region, which arise from S-S stretching modes. It has been shown (Spector, 1971; Bjork, 1970) that there are no disulfide bonds in either α - or γ -crystallin; therefore, the 535 cm^{-1} bands in the spectra of both α - and γ -crystallin are not due to the S-S mode. However, in the spectrum of β -crystallin there is a medium line at 510 cm^{-1} , indicating that there are disulfide bonds in β -crystallin. Armand et al. (1970) found by biochemical assays that at least one of the β -crystallins contained disulfide bonds. The correlation between the disulfide bond conformation and its stretching frequency has been discussed in Chapter I. From this correlation, it is concluded that the geometry of the disulfide bonds in β -crystallin is in gauche-gauche-gauche conformation.

In the amide I ($1630\text{-}1680\text{ cm}^{-1}$) and amide III ($1220\text{-}1300\text{ cm}^{-1}$)

regions, each spectrum of these proteins displays the strong and sharp amide I frequency at 1672 cm^{-1} and amide III frequency at 1240 cm^{-1} , indicating that these proteins in lyophilized powder state exist in predominantly anti-parallel β -sheet conformation (Table 2).

The peak intensity ratio of tyrosine doublet, $I(857)/I(830)$, in each crystallin or albuminoid is about 10:9 to 10:10, indicating that the hydroxyl groups of tyrosine residues in these proteins form weak hydrogen bonds.

By comparing the spectra of both intact lens proteins and isolated lens proteins, the amide I and amide III frequencies which appear at 1672 and 1240 cm^{-1} are exactly the same. This means that the backbone conformation of the lens proteins does not change when they are fractionated.

To determine whether the anti-parallel β -sheet conformation is uniformly distributed throughout the whole lens, we have obtained Raman spectra from various locations and found that the frequencies and line shapes of the amide I and amide III bands are independent of this parameter. However the intensity ratios of 624 cm^{-1} due to phenylalanine to 644 cm^{-1} due to tyrosine show variations, indicating that the α -, β -, and γ -crystallin are heterogeneously distributed in the lens. Based on the ratios for α -, β -, and γ -crystallin, we may conclude that γ -crystallin is mainly in the nucleus in good agreement with the work of Bours and Brahma (1973).

III. Prevalence of α -Helical Form in Chick and Pigeon Lens Proteins

The avian lens is unlike other vertebrate lenses in several respects: it contains a unique crystallin, FISC or δ -crystallin (Rabaey, 1962; Zwaan, 1966); it does not develop cold cataract and is generally

less susceptible to other types of cataract (Kuck, 1974); it has a low proportion of protein; it is extremely soft with no distinct nucleus; it lacks the equivalent of mammalian lens albuminoid; it has no grossly visible fluorescence; it has a low-protein-thiol content (Zwaan, 1966); it has relatively low amounts of γ -crystallin, especially in birds of flying habit, which also have a remarkably high level of glycogen in the nucleus (Rabaey, 1963; Rabaey, et al., 1972).

The Raman spectra of an intact chick (~ 10 days old) lens and an intact pigeon (~ 8 weeks old) lens maintained in a modified T-K medium are shown in Figure 10. Included for comparison is the spectrum of a monkey (~ 3 years old) lens, which is virtually identical to the spectrum of a bovine (~ 2 years old) lens (Yu and East, 1975).

The information pertaining to the secondary structure of proteins may be found from two spectral regions: amide I and amide III (Chapter I). The examination of the chick lens spectrum immediately suggests that the proteins are mainly in the α -helical conformation (Table 2). The spectral features in the amide I and III regions are identical to those of isolated δ -crystallin solution at pH 7.0 (latter result). The strong line at 940 cm^{-1} due to the C-C stretching vibration provides another good indication of the high level of α -helix. It was shown that this frequency is different for α -helix (945 cm^{-1}) and β -sheet (1002 cm^{-1}) in the case of poly-L-lysine (Yu, Lippert, and Peticolas, 1973).

The major Raman lines of the spectrum of the intact pigeon lens at 482, 864, 942, 1087, 1129, 1342, 1387, and 1461 cm^{-1} are due to glycogen component (Figure 11). The protein signals appear at 1654 cm^{-1} for amide I vibrational mode and at 1006 cm^{-1} due to phenylalanine.

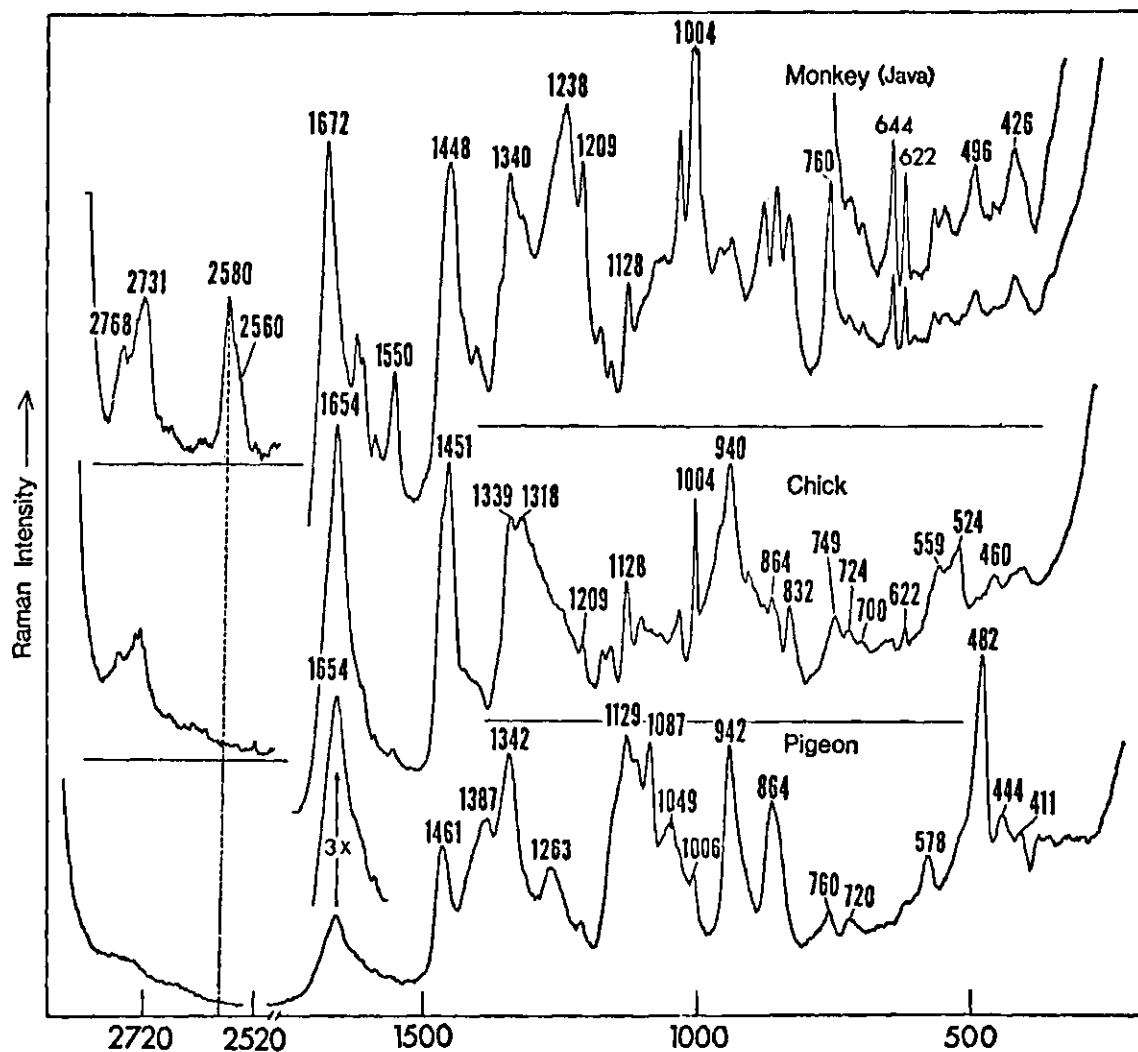


Figure 10. Comparisons of the Raman Spectra of Monkey (~ 3 years old), Chick (~ 10 days old), and Pigeon (~ 8 weeks old). (The Raman signals are obtained from the nucleus of the lens.)

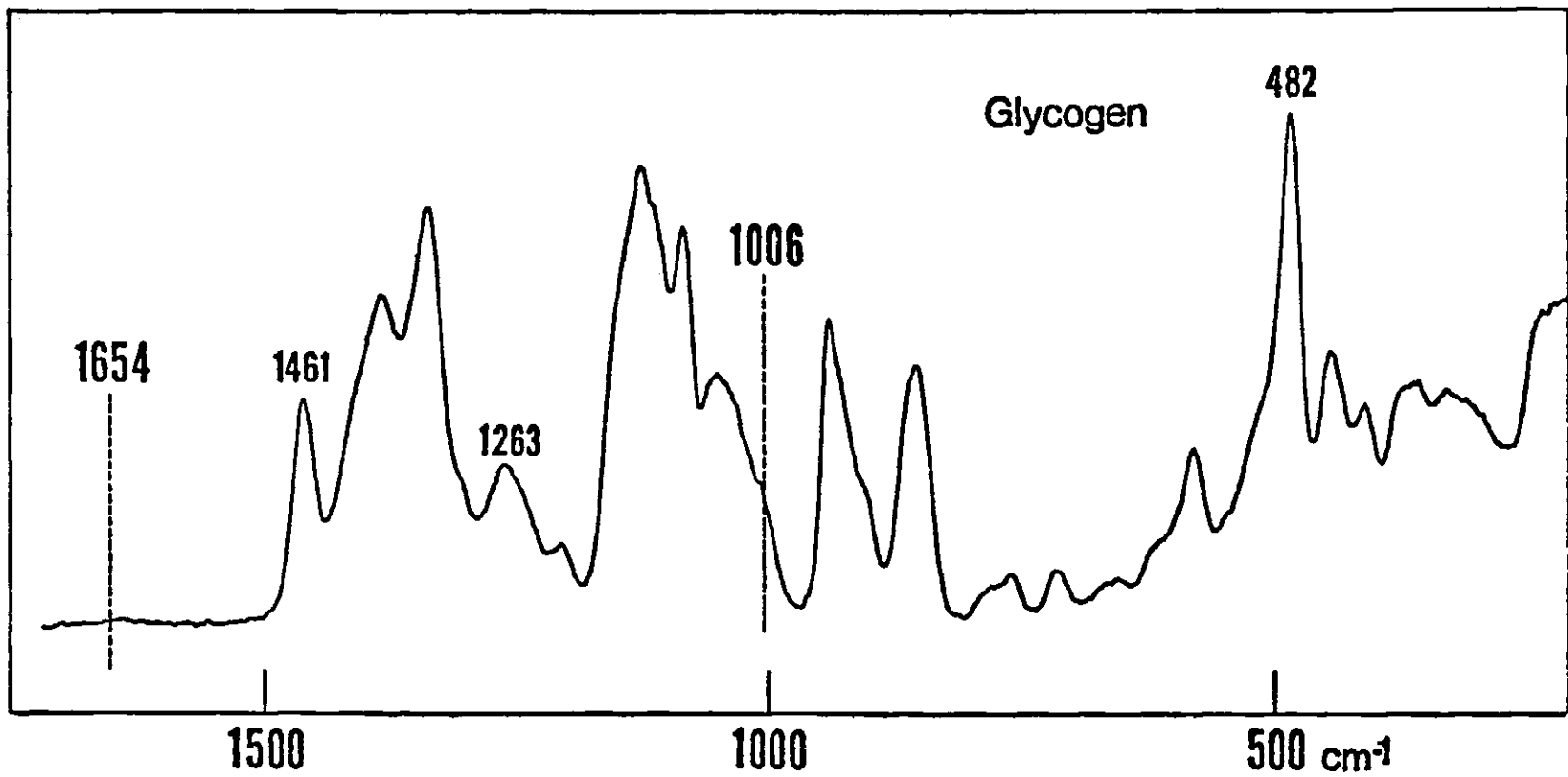


Figure 11. Raman Spectrum of Glycogen (solid, liver glycogen from Pfanstiehl Laboratory)

The medium peak at 1263 cm^{-1} is also due to glycogen and should not be confused with the amide III vibrational mode. The spectral features displayed in the amide I and amide III regions indicate that the conformation of the proteins in the presence of high concentration of glycogen in the central portion (nucleus) of a pigeon lens also exists in a predominantly α -helical form. Schachar and Solin (1975) have suggested that the similarity between the hexagonal cross section of lens fibers and hexagonal arrangement of atoms in antiparallel β -pleated structure are causal. However, the result that bird lens protein is chiefly α -helical appears to contradict the suggestion of Schachar and Solin, because the cross section of avian lens fibers is also hexagonal (Hockwin, 1973).

The Raman signal due to thio groups appears near 2582 cm^{-1} . It is quite strong in monkey lens, but completely absent in the spectra of chick and pigeon lenses. Since the thiol level in α -crystallin (~ one per 20,000 daltons) is detectable in the Raman effect (Yu and East, 1975), the protein SH in δ -crystallin must exist in only trace amounts, consistent with the reported analysis (Waley, 1969).

IV. Heterogeneous Nature of Chicken Lens

Spectra from the nucleus, intermediate zone and cortex of an old hen lens (~ 10 years) are shown in Figure 12. These Raman spectra show that the proteins in the nucleus of such a lens are different from the proteins in the cortex in both amino acid composition and conformation. All of the Raman lines from each region of the chicken lens can be assigned to protein vibrations (Lord and Yu, 1970a,b). The C-N stretching mode of the protein backbone at 1128 cm^{-1} is used as an internal reference

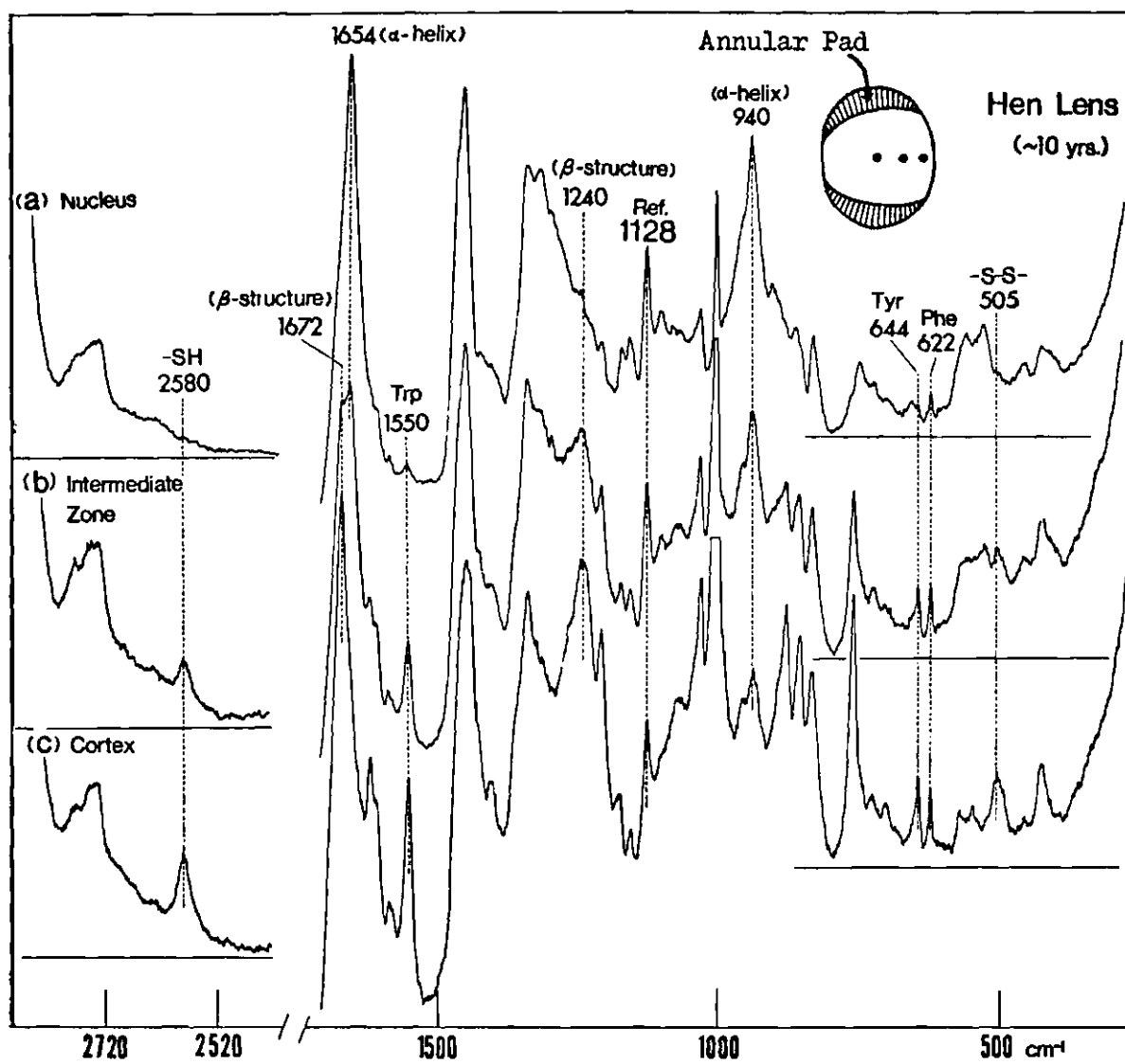


Figure 12. Raman Spectra of Old Hen Lens (~ 10 years old) as a Function of Location

irradiation. The fluorogen is considered a photooxidation product of tryptophan and may play a role in the lens aging process (Lerman, 1972; Lerman, *et al.*, 1976; Augusteyn, 1975; Pirie, 1972; Zigman, *et al.*, 1973; Kurzel, *et al.*, 1973), although Spector, *et al.* (1975) have suggested that the fluorescent compound is not closely related to tryptophan, but instead, is a β -carboline (Dillon, *et al.*, 1976).

V. Comparison of δ -Crystallin Conformation in Intact Lens and in Isolated State

Figure 13 shows the chromatogram of the separation of the δ -crystallin of one day old chick lenses from other fractions. The extinction coefficient of δ -crystallin at 280 nm is lower than those of peak 1 and peak 3. Thus the area under peak δ does not reflect the relative percent of δ -crystallin in the chick lens composition.

In Figure 14 the Raman spectra are given of (a) δ -crystallin solution at pH 7.0 and (b) δ -crystallin lyophilized powder. The dotted line indicates the contribution of water to the Raman spectrum of aqueous δ -crystallin solution.

The Raman spectrum of δ -crystallin in solution is almost identical to the spectrum of an intact 10 day old chick lens (Figure 10) or the nucleus of the old hen lens (Figure 12). One difference is due to the water contribution.

Delta-crystallin has the same conformation in lyophilized powder form and in aqueous solution as it does in an intact chick lens. Raman lines at 1652, 1654, 940 and 525 cm^{-1} along with the absence of an amide III line below 1264 cm^{-1} indicate that δ -crystallin exists mainly in the α -helical conformation.

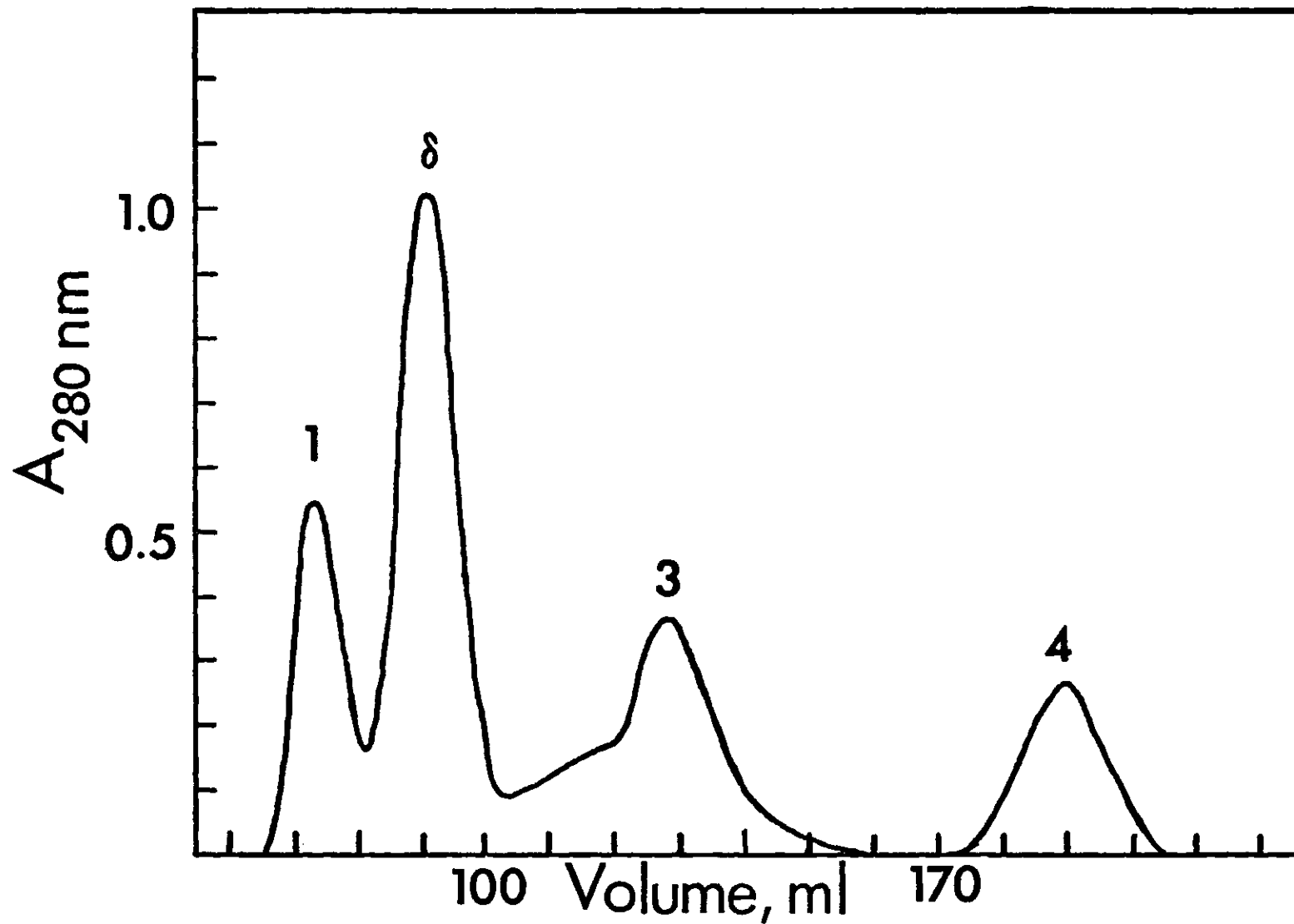


Figure 13. Separation of δ -Crystallin of One Day Old Chick Lens Proteins by Gel Chromatography on Sephadex G-200 Column

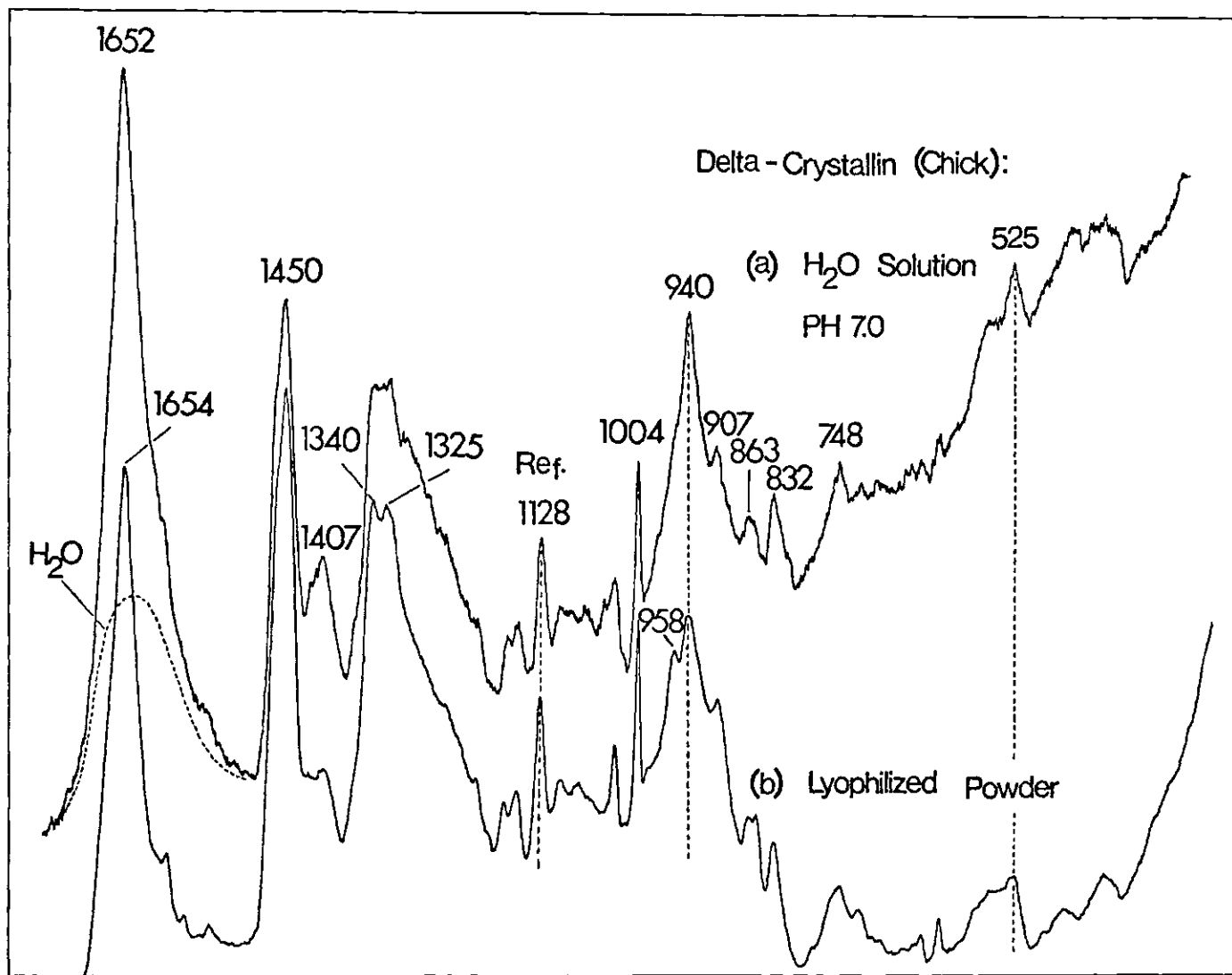


Figure 14. Raman Spectra of Isolated δ -Crystallin in pH 7.0 H₂O Solution and in Lyophilized Powder

The circular dichroism spectra of bovine α -crystallin (Li and Spector, 1974) and rat lens proteins (Kuck, et al., 1976) displayed a single negative band with a minimum at 215 nm characteristic of the β -sheet structure. In Figure 15 a quantitative CD spectrum of δ -crystallin solution at pH 7.0 is presented. In contrast, the spectrum shows two distinct minima at 208 and 222 nm, characteristic of α -helix. According to Greenfield and Fasman (1969) the percent of α -helix in a protein can be estimated by using the following equation:

$$\% \alpha\text{-helix} = \frac{[\theta]_{208 \text{ nm}} + 4,000}{-33,000 + 4,000}$$

The mean residue ellipticity of δ -crystallin at 208 nm is -2.56×10^4 degrees $\text{cm}^2/\text{decimole}$. Therefore, δ -crystallin can be estimated to have a helical content of 74%.

The molecular weight of purified native δ -crystallin obtained from lens fibers of 13-17 day old chick embryos was determined to be approximately 200,000 daltons by gel filtration and sedimentation centrifugation. The subunit molecular weight of δ -crystallin was found to be between 45,000 and 50,000 daltons when examined in the presence of sodium dodecyl sulfate (Piatigorsky, et al., 1974). Delta-crystallin is completely dissociated by sodium dodecyl sulfate without reduction, indicating that the subunits are not covalently bound by disulfide bonds. Thus, native δ -crystallin appears to consist of four polypeptides of the same size.

The amino acid composition of δ -crystallin is known (Waley, 1969; Piatigorsky, et al., 1974): Glu 14.7, Leu 13.3, Ser 8.4, Ala 7.6, Ile 7.4,

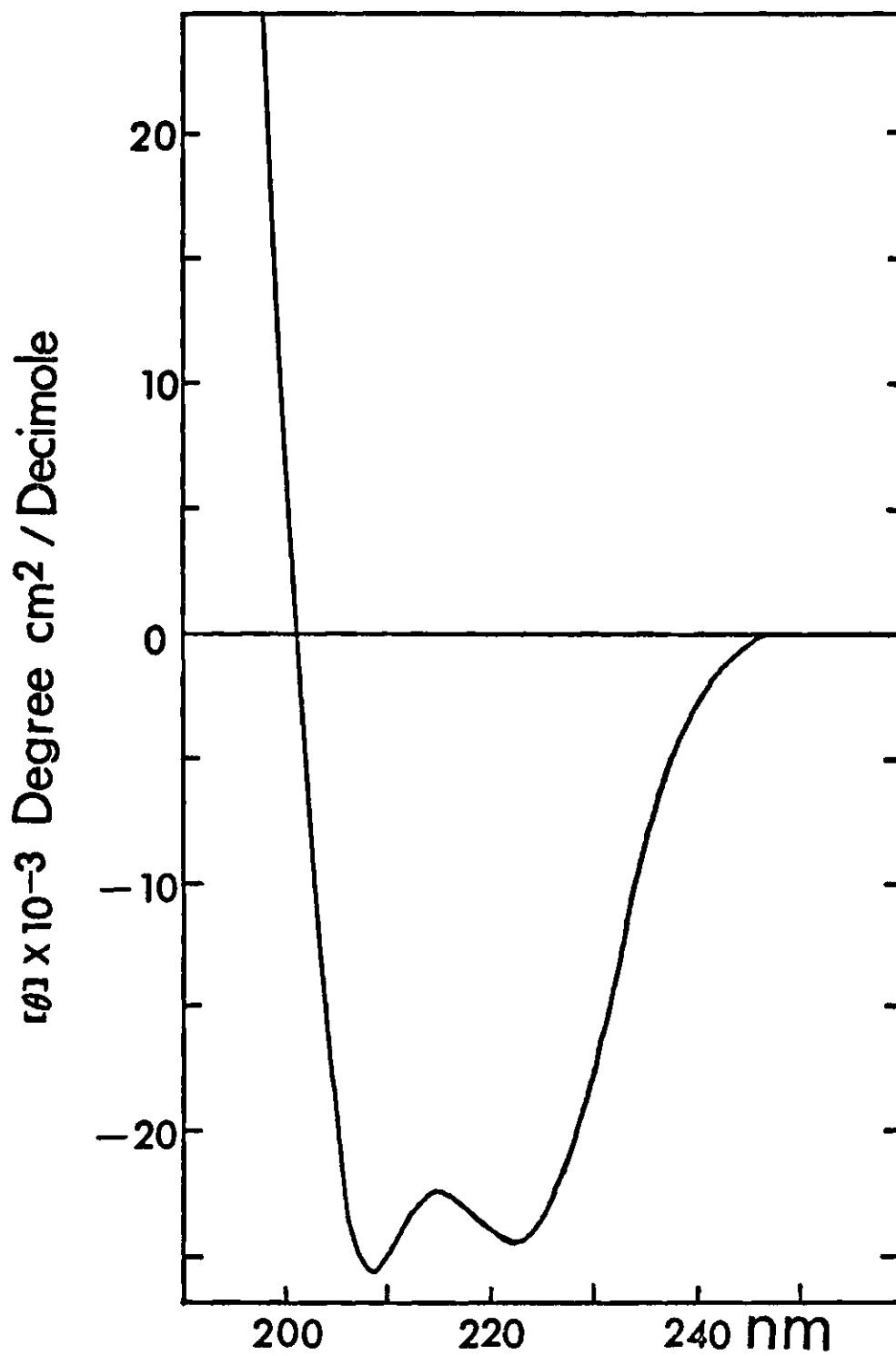


Figure 15. Circular Dichroism Curve of Isolated δ -Crystallin in H_2O (pH 7.0) Solution (2 mg/ml) in the 200-260 nm Region

Asp 7.2, Val 6.7, Lys 6.7, Thr 6.6, Gly 6.0, Arg 4.6, Pro 2.9, Phe 2.3, Met 1.8, His 1.7, Tyr 1.5, $\frac{1}{2}$ Cys trace and Trp 0.7 mole %. The small peak of Raman lines of δ -crystallin at 622 cm^{-1} due to Phe, 642 cm^{-1} due to Tyr and 760 cm^{-1} due to Trp is consistent with the results of amino acid analysis. The absence of Raman lines at 510 and 2580 cm^{-1} is also consistent with trace amounts of the disulfide and sulfhydryl groups.

Since experimental evidence has shown that the conformation of proteins is determined predominantly by their amino acid sequence (Anfinsen, et al., 1961), many attempts have been made to predict protein structure from their primary sequence. Chou and Fasman (1974a,b) have developed a predictive model for the secondary structure (α -helix and β -sheet structure) of globular proteins utilizing the α -helix and β -sheet conformational parameters, P_{α} and P_{β} , of the 20 amino acids. Although detailed prediction of the secondary structure of δ -crystallin must await the determination of amino acid sequence, the high α -helix content in δ -crystallin is supported by the facts that δ -crystallin contains unusually high percentages of Glu and Leu which have high helix-forming potential and that the calculated average helix-forming potential is indeed high, $\langle P_{\alpha} \rangle = 1.10 > 1.03$ which is the value required for helix formation (Chou and Fasman, 1974a,b).

Cold cataracts are observed in young mammalian lenses which contain a large percentage of γ -crystallin, but cold cataracts are not observed in chick lenses where γ -crystallin has been largely replaced by δ -crystallin. It is of interest to point out that γ -crystallin contain a segment of structural instability (residues 108-120) which has nearly equal potential for β -structure and α -helix according to the method of

Chou and Fasman. The reversible cold cataract phenomenon in young mammalian lenses may be caused by the conformational change involving this segment. It is beyond present Raman techniques to establish a change in conformation which may involve only 8% of the γ -crystallin residues. In fact the Raman spectra of lyophilized normal and cold cataract rat lenses are identical.

VI. Effect of Heat Denaturation on the Conformation of δ -Crystallin

The Raman spectrum of heat denatured δ -crystallin (Figure 16) has the same β -pleated sheet structure features as the Raman spectrum of heat denatured one-day old chick lens nucleus. (Kuck, et al., 1976). The 525 and 940 cm^{-1} lines, characteristic of α -helix, are each much weaker in the heat denatured δ -crystallin spectrum. The amide III line at 1240 cm^{-1} is strong and the amide I line is at 1672 cm^{-1} in the spectrum of heat denatured δ -crystallin. Therefore, it is concluded that δ -crystallin is changed from a protein with largely α -helical structure to a protein with largely β -pleated sheet structure by heat denaturation.

VII. Distribution of Glycogen and Proteins in Pigeon Lens

The Raman spectra obtained from the different zones of an adult pigeon lens (~ 8 weeks old) are compared in Figure 17. The amide I lines at 1656 and 1667 cm^{-1} indicate the presence of both α -helical δ -crystallin and β -pleated crystallins (α - and/or β -crystallin) in the cortical and the intermediate regions of the pigeon lens while the 1656 cm^{-1} line indicates that the only protein in the nucleus is δ -crystallin.

The Raman light collected from the annular pad of an adult pigeon (Figure 18) shows similarities with that of hen's cortex (Figure 12), but differences from the cortex of a pigeon lens (Figure 17). This Raman

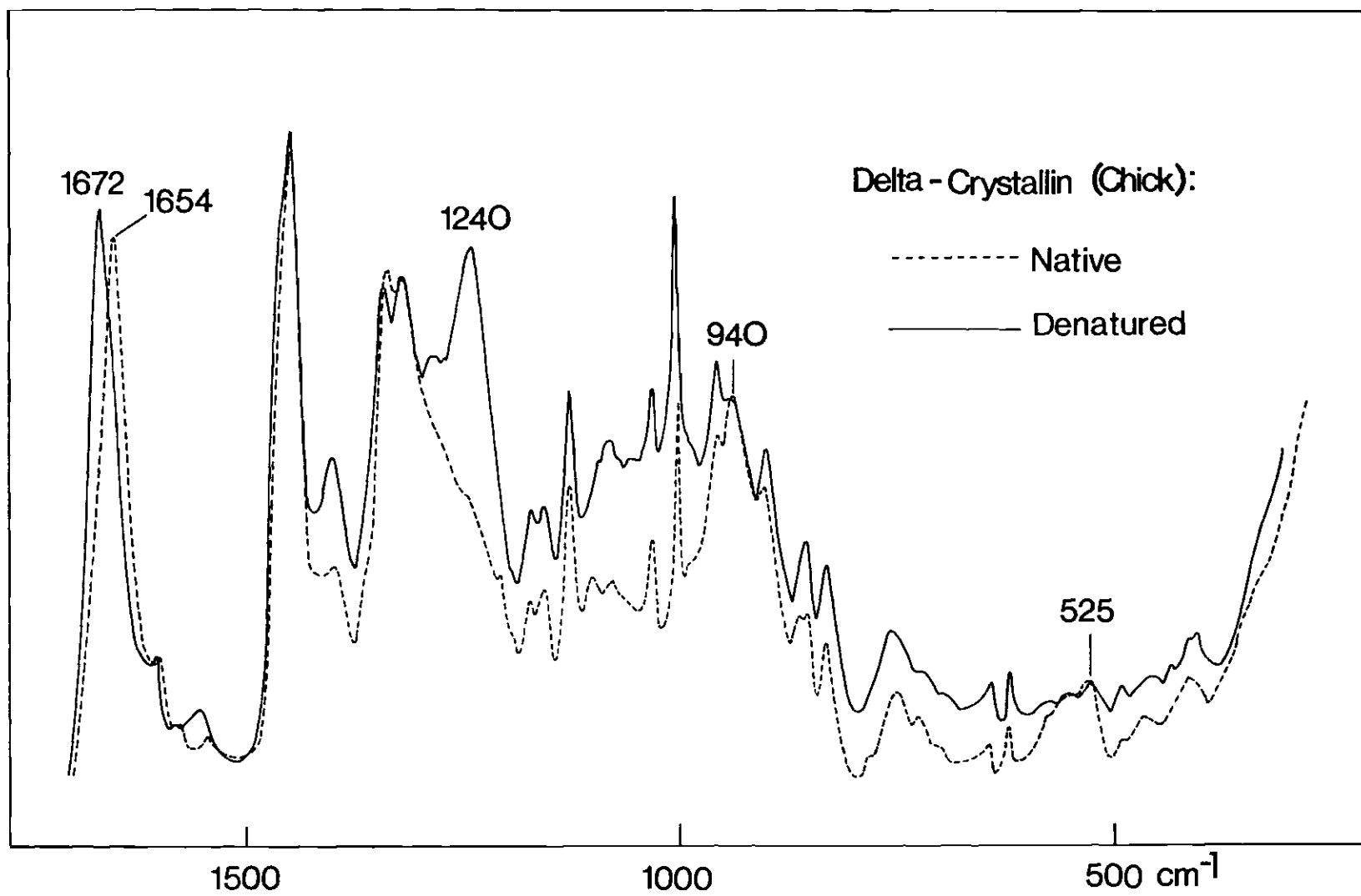


Figure 16. Raman Spectra of Native and Heat-denatured δ -Crystallin

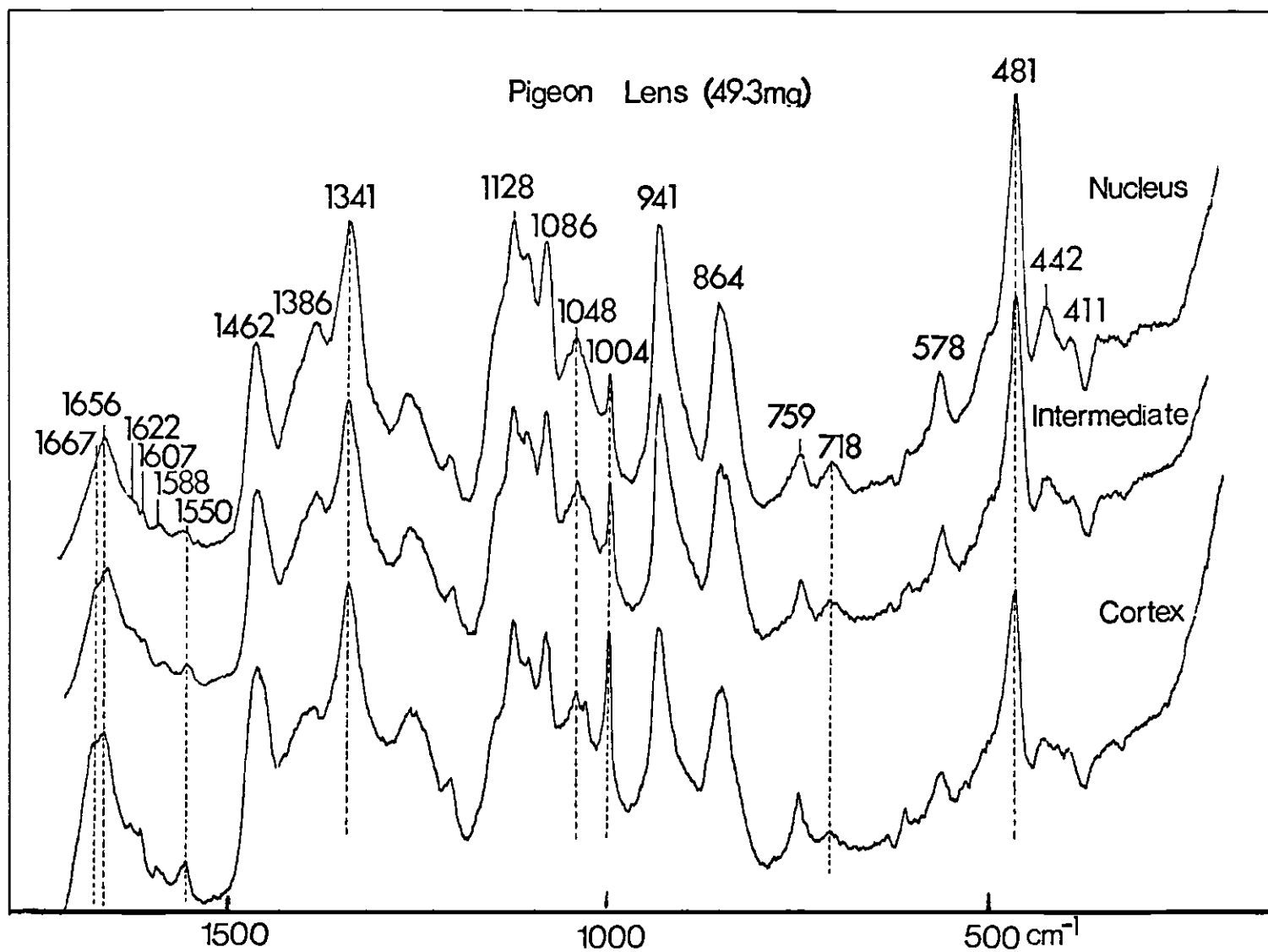


Figure 17. Raman Spectra of Adult Pigeon Lens as a Function of Location

spectrum (Figure 18) indicates that the proteins synthesized at this stage (~ 8 weeks old) have primarily a β -pleated sheet structure.

The presence of glycogen in lenses has been studied mostly by histochemical methods, but quantitative estimation is often difficult. Raman spectroscopy is well suited for the in situ estimation of this polymeric carbohydrate because the Raman signals due to glycogen are strong and can be readily measured. The best indicator for the presence of glycogen is the Raman line at 481 cm^{-1} where protein vibrations do not normally interfere.

The Raman spectrum of an adult pigeon lens annular pad (Figure 18) indicates that the annular pad contains no glycogen. It is of interest to note that young pigeon (2 days old) annular pad does not contain detectable glycogen either. Thus, it appears that glycogen is not synthesized in the annular pad in the period 2 days to 3 years (the oldest pigeon available to our laboratory). From the spectral features in Figure 17, it is concluded that glycogen is present throughout the adult pigeon lens (annular pad excluded) with the highest concentration in the nucleus. The glycogen/protein ratio is about 2:1 in the nucleus (methods) and is about five times greater in the nucleus than in the anterior cortex.

VIII. Direct Evidence for the Existence of α -Helical δ -Crystallin in Reptilian Lenses

Reptiles share with birds the distinction of possessing the unique δ -crystallin (Clayton, 1974). To indicate the presence of α -helical δ -crystallin in certain reptilian lenses, Raman spectra of young lizard and snake lenses are obtained (Figure 19). Because of the small sizes (~ 2 mg) of these lenses the distinction between nucleus and cortex is somewhat

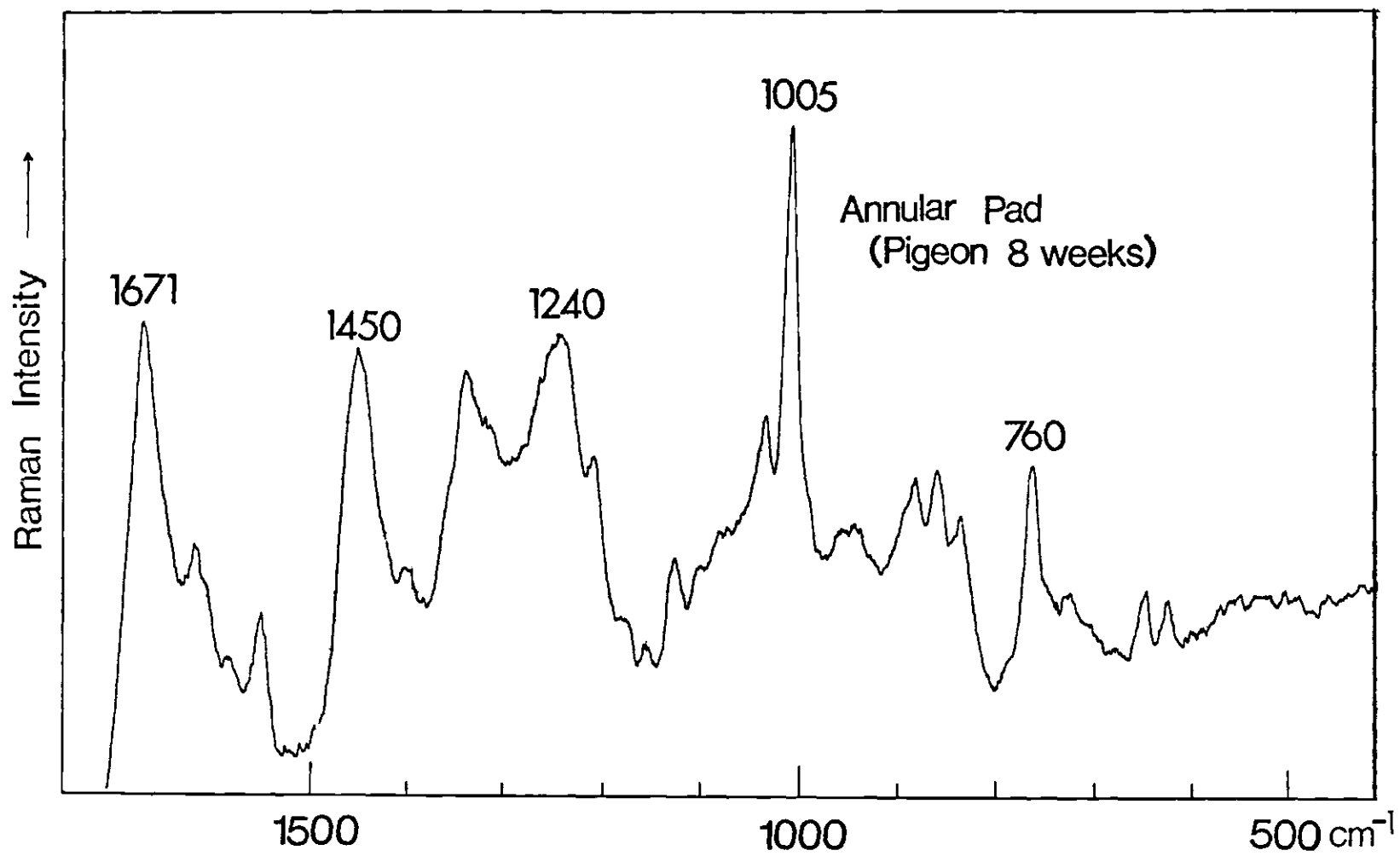


Figure 18. Raman Spectrum of the Annular Pad of an Adult Pigeon

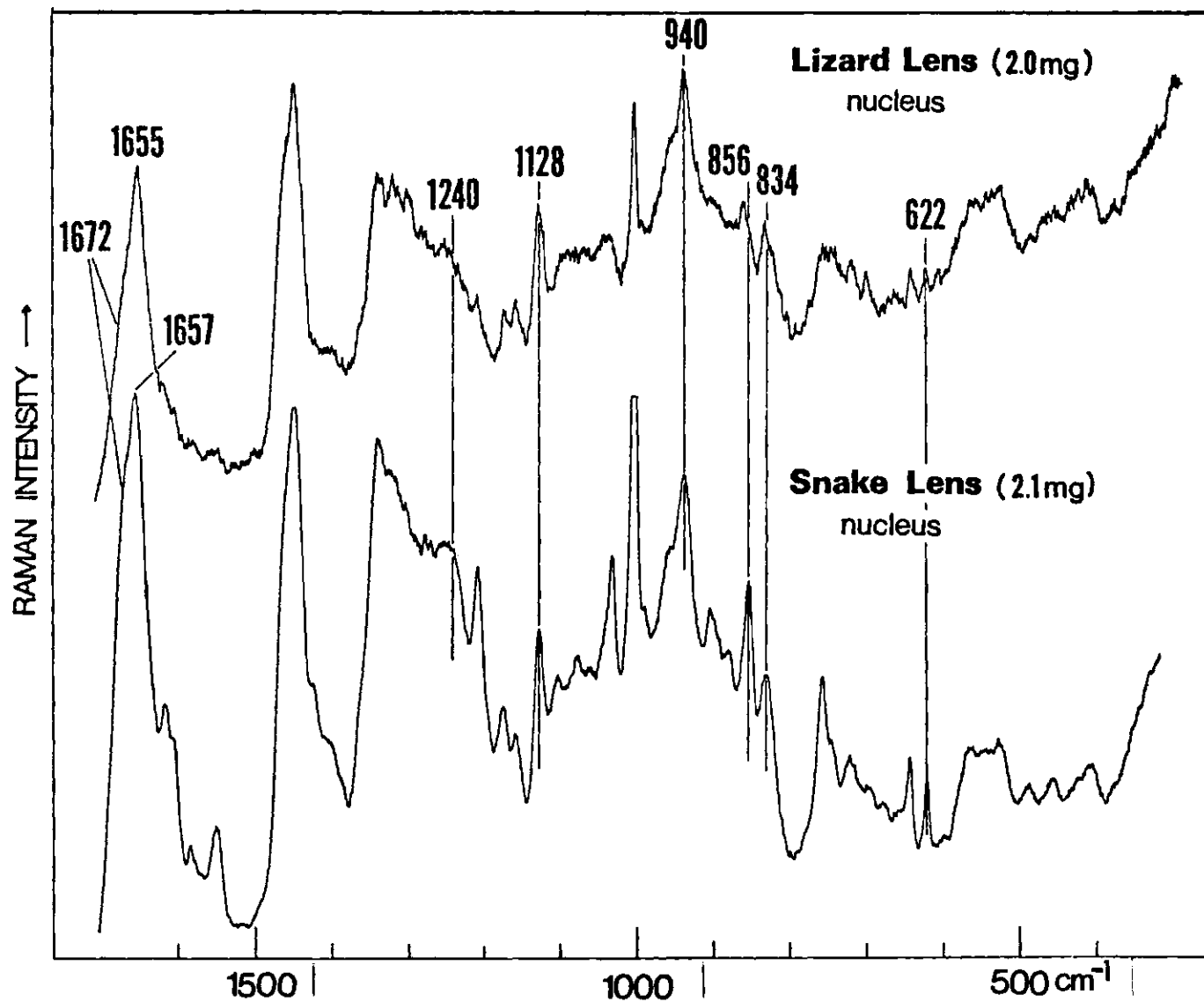


Figure 19. Raman Spectra of Intact Lizard and Snake Lenses

difficult. A small fraction of the Raman light from the cortex may have been mixed with that of the nucleus. The Raman lines at 1655, 1657, 940, and 525 cm^{-1} provide the evidence that δ -crystallin in the lenses of lizard and snake also exists in α -helical conformation. The Raman spectrum of lizard lens is indeed very similar to that of isolated δ -crystallin (Figure 14) or the nucleus of chicken lens (Figure 12). In the snake lens spectrum, the amide I and III lines at 1672 and 1240 cm^{-1} indicate the presence of α - and β -crystallin like proteins in β -pleated structure.

Old snapping turtle and caiman lenses, also investigated by Raman spectroscopy (Figure 20), show no evidence (snapping turtle lens) or only trace evidence (caiman lens) of α -helical δ -crystallin. The spectral features display remarkable similarities with those of human and monkey lenses (Figures 7 and 10).

IX. Polarized Raman Studies of Chick Lens

Like infrared dichroism, the polarized Raman scattering method may be employed to determine whether polypeptide chains are uniquely oriented and, if so, in what direction.

Figure 21 shows three scattering geometries. A combination of these scattering geometries permits one to determine the following polarization components: (Z,Z), (X,X), (X,Z), (Z,X), (Y,X), (X,Y), (Y,Z), and (Z,Y) where the first and second letters indicate the polarization direction of the incident and scattered light. The components (Z,Z) and (X,X) are of particular interest because they should be identical for randomly oriented molecules, but quite different in a well-oriented system. This has been demonstrated in the amide I region of the Raman spectra of oriented α -helical poly- γ -benzyl-L-glutamate (Wilser and Fitchen, 1975).

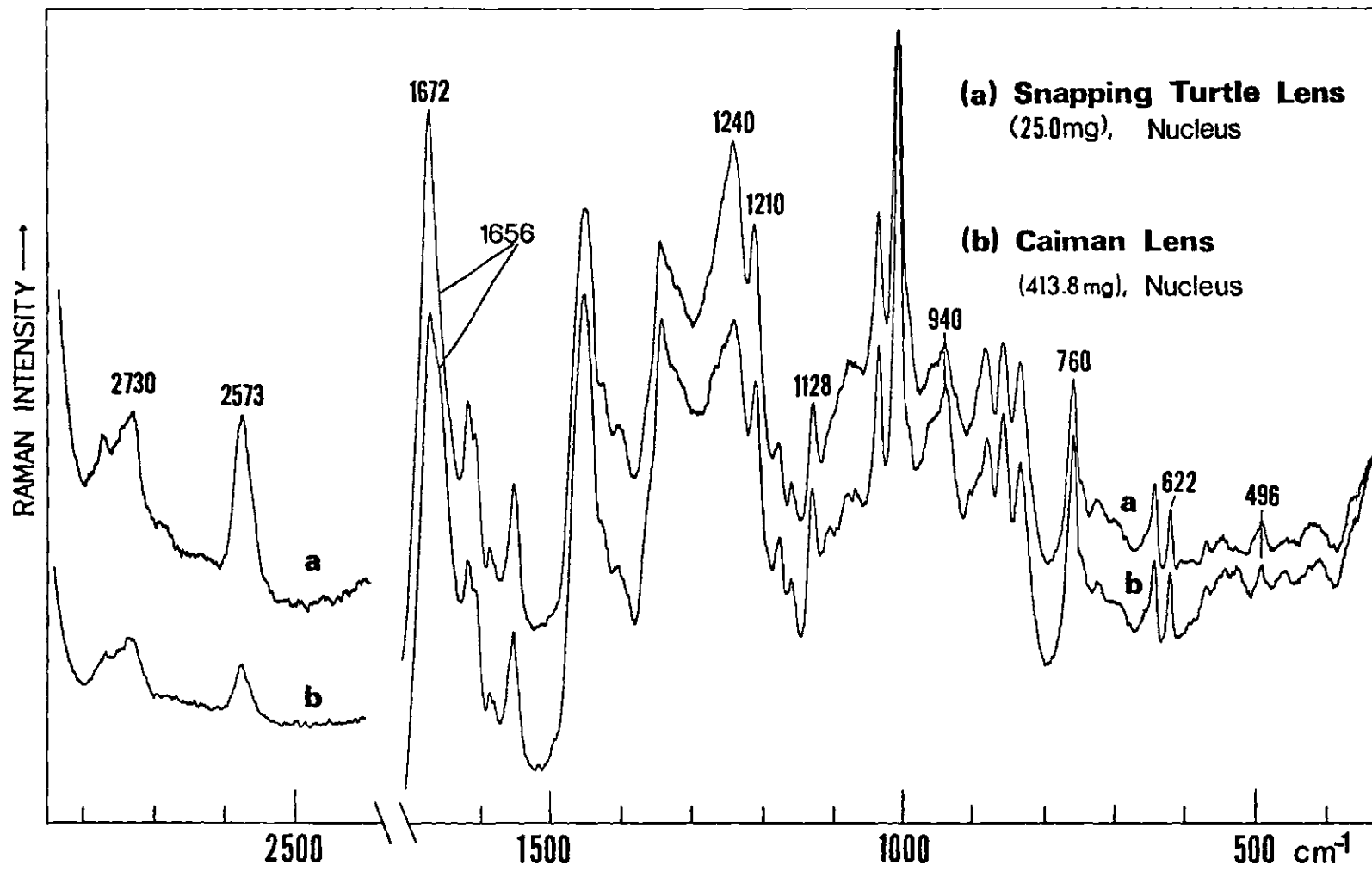


Figure 20. Raman Spectra of Intact Snapping Turtle and Caiman Lenses

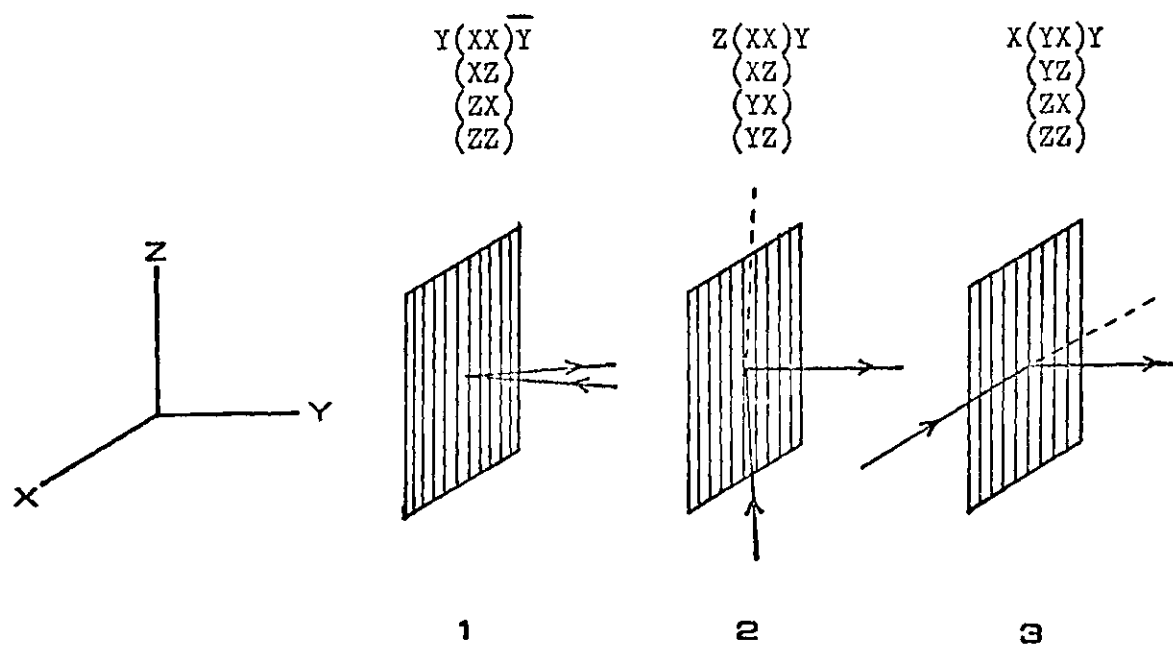


Figure 21. Three Scattering Geometries for Oriented Polypeptides

The intensity ratio, $I(Z,Z)/I(X,X)$, for amide I was 3.7 ± 0.5 . It should be noted that in the (Z,Z) measurements the polarization direction of the incident and scattered light is nearly parallel to the C=O and N-H bonds. Since the induced polarizability change along a bond may be quite different from that perpendicular to the bond, they should be relatively different Raman scattering intensities (Hsu, et al., in press).

It is of interest to apply the polarized Raman scattering method to examine further whether δ -crystallin is uniquely oriented in the intact chick lens since δ -crystallin of the chick lens exists mainly in the α -helical conformation (Figure 10).

Figure 22 shows the Raman spectra (1400 - 1700 cm^{-1}) of an intact chick (8 days old) lens in parallel polarization. The CH_2 deformation vibration at 1450 cm^{-1} is used as an internal reference for the amide I (1652 cm^{-1}) mode. The spectra (a)-(g) are taken by shining the laser beam through the center of the chick lens with the polarization of the laser beam perpendicular to the optical axis of the chick lens. The scattered light is collected at 90° from the very center of the lens. The lens is rotated about 30° for two sequential spectra and a total of about 180° is rotated from (a) to (g) (Figure 23). The spectra (h) and (i) are taken by shining the laser beam through the point about half way between the center and the edge. All other conditions are the same as spectra (a) and (b). The spectrum (j) is taken by shining the laser beam through the center of the chick lens with the polarization of the laser beam parallel to the optical axis of the chick lens. The scattered light is also collected at 90° from the center of the lens.

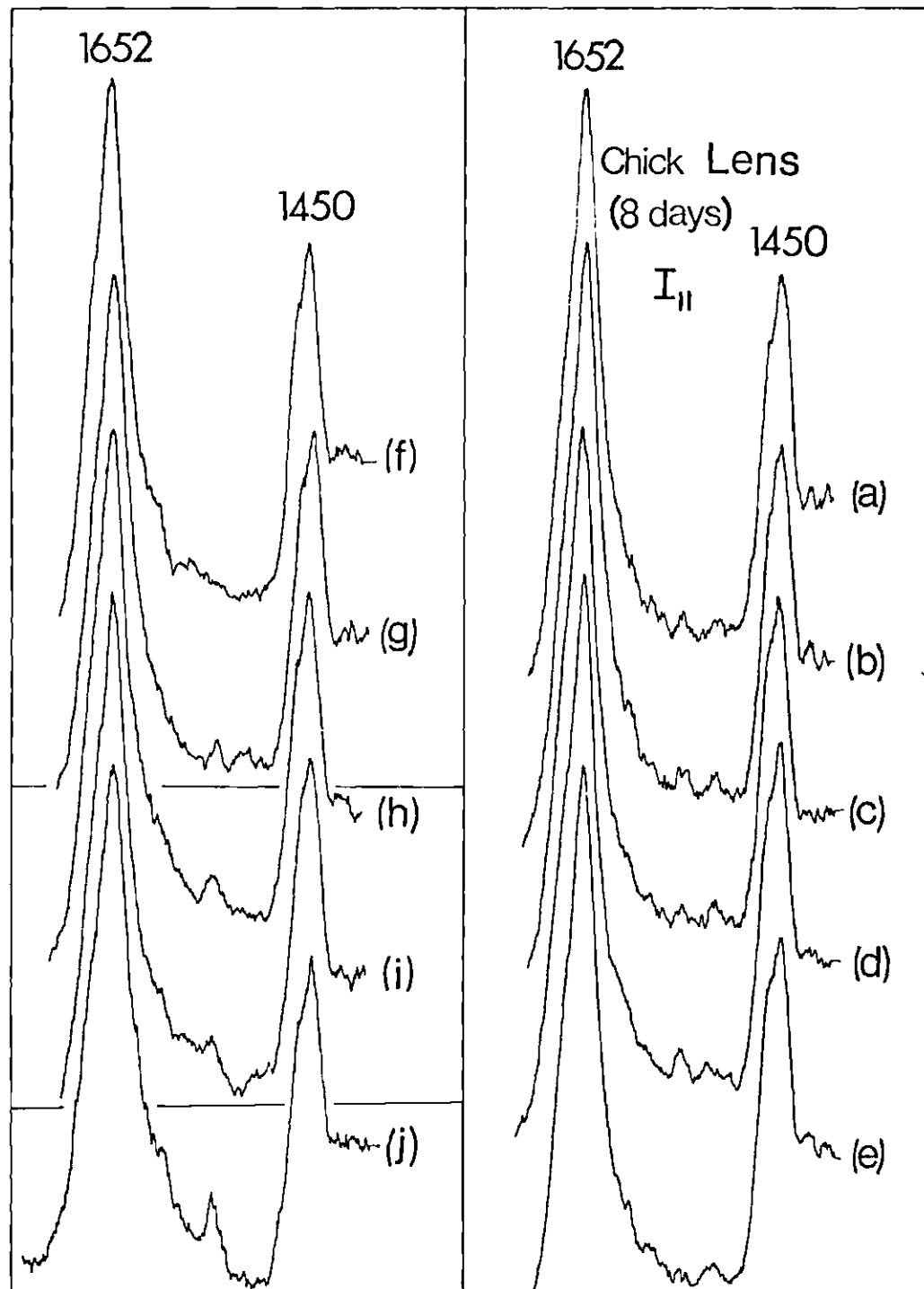


Figure 22. Raman Spectra of Intact Chick Lens in the Amide I Region
(The spectra are taken from different orientations.)

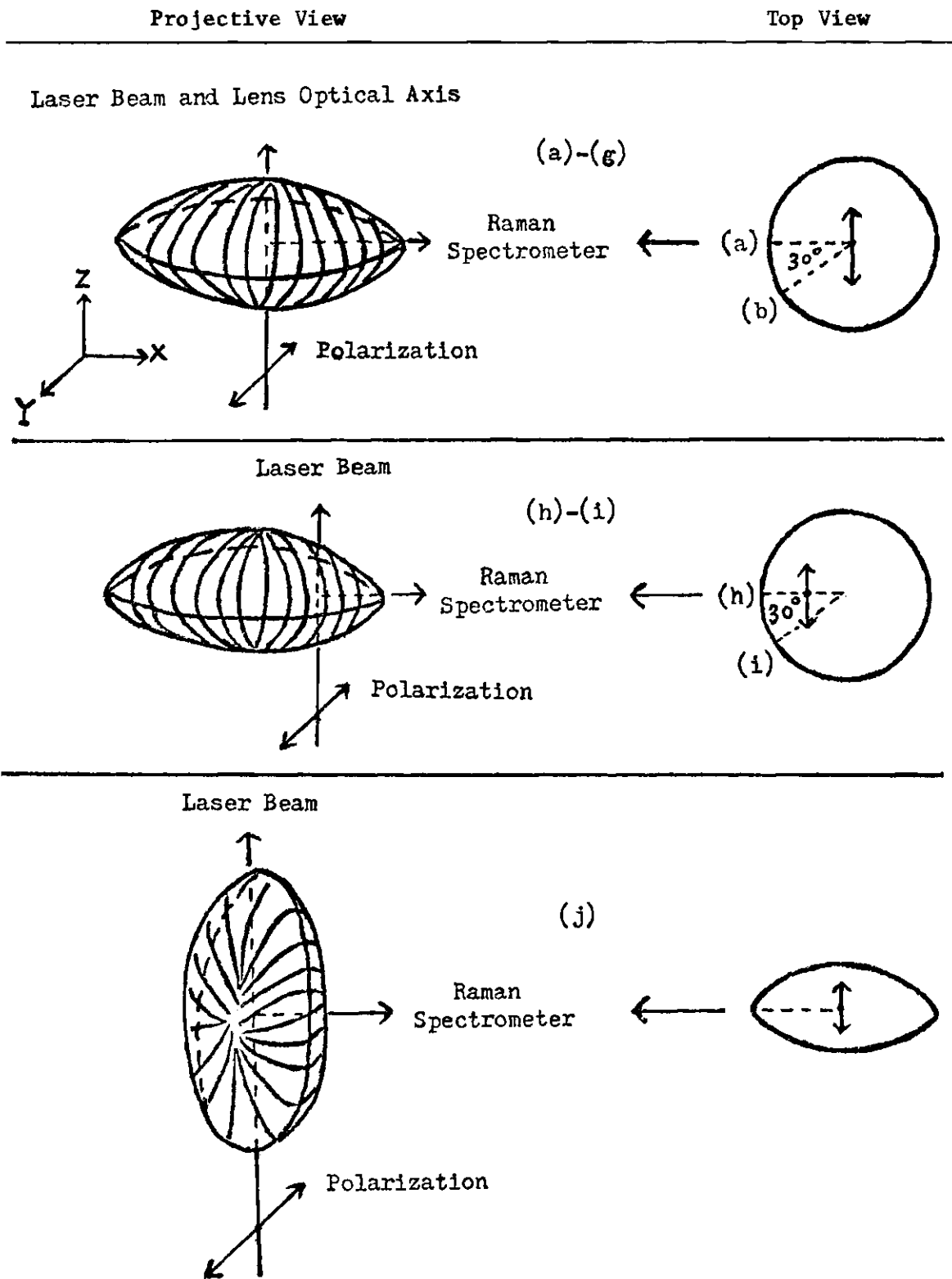


Figure 23. Schematic Arrangement of Polarized Raman Studies of Chick Lens

In Figure 22 all of the spectra are virtually identical. Therefore it can be concluded that the δ -crystallin in the chick lens is not oriented parallel or perpendicular to the optical axis of the chick lens. Although this result cannot exclude the other possible orientations, it is also quite possible that δ -crystallin is a globular protein.

X. Effects of Aging and UV Irradiation on Sulfhydryl Groups of Intact Rat and Mouse Lenses

There are many changes in composition and metabolism in the aging lens (Kuck, 1970; Waley, 1969). Among these alterations with age, usually the following three parameters are more significant: (1) increase of water insoluble albuminoid (Kuck, 1970); (2) increase of pigment (Lerman, et al., 1976); and (3) decrease of sulfhydryl groups (Dische, et al., 1956). Laser Raman scattering is a noninvasive, sensitive, and selective probe of lens structures at the molecular level. In contrast to most biochemical methods requiring classical isolation procedures, it is employed to extract structural and conformational information directly from a living intact lens and thus avoids possible aerobic oxidation of the sulfhydryl groups. The sulfhydryl groups which play a role in the function of some lenses can be readily detected and measured quantitatively in the Raman effect.

The aging effects on the oxidation of sulfhydryl groups of intact rat lens are shown in Figure 24 (nucleus) and Figure 25 (cortex). The drop of S-H peak intensity at 2580 cm^{-1} with a concomitant increase of the S-S peak at 508 cm^{-1} indicates that the S-S bonds do form in vivo in the process of aging. Since only γ -crystallin contains an appreciable number of free sulfhydryl groups (Yu and East, 1975), the decrease in

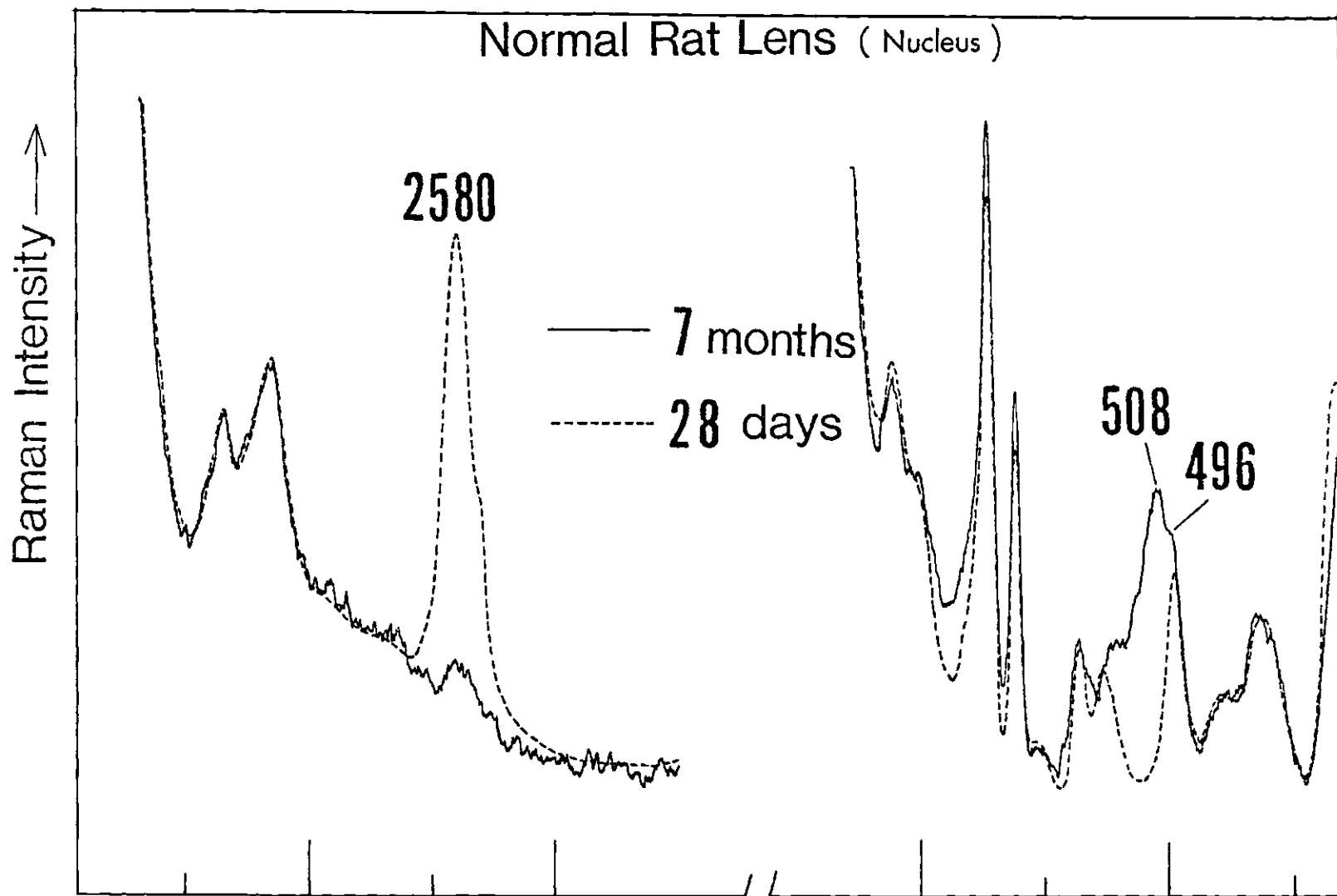


Figure 24. Raman Spectra of Intact Rat Lens (nucleus) as a Function of Age in the S-H and S-S Vibrational Regions

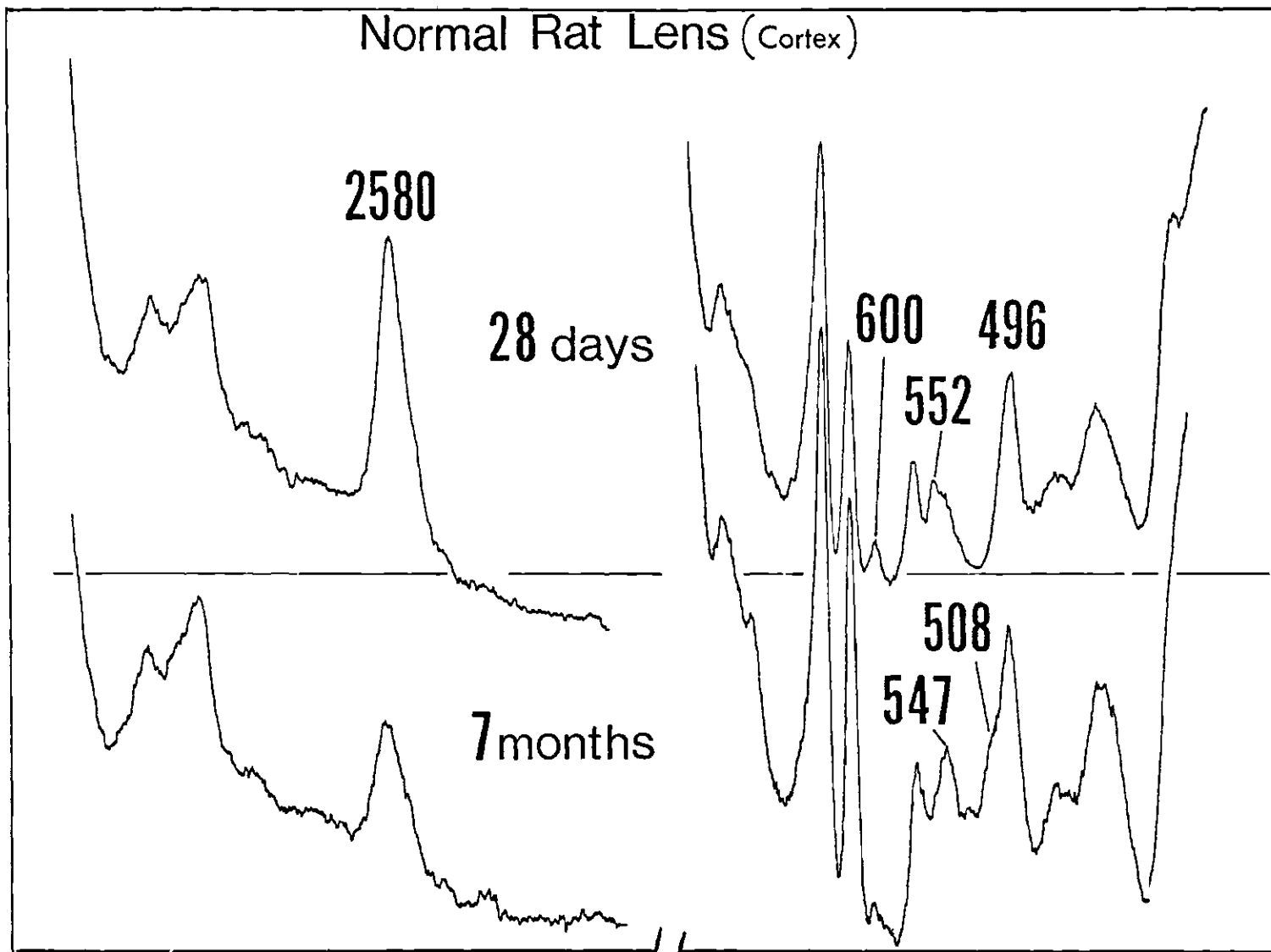


Figure 25. Raman Spectra of Intact Rat Lens (cortex) as a Function of Age in the S-H and S-S Vibrational Regions

sulfhydryl groups may also indicate the decrease in γ -crystallin in the aging rat lens. Lerman and Zigman (1967) showed that over the period of 1-11 months of age, the amount of γ -crystallin decreased from 60% to about 12% of total soluble proteins.

The lens can be affected only by radiation of wavelengths that are absorbed. The adult human lens cannot be affected by radiation of a wavelength greater than 2000 nm or below 293 nm since these rays are absorbed by the cornea. Within this range, the lens absorbs much of the radiation between 1100 and 1400 nm (near infrared) and between 320 and 400 nm (near ultraviolet). Wavelengths between 293 and 400 nm are transmitted by the cornea and effectively absorbed by the lens, so this is the range of ultraviolet potentially most damaging to the lens. Figure 26 shows the effects of long-wave UV irradiation on the sulfhydryl groups of the mouse lens. The SH contents were measured from the 2580 cm^{-1} peak area. The peak area of CH deformation at 2730 cm^{-1} was used as an internal reference. The SH contents in the cortex of one month old mouse lens were assumed to be 100%. In the cortex of one month old control mouse lens nearly all protein-S is present in S-H form, whereas at 11 months old, only about 40% is present as S-H form. Over the same interval the value for sulfhydryl groups in the nucleus of control mouse lens falls from 80% to nearly zero. Figure 26 also indicates that the effect of long-wave UV irradiation in lowering the S-H contents reaches the maximum after nine months of irradiation in the cortex of mouse lens. In the nucleus this effect is smaller than that of cortex because the sulfhydryl groups in the nucleus of mouse lens are usually low.

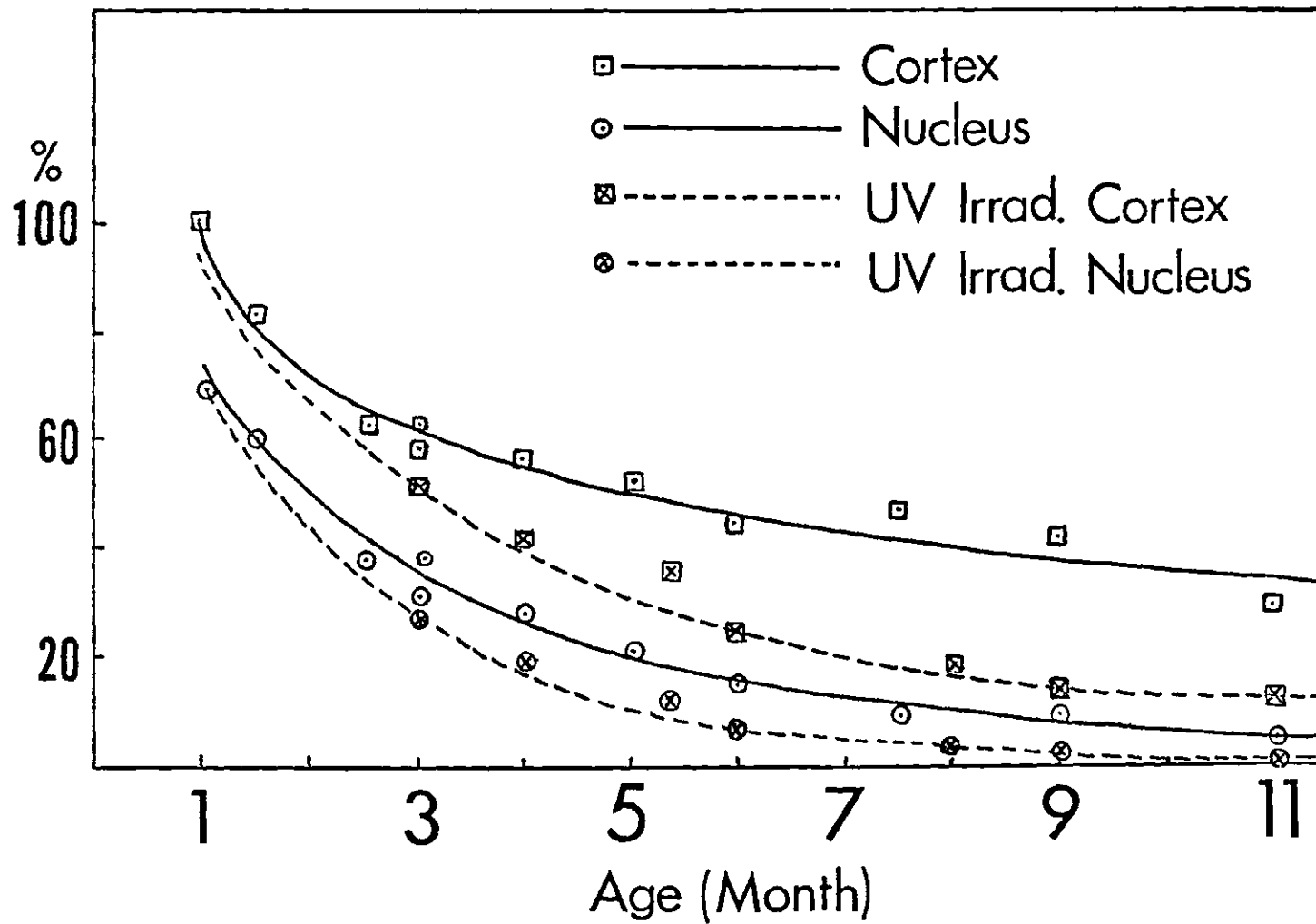


Figure 26. SH Contents of Both Normal and UV Irradiated Mouse Lenses as a Function of Age: Nucleus and Cortex

CHAPTER III

RESONANCE RAMAN SPECTROSCOPIC STUDIES OF METALLOPORPHYRINS
AND HEMEPROTEINS1. Introduction

From the previous chapter, we have seen that non-resonance laser Raman spectroscopy is a powerful technique to study colorless biological materials. Moreover, if a biological molecule absorbs light in the electronic absorption region, Raman spectroscopy can provide new structural information via the resonance Raman effect. Tuning the laser exciting frequency into the electronic absorption region can produce selective enhancement of certain Raman bands which correspond to the vibrational modes of the chromophore. Therefore the resonance effect provides a means where the vibrational modes of biological chromophores can be distinguished from the vibrational modes of their biological matrix. Resonance enhancement factors can be quite large so that the chromophore vibrations completely dominate the spectrum and can be detected at very high dilution. Since biological chromophores are often loci for biological function, Raman spectroscopy also provides a powerful technique to study the structure-function relationships in colored biological molecules.

The utility of this technique as a structural probe of the chromophore in hemeproteins has stimulated several studies on protein-free porphyrins and metalloporphyrins (Spiro and Streckas, 1974; Felton, et al.,

1974; Verma and Bernstein, 1974; Verma, et al., 1974).

Metalloporphyrins are important both as a class of compounds of chemical interest and for their important role in certain biological processes; moreover, it is essential to understand the resonance Raman spectra of the basic protein-free porphyrins and metalloporphyrins before attempting to investigate the effects of protein and other axial ligands on the vibrational modes of the chromophore in heme proteins.

2. Materials and Methods

Nickel(II) Etioporphyrin I

Ni(II)Etio was prepared by heating pure $H_2Etio-h_4$ (supplied by Dr. R. H. Felton) with nickel acetate in glacial acetic acid under reflux until no trace of free base porphyrin was detectable in the visible absorption spectrum. The nickel complexes were purified by neutral alumina chromatography and recrystallization from CH_2Cl_2 -hexane solution (Falk, 1964).

Nickel(II) Octaethylporphyrin-meso-d₄; Nickel(II) Etioporphyrin I-meso-d₄;

Nickel(II) Mesoporphyrin IX Dimethyl Ester-meso-d₄

Ni(II)OEP-d₄, Ni(II)Etio-d₄, and Ni(II)MesodME-d₄ were prepared from H_2OEP-h_4 (supplied by Dr. R. H. Felton), $H_2Etio-h_4$, and $H_2MesodME-h_4$ (Sigma), respectively, by first exchange in $D_2SO_4-D_2O$ (9:1) solution and then metal insertion. After three hours of exchange, the product extracted was subjected to the same metal insertion procedures as those for Ni(II)-Etio-h₄ except using pyridine instead of glacial acetic acid as solvent. After one exchange, a minimum of 92% deuterium incorporation at meso carbons was observed (¹H NMR spectrum).

Protoporphyrin IX Dimethyl Ester-meso-d₄

A standard solution of hexapyridyl magnesium iodide was prepared as follows: a mixture of magnesium (800 mg), iodine (1.5 g), and diethyl ether (30 ml) was heated under reflux, in an atmosphere of nitrogen, until colorless, before being filtered and the filtrate evaporated to dryness. The residual yellow solid was quenched with pyridine (50 ml) and deuteriomethanol (2 ml). In a typical deuteration experiment, 20 ml of this standard solution was added to protoporphyrin IX dimethyl ester (100 mg) (Sigma) in dry pyridine (3 ml) and the mixture was heated under reflux in an atmosphere of nitrogen, during four hours. The product was extracted and washed. The residue was chromatographed on alumina and the CH₂Cl₂ eluates were evaporated; crystallization of the residue from CH₂Cl₂-methanol solution. NMR showed that the meso carbons were deuterated to the extent of 94% (Kenner, *et al.*, 1973).

Nickel(II)Protoporphyrin IX Dimethyl Ester-meso-d₄

Protoporphyrin IX dimethyl ester-meso-d₄ (50 mg) was added to a solution of nickel acetate (50 mg) in CH₃COOD (12 ml) at 80°C under nitrogen. After 12 minutes, the solution exhibited only a two-banded metalloporphyrin visible spectrum; 1,2-dichloroethane (3.5 ml) was added and the mixture was washed with water. The washed, nonaqueous phase was dried over sodium sulfate, concentrated, and added to a column (1 x 40 cm) of alumina wet with 1,2-dichloroethane. Dichloroethane elute fractions were concentrated, heated, and treated with CH₃OD to give crystals which were dried at 100°C under vacuum. NMR showed that the meso carbons were deuterated to the extent of 94% (McLees and Caughey, 1968).

Other Metalloporphyrins

All the other metalloporphyrins used in this work were prepared by Dr. L. D. Spaulding (Spaulding, et al., 1975).

Raman Spectroscopic Methods

The laser Raman system and the sample handling techniques for obtaining the resonance Raman spectra of metalloporphyrins in crystalline, KBr pellets, or solution have been described in Chapter I.

3. Results and Discussion

I. Structure Sensitive Vibrational Bands of Resonance Raman Spectra of Metallooctaethylporphyrins

Figure 27 shows the Raman spectra of both triclinic and tetragonal crystal forms of nickel(II) octaethylporphyrin (Ni(II)OEP) with their CH_2Cl_2 solution spectrum. Both crystal forms have the identical solution spectra. The scattered light is analyzed into components parallel (I_{\parallel}) and perpendicular (I_{\perp}) to the incident polarization. The crystals, especially the tetragonal form, are sensitive to photodecomposition; therefore, reduced laser power was used during the recording of the spectra. From Figure 27, it is indicated that the high frequency lines are structure sensitive. In the Ni(II)OEP crystals with D_{4h} symmetry, the structure sensitive bands are shown at 1660, 1609, 1581, and 1524 cm^{-1} while in D_{2d} crystals these bands are shifted to 1641, 1590, 1573, and 1512 cm^{-1} , respectively. Similar spectral features are shown in Figure 28 for both crystalline and solution spectra of Ni(II)OEP-meso- d_4 which is deuterated at meso carbons. The spectra of tetragonal crystals whether in crystalline form or embedded in a KBr pellet show the same Raman frequencies.

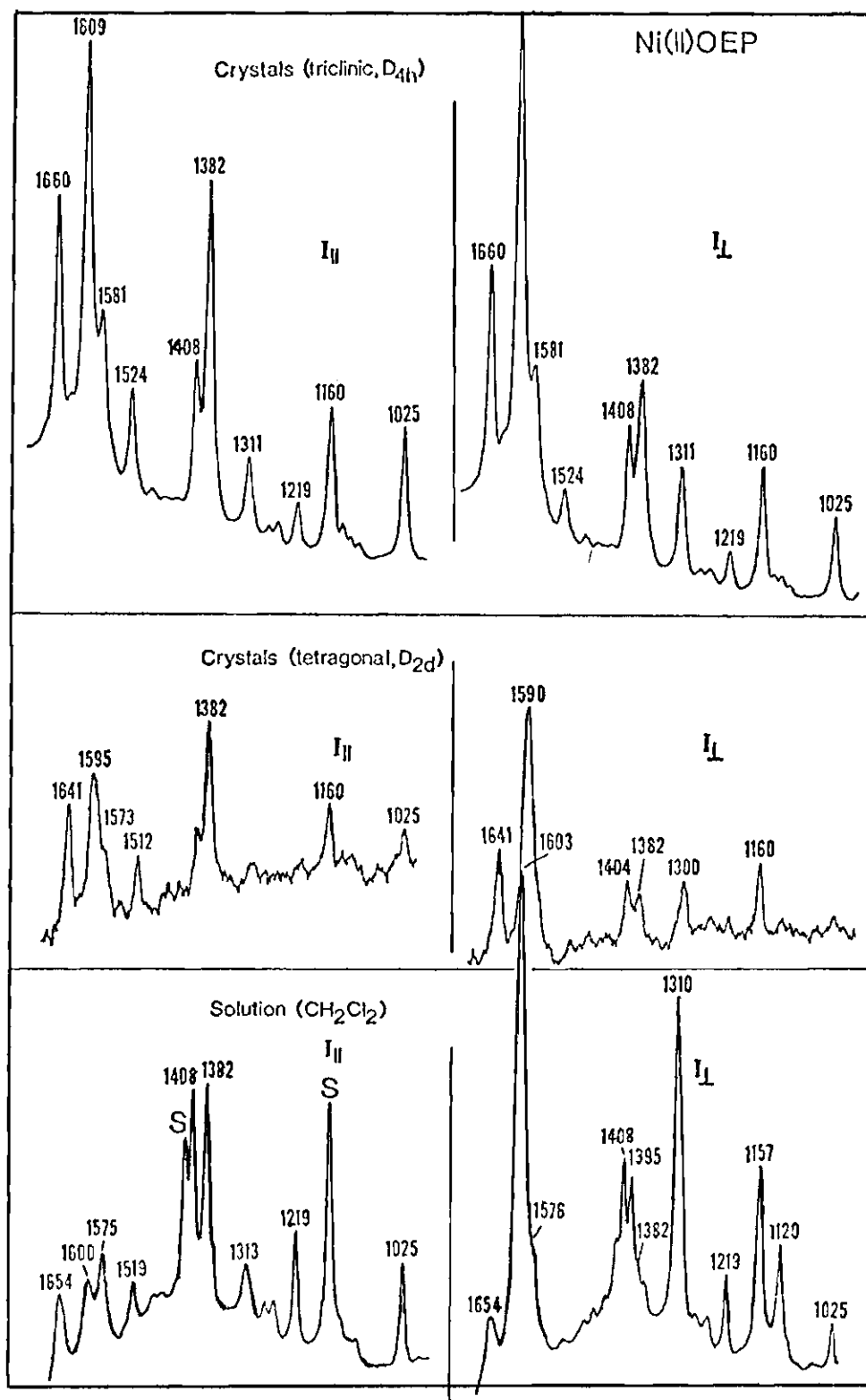


Figure 27. Resonance Raman Spectra of Crystalline and Solution Samples of Ni(II)OEP-meso-h₄

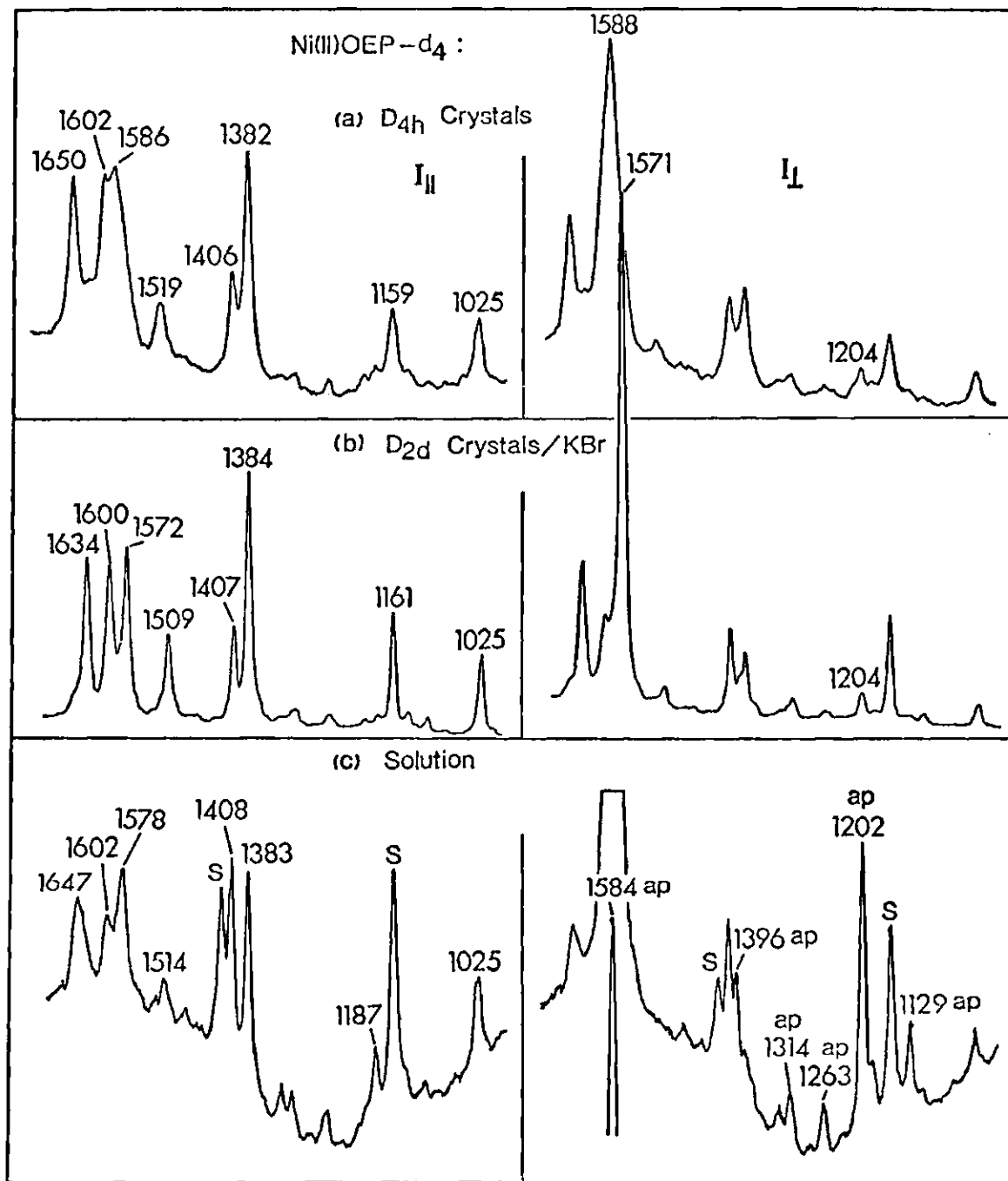


Figure 28. Resonance Raman Spectra of Crystalline and Solution Samples of Ni(II)OEP-meso-d₄

In the Ni(II)OEP-meso-d₄ crystals with D_{4h} symmetry the 1650, 1586, and 1519 cm⁻¹ lines are shifted to 1634, 1572, and 1509 cm⁻¹, respectively, in the D_{2d} symmetry form. There is no structure sensitive band below 1500 cm⁻¹.

Hoard (1973) has assumed that, in the absence of external constraints, the same basic conformation of the core is utilized in the Ni(II)OEP molecules, and the planar conformation (D_{4h}) is preferred in the unconstrained species at experimental temperature. The spectra of the solution and triclinic crystals (D_{4h}) of Ni(II)OEP are similar to each other. The 0-6 cm⁻¹ frequency difference between these two spectra is due to CH₂Cl₂ solvent effect. In tetragonal crystals of Ni(II)OEP, the porphinato core is highly ruffled in exact agreement with S₄ symmetry while closely approximating the higher symmetry of D_{2d}. However, when tetragonal crystals are dissolved in CH₂Cl₂, the solution spectrum is identical with that of triclinic crystals and indicates that the tetragonal crystal molecules relieve the packing constraints and assume a planar conformation. These results are in good agreement with Hoard's assumption.

The vibrational frequencies and the assessment of depolarization ratios, ρ , for Ni(II)OEP-meso-h₄ and Ni(II)OEP-meso-d₄ are tabulated in Table 3. McClain (1971) has shown that the scattering tensor patterns in D_{4h} and D_{2d} molecular symmetries for two-photon processes are identical. Therefore lowering of molecular symmetry from D_{4h} to D_{2d} will not affect the depolarization ratios. The classification of a line as polarized ($\rho < 3/4$), depolarized ($\rho = 3/4$), or anomalously polarized ($\rho > 3/4$) is still valid in D_{2d} symmetry.

Table 3. Resonance Raman Frequencies (cm^{-1}) and Polarizations for NiOEP^a

NiOEP Triclinic (D_{4h})		NiOEP Tetragonal (D_{2d})		NiOEP Solution (CH_2Cl_2)	
H	D	H	D	H	D
1660 (s,dp)	1650 (s,dp)	1641 (s,dp)	1634 (s,dp)	1654 (s,dp)	1647 (s,dp)
	1602 (s)	1595 (s,p)	1600 (s,p)	1600 (s,p)	1602 (s,p)
1609 (s,ap)	1588 (s,ap)	1590 (s,ap)	1571 (s,ap)	1603 (s,ap)	1584 (s,ap)
1581 (m,dp)	1586 (s)	1573 (m,dp)	1572 (s,dp)	1575 (s,dp)	1578 (s,dp)
1524 (m,p)	1519 (m,p)	1512 (m,p)	1509 (m,p)	1519 (m,p)	1514 (m,p)
1491 (w,dp)				1480 (w,dp)	1480 (w)
				1466 (w,dp)	
1408 (m,dp)	1406 (m,dp)	1404 (m,dp)	1407 (m,dp)	1408 (s,dp)	1408 (s,dp)
			1393 (w,ap)	1395 (s,ap)	1396 (s,ap)
1382 (s,p)	1382 (s,p)	1382 (s,p)	1384 (s,p)	1382 (s,p)	1383 (s,p)
	1334 (w)		1334 (w)	1313 (m)	1329 (m,dp)
1311 (m,ap)	1312 (w,ap)	1311*(m,ap)	1312 (w,ap)	1310 (s,ap)	1314 (m,ap)
1274 (w,dp)		1274*(w,dp)		1276 (w,dp)	
1258 (w,dp)	1259 (w)	1258*(w,dp)	1260 (w)	1260 (w,dp)	1263 (m,ap)
1219 (w,dp)		1218*(w,dp)		1219 (s,dp)	
	1202 (w,ap)		1204 (w,ap)		1202 (s,ap)
	1184 (w,dp)		1185 (w,dp)		1187 (m,dp)
1160 (m,dp)	1159 (m,dp)	1160 (m,dp)	1161 (m,dp)	1160 (Overlapped with a solvent band)	1160

Table 3. Continued

NiOEP Triclinic (D_{4h})		NiOEP Tetragonal (D_{2d})		NiOEP Solution (CH_2Cl_2)	
H	D	H	D	H	D
1139 (w,p)	1136 (w,p)	1138*(w,p)	1139 (w)	1140 (w,p)	1141 (w)
1124 (w,ap)	1127 (w,ap)			1120 (s,ap)	1129 (s,ap)
1108 (w)	1109 (w)	1107*(w)	1109 (w)	1110 (w)	1111 (w)
1025 (m,p)	1025 (m,p)	1025 (m,p)	1025 (m,p)	1025 (s,p)	1025 (s,p)
958*(w)	959 (w)	964*(w)	965 (w)		
		943*(w)			
904*(w)		899*(w)			
		844*(w)			
802*(w)	769 (w)	803*(w)	798 (w)	Masked by solvent	
	773 (w)	774*(w)	773 (w)		
		761*(w)	763 (w)		
749*(w)	755 (w)	749*(w)			
673*(w)	686 (w)	673*(w)	680 (w)		
	668 (w)	609*(w)	667 (w)		
		551*(w)			
		526*(w)			
		481*(w)			
353*(w)	349 (w)	352*(w)	348 (w)		
276*(w)	274 (w)	283*(w)			

Table 3. Concluded

NiOEP Triclinic (D_{4h})		NiOEP Tetragonal (D_{2d})		NiOEP Solution (CH_2Cl_2)	
H	D	H	D	H	D
			242 (w)		
225*(w)	236 (w)	243*(w)	219 (w)		

^aSpectra are taken with crystalline samples excepting lines marked by asterisks; these are measured with sample in KBr support.

Abbreviations: ap, anomalously polarized
 dp, depolarized
 p, polarized
 s, strong
 m, medium
 w, weak

Deuteration at meso carbons of Ni(II)OEP decreases vibrational frequencies which are derived from the vibrations involving meso carbons. In addition to frequency shifts, deuteration at meso carbons induces two new anomalously polarized lines (1202 and 1263 cm^{-1}) and decreases the intensity of 1310 cm^{-1} anomalously polarized line. The line intensity of 1202 cm^{-1} is shown in the perpendicular component only; therefore, this line is an inversely polarized line ($\rho \rightarrow \infty$). All these changes are also observed in the spectrum of Fe(III)OEPCl-meso-d₄. The Raman frequencies of both Fe(III)OEP-meso-h₄ and -d₄ are tabulated in Table 4.

Improved interpretations of resonance Raman data require an understanding of the nature of the Raman active normal modes (a_{1g} , a_{2g} , b_{1g} , and b_{2g} under D_{4h} symmetry). Several investigators (Abe, et al., 1976; Kitagawa, et al., 1976; Stein, et al., 1975) have undertaken the normal coordinate analysis of model metalloporphyrins. Abe, et al. (1976), using the adjusted force constants of Ogoshi, et al. (1972), have analyzed the normal coordinates of Ni(II)OEP with D_{4h} symmetry. Table 5 shows the important internal coordinate contributions to the potential energy of normal modes above 1500 cm^{-1} in Ni(II)OEP (D_{4h}). Abe's result indicates that with the exception of the a_{1g} vibration the high frequency modes shown in Table 5 share a common feature of possessing a total of about 60-80% contribution from (C_a-C_m) stretching, (C_a-N) stretching, and ($C_b C_a N$) bending where C_m is the meso carbon and C_a and C_b are the α - and β -carbon of pyrrole, respectively (Figure 29). The 1660 (dp) and 1609 (ap) cm^{-1} lines of Ni(II)OEP (D_{4h}) contain the largest percentage of (C_a-C_m) stretching, about 70%. These lines which show the greatest shift are shifted by 19 cm^{-1} to lower frequencies in the D_{2d} symmetry form.

Table 4. Resonance Raman Frequencies (cm^{-1}) and Polarizations for FeOEPC1

Fe(III)OEPC1 KBr		Fe(III)OEPC1 Solution (CH_2Cl_2)	
H	D	H	D
1630 (s,dp)	1620 (s,dp)	1632 (s,dp)	1620 (s,dp)
1585 (s,p)	1585 (m)		
1568 (s,ap)	1552 (s,ap)	1567 (s,ap)	1553 (s,ap)
1562 (s,dp)	1560 (s,dp)	1561 (m,dp)	1560 (s,dp)
1486 (m,p)	1523 (w,p)	1473 (?)	
1454 (m,p)			
1407 (s,dp)	1403 (s,dp)	1407 (s,dp)	1406 (s,dp)
1393 (m,ap)	1393 (m,ap)	1394 (m,ap)	1394 (w,ap)
1378 (s,p)	1375 (s,p)	1376 (s,p)	1376 (s,p)
1312 (s,ap)	1313 (m,ap)	1308 (s,ap)	1315 (w,ap)
	1267 (w,ap)		1267 (w,ap)
1214 (m,dp)		1213 (m,dp)	
	1203 (s,ap)		1204 (w,ap)
	1189 (w,dp)		1189 (w,dp)
1160 (s,dp)	1158 (s,dp)	1159 (s,dp)	1159 (s,dp)
1141 (m,p)	1139 (w,p)		
1126 (m,ap)	1129 (w,ap)	1126 (w,ap)	1130 (w,ap)
1028 (m,p)	1028 (s,p)	1028 (w,p)	1030 (m,p)
964 (m,p)	965 (w,p)		

Table 4. Concluded

Fe(III)OEPCl KBr		Fe(III)OEPCl Solution (CH ₂ Cl ₂)	
H	D	H	D
937 (w,p)	935 (w)	Masked by solvent	
812 (w)			
786 (w)	783 (w)		
752 (m,p)			
736 (w)			
676 (w)	686 (w)		
354 (m,p)	353 (w,p)		
	310 (w)		
274 (w)			
220 (w)	233 (w)		

Abbreviations: ap, anomalously polarized
 dp, depolarized
 p, polarized
 s, strong
 m, medium
 w, weak

Table 5. Important Internal Coordinates Contributing to the Potential Energy of Normal Modes above 1500 cm^{-1} in NiOEP (D_{4h})

Symmetry	Observed (CH_2Cl_2)	Internal Coordinates
b_{1g}	1654	$\nu(\text{C}_a-\text{C}_m) \gg \nu(\text{C}_a-\text{C}_b) \sim \delta(\text{C}_b\text{C}_a\text{N}) > \nu(\text{C}_b-\text{C}_b)$
a_{2g}	1603	$\nu(\text{C}_a-\text{C}_m) \gg \nu(\text{C}_a-\text{N})$
a_{1g}	1600	$\nu(\text{C}_b-\text{C}_b) \gg \nu(\text{C}_a-\text{C}_m) \sim \delta(\text{C}_b\text{C}_a\text{N})$
b_{2g} (?)	1575	$\nu(\text{C}_a-\text{N}) > \nu(\text{C}_a-\text{C}_m)$
a_{1g}	1519	$\nu(\text{C}_a-\text{N}) > \nu(\text{C}_a-\text{C}_m)$

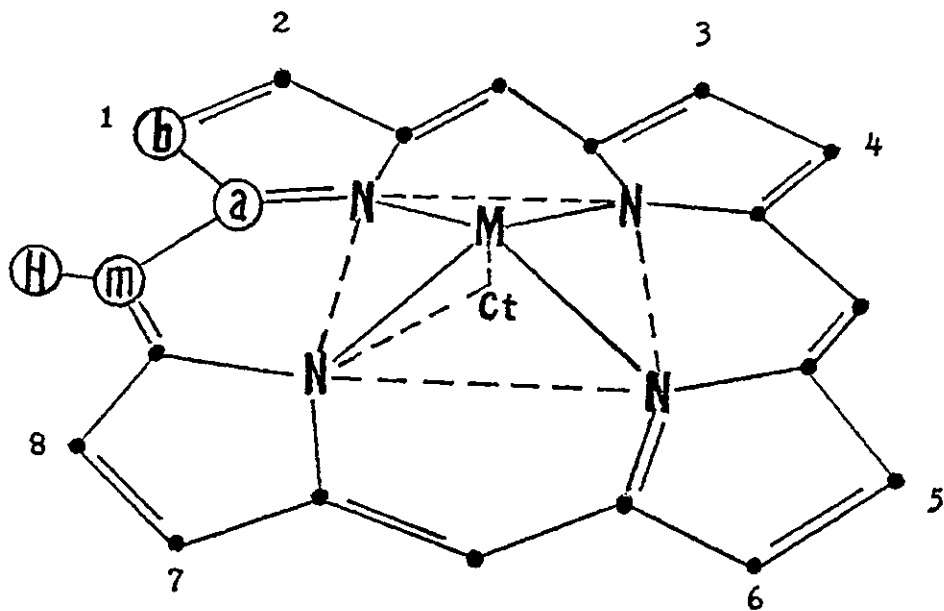


Figure 29. Labeling Scheme for the Porphinato Moiety and Structure of Porphyrins

Porphyrins	Substituents on Position							
	1	2	3	4	5	6	7	8
Octaethylporphyrin	E	E	E	E	E	E	E	E
Etioporphyrin I	M	E	M	E	M	E	M	E
Mesoporphyrin IX dimethyl ester	M	E	M	E	M	P	P	M
Protoporphyrin IX dimethyl ester	M	V	M	V	M	P	P	M

Abbreviations: E, $-\text{CH}_2\text{CH}_3$; M, $-\text{CH}_3$; V, $-\text{CH}=\text{CH}_2$; P, $-\text{CH}_2\text{CH}_2\text{COOCH}_3$

On the other hand, the 1602 (p) cm^{-1} of Ni(II)OEP-meso- d_4 contains reduced amounts of (C_a-C_m) stretching, about 15%, or (C_a-N) stretching and is not structure sensitive. The contribution of (C_a-C_m) stretching to the a_{2g} vibration at $\sim 1590 \text{ cm}^{-1}$ is of particular interest because it involves the stretching and contraction of the chemical bonds in the inner 16-membered ring (Figure 29). A vibration of this kind is likely to reflect the properties of the porphyrin core. It will be shown later that expansion of the inner 16-membered ring will lower this a_{2g} Raman frequency.

Figure 30 shows the Raman spectra obtained for Cu(II)OEP in parallel and perpendicular polarization. Sample (a) which was supplied by Dr. D. Dolphin is Cu(II)OEP crystals embedded in KBr pellet. The same spectrum is obtained when this crystal sample is irradiated without KBr support. Sample (b) is also Cu(II)OEP crystals crystallized from CH_2Cl_2 -hexane solution. When both crystal forms are dissolved in CH_2Cl_2 the solution spectra are identical (Figure 30c).

The spectrum of Cu(II)OEP in KBr pellet (Figure 30a) shows 1660, 1605, 1578, and 1513 cm^{-1} lines which are not observed in the spectra of the crystals or solution (Figure 30b,30c). By analogy to the frequency shifts observed in the Ni(II)OEP- h_4 and $-\text{d}_4$ spectra, it is concluded that the Cu(II)OEP supplied by Dolphin is a mixture containing two crystal forms of Cu(II)OEP. A simpler Raman spectrum which displays 1660 (dp), 1605 (ap), 1578 (dp), and 1513 (p) should be observed for the second crystal form of Cu(II)OEP.

The crystal molecular configuration changes from a planar to a buckled, nonplanar depending on the crystal packing and on the substitu-

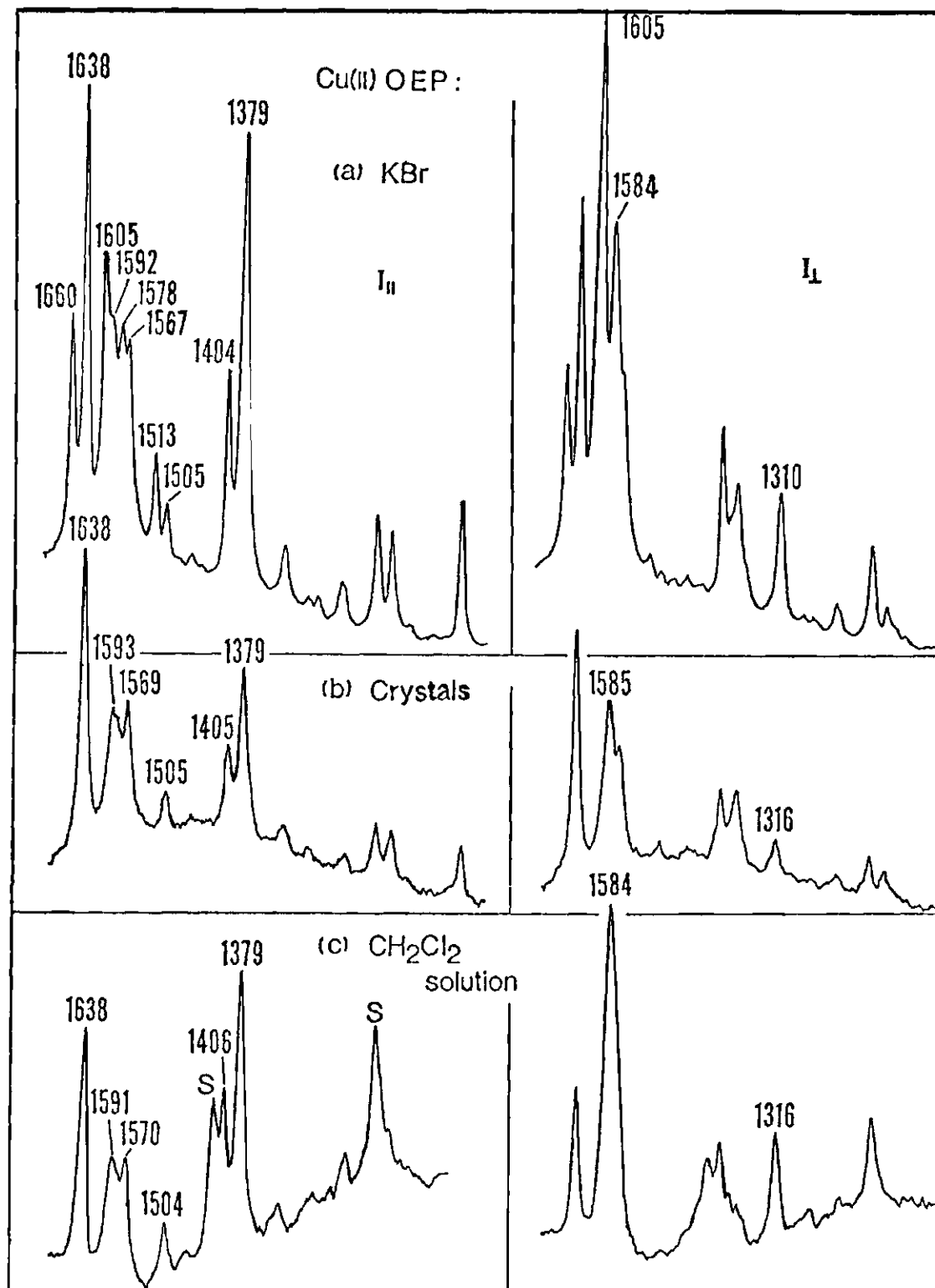


Figure 30. Resonance Raman Spectra of Cu(II)OEP: (a) Sample supplied by Dr. D. Dolphin; (b) Sample obtained from CH₂Cl₂-hexane solution; (c) CH₂Cl₂ solution sample of (a) and (b)

ents attached to the porphinato core (Hoard, 1973; Fleischer, et al., 1964). In addition to Ni(II)OEP which has triclinic (D_{4h}) and tetragonal (D_{2d}) crystal forms, the crystal structure of other porphyrins has been determined. Silvers and Tulinsky (1967) solved the crystal molecular structure of triclinic tetraphenylporphyrin and found that, although the porphyrin ring is nonplanar, the atoms of the inner 16-member ring are planar. However, Harmor, et al. (1964) analyzed the tetragonal single crystal of tetraphenylporphyrin and concluded that the molecular symmetry of this crystal is S_4 , suggesting that this crystal is ruffled. Moustakali and Tulinsky (1973) have revealed that, since the porphine macrocycle of copper-tetrapropylporphyrin is essentially planar and the geometry of the independent pyrroles is identical, the porphine skeleton closely approximates D_{4h} symmetry. On the other hand, the crystal structure of copper tetraphenylporphyrin has been determined to be tetragonal (Fleischer, et al., 1964). Therefore the existence of two crystal molecular forms of Cu(II)OEP as evinced from the resonance Raman data is quite reasonable.

When the crystal mixture of Cu(II)OEP is dissolved in CH_2Cl_2 , the molecular form which shows the lower frequency lines in the Raman spectrum is stable in solution. This behavior contrasts with that of Ni(II)OEP, in which the molecular form displaying higher frequency lines in Raman spectrum is stable in solution. Nonetheless, the solution spectrum of Cu(II)OEP is still assigned to a planar form since there is no apparent reason for the retention of a ruffled core in solution.

II. An Anomalous Polarized Line in Resonance Raman Spectra of Metalloporphyrins and Hemoproteins as a Structural Probe of Metal Displacement

Table 6 shows a correlation of the anomalously polarized line at $\sim 1590 \text{ cm}^{-1}$ in a series of known structure metalloporphyrins with Ct-N distance, a distance between the center of the porphyrin core and the pyrrole nitrogen (Figure 29). The metalloporphyrins are listed in the order of decreasing Ct-N distance. The correspondence between a decrease in Ct-N distance and an increase in the a_{2g} frequency is clearly indicated. Rh(III)Etio(DMA)₂Cl and Ni(II)OEP (D_{2d}) are two exceptions. Rh(III)Etio(DMA)₂Cl displays its a_{2g} frequency at $\sim 10 \text{ cm}^{-1}$ higher than that which might be expected and Ni(II)OEP (D_{2d}) shows its a_{2g} frequency at 1590 cm^{-1} although its Ct-N distance is shorter. The following "core expansion" mechanism can be used to account for the change in the a_{2g} frequency with Ct-N distance. If $d(\text{Ct-N})$ is a measure of the radius of the inner 16-membered ring, then expansion of the ring will increase $d(\text{C}_a-\text{C}_m)$ and $d(\text{C}_a-\text{N})$. Changes in the force constants of the C_a-C_m and C_a-N bonds associated with the core expansion are probably responsible for the observed frequency lowering.

This "core expansion" correlation suggests assessment of the out-of-plane displacement of the metal is possible, if the metal-to-pyrrole nitrogen distance, $d(\text{M-N})$ can be estimated. In oxyhemoglobin $d(\text{Fe-N}) = 2.00 \text{ \AA}$ is appropriate for a low-spin iron(II) complex. The anomalously polarized line of oxyhemoglobin appears at 1585 cm^{-1} (Spiro and Streckas, 1974), implying a $d(\text{Ct-N})$ of $\sim 2.00 \text{ \AA}$. It is therefore concluded that oxyhemoglobin contains in-plane iron, which is well known (Hoard, 1971;

Table 6. Correlation of the Anomalous Polarized Frequency (cm^{-1}) with Ct-N Distance (\AA)

Compound	Frequency (cm^{-1})	Ct-N (\AA)	Structure
SnOEPCl ₂	1545	2.082 (2)	SnOEPCl ₂
AgOEP	1550	2.08	AgTPP
MgOEP	1558	2.055 (6)	MgTPP (H ₂ O)
ZnOEP	1565	2.047 (2)	PyZnTPyP
RhEtio(DMA) ₂ Cl	1578	2.038 (6)	RhEtio(DMA) ₂ Cl
(FeOEP) ₂ O	1570	2.027	(FeTPP) ₂ O
FeOEPCl	1568	2.019 (3)	Average Hemin
FeProtoDMECl	1575	2.007 (5)	FeProtoCl
VOEtio	1574	2.01 (4)	VODPEP
PdOEP	1585	2.009 (9)	PdTPP
Fe(II)Etio(py) ₂	1587	2.004 (4)	Fe(II)TPP(Im) ₂
CuOEP	1585	2.000 (5)	CuTPPrP
Fe(III)OEP(Im) ₂ Cl	1590	1.989 (5)	Fe(III)TPP(Im) ₂ Cl
FeOEP(NO)	1593	1.990	FeTPP(NO)
MnOEPCl	1591	1.99	MnTPPCl
CuOEP	1605	1.981 (7)	CuTPP
CoOEP(NO)	1605	1.976 (3)	CoTPP(NO)
NiOEP (D _{4h})	1609	1.958 (2)	NiOEP
NiOEP (D _{2d})	1590	1.929 (3)	NiOEP

Table 6. Concluded

Compound	Frequency (cm^{-1})	Ct-N (\AA)	Structure
----------	-----------------------------------	-----------------------	-----------

Abbreviations:

py, pyridine	Im, imidazole
TPP, tetraphenyl porphyrin	TPyP, tetra(4-pyridyl) porphyrin
Etio, etioporphyrin	DMA, dimethyl amine
Proto, protoporphyrin IX	DPEP, deoxyphylloerythroetio- porphyrin
TPrP, tetra(n-propyl) porphyrin	DME, dimethyl ester

Figures in parentheses are the standard deviation of the average bond length.

Numerical value refers to lest significant figure.

Collman, et al., 1974). More interesting is an assessment of iron displacement in deoxyhemoglobin. The anomalously polarized line appears at 1552 cm^{-1} (Spiro and Strekas, 1974). Adjustment of this frequency by addition of $\sim 4\text{ cm}^{-1}$ is required when comparison of frequencies taken with solid samples is made with those in solution. The corrected anomalously polarized line of deoxyhemoglobin at 1556 cm^{-1} implies the Ct-N distance is 2.05 \AA . Upon setting $d(\text{Fe-N}) = 2.086\text{ \AA}$ (Hoard and Scheidt, 1973), a Ct-Fe displacement of 0.39 \AA is obtained for the iron in deoxyhemoglobin. This value is in good agreement with the 0.42 \AA displacement found in the model high-spin iron(II) porphyrin (Hoard, 1971), but is considerably smaller than the estimated 0.75 \AA by Perutz (1972). It is of interest to note that recent refinement of the x-ray diffraction data from deoxyhemoglobin crystals has reduced this estimate to 0.60 \AA (Perutz and Fermi, unpublished results). The estimated $0.5 \pm 0.1\text{ \AA}$ by Eicher, et al. (1976) from Mossbauer experiments for the ferrous iron out-of-plane displacement in deoxyhemoglobin agrees well with that from resonance Raman data.

Spiro and Strekas (1974) have labeled the anomalously polarized line at 1590 cm^{-1} as a spin state marker since conversion of iron from low-spin to high-spin without change in oxidation state causes this anomalously polarized line to shift to lower frequency. They have suggested that "doming" of the porphyrin ring accompanying out-of-plane displacement of the iron is responsible for the observed shifts. However, normal coordinate calculations on domed octamethylporphyrin cannot produce a large frequency shift without simultaneously adjusting the bond stretching force constants (Stein, et al., 1975). Since adjustments of the bond force constants imply changes in bond lengths and thus the size of the

porphinato core, the "doming" mechanism of Spiro is not completely incompatible with the "core expansion" mechanism. It should be noted that there is no clear evidence that heme structure is considerably "domed" in deoxyhemoglobin or other high-spin heme proteins.

The structural implication of the two interpretations differs when the anomalously polarized line is lower than $\sim 1580 \text{ cm}^{-1}$. Since doming is induced by the out-of-plane displacement of metal, this mechanism would predict a maximum $d(\text{Ct-Fe})$ in the high-spin ferric heme proteins such as methemoglobin fluoride. Methemoglobin fluoride has an anomalously polarized line at 1555 cm^{-1} while the model high-spin ferric complex such as Fe(III)OEPCl has an anomalously polarized line at 1576 cm^{-1} . In order to explain the difference between 1576 and 1555 cm^{-1} by doming mechanism, an additional protein-induced doming is required. On the other hand, the 1555 cm^{-1} in methemoglobin fluoride can be explained by core expansion mechanism as indicating an increase in $d(\text{Ct-N})$. The increase in $d(\text{Ct-N})$ with a fixed value of $d(\text{Fe-N})$ implies a decrease in $d(\text{Ct-Fe})$. Thus, $d(\text{Ct-Fe})$ is about $0.3 - 0.4 \text{ \AA}$ in high-spin ferric heme proteins.

III. Dispersion of Depolarization Ratio

It has been shown that deuteration at meso carbons of Ni(II)OEP induces a new inversely polarized ($\rho = \infty$) line at 1202 cm^{-1} (Figure 28). Deuteration at meso carbons of $\text{Ni(II)etioporphyrin I}$, $\text{Ni(II)mesoporphyrin-IX dimethyl ester}$, and $\text{Ni(II)protoporphyrin dimethyl ester}$ (Figure 29) also appears as an inversely polarized or as an anomalously polarized ($3/4 < \rho < \infty$) line at 1206 (ip), 1207 (ap), or 1211 cm^{-1} (ap), respectively. Figures 31-34 show the resonance Raman spectra of $\text{Ni(II)OEP-meso-d}_4$,

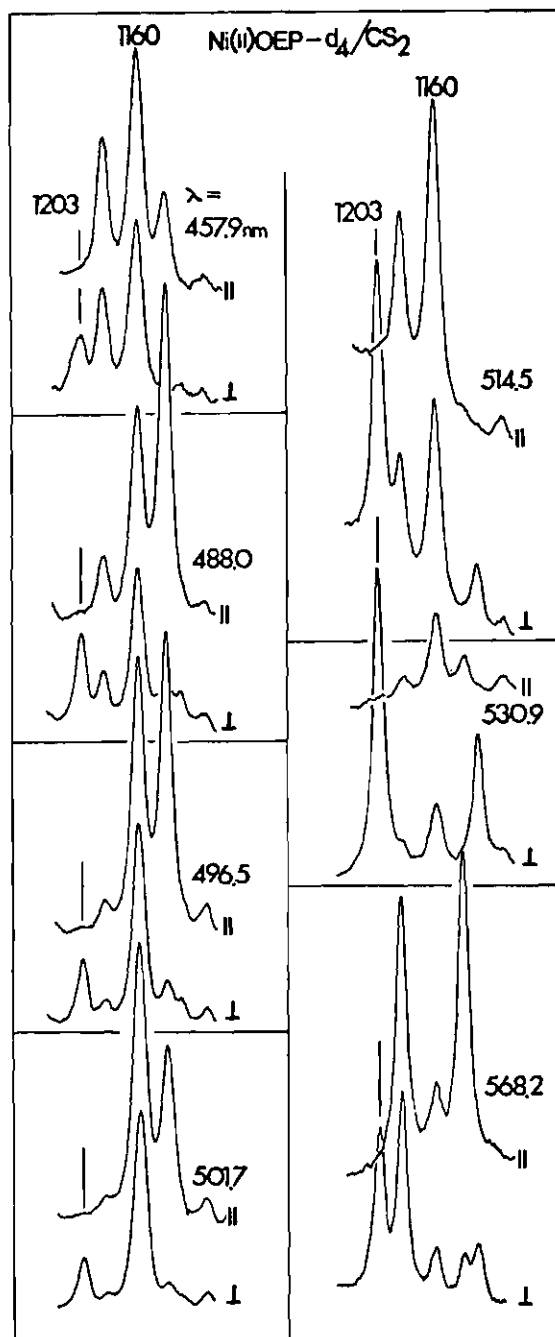


Figure 31. Resonance Raman Spectra of Ni(II)OEP-meso- d_4 in CS_2 Solution (The scattered light is analyzed into components perpendicular (\perp) and parallel (\parallel) to the incident polarization. The exciting wavelengths are 457.9, 488.0, 496.5, 501.7, 514.5, 530.9, and 568.2 nm.)

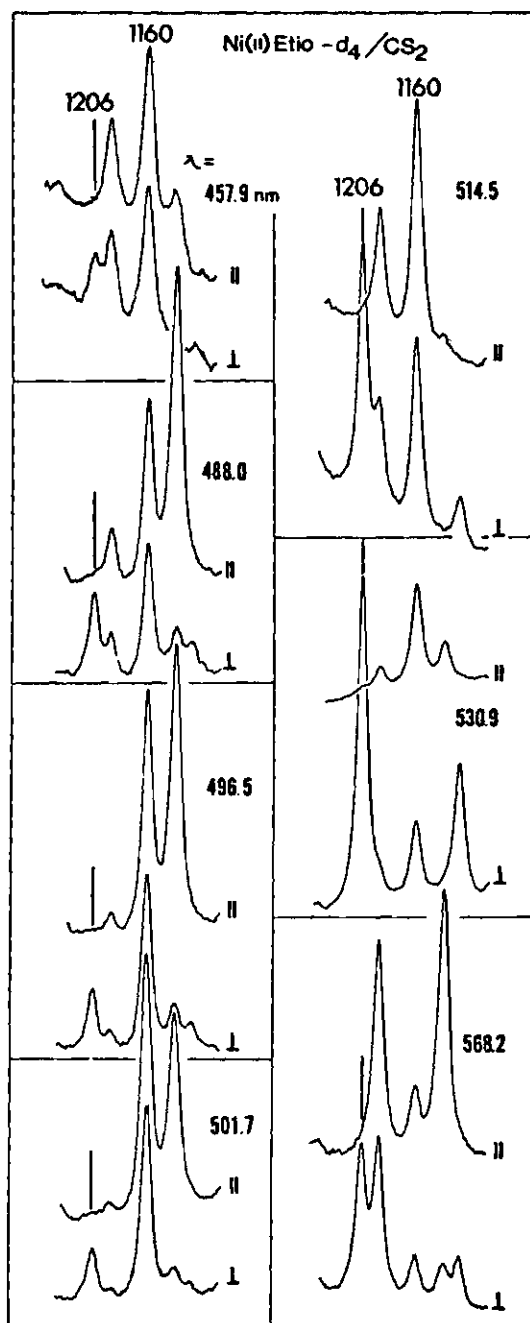


Figure 32. Resonance Raman Spectra of Ni(II)Etio-meso-d₄ in CS₂ Solution (Other conditions are the same as Figure 31.)

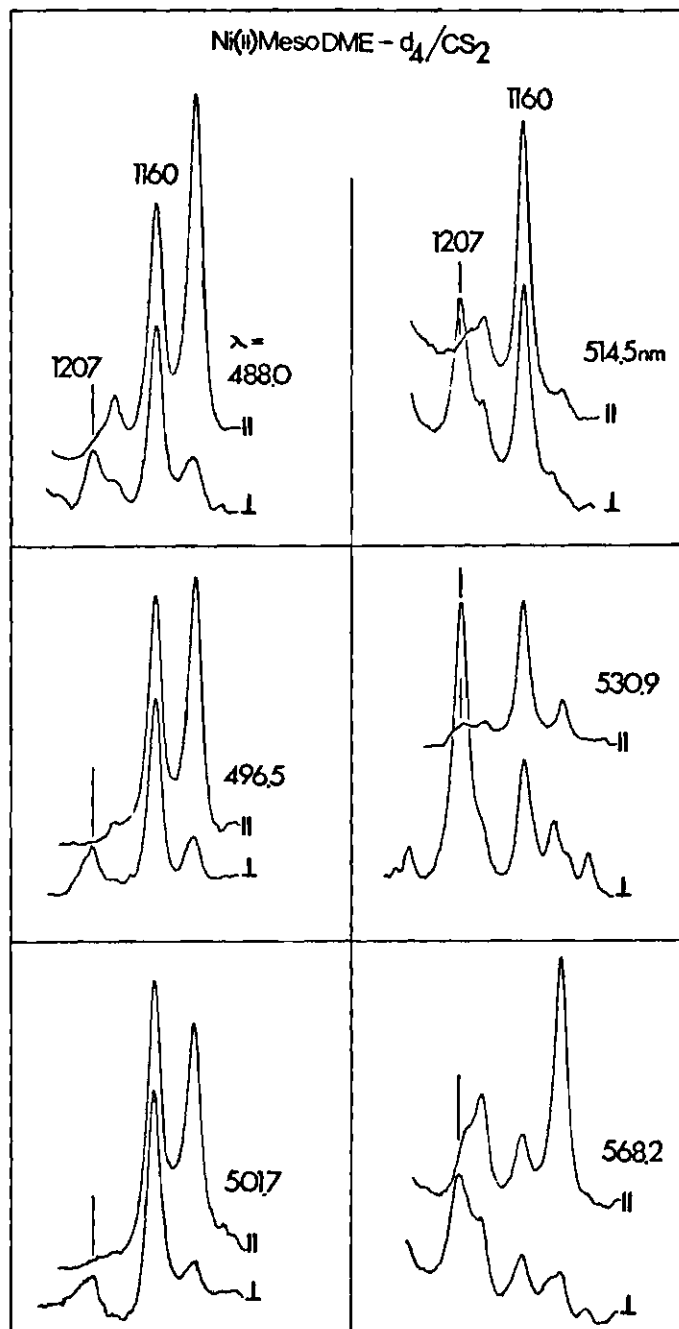


Figure 33. Resonance Raman Spectra of Ni(II)MesO DME-meso-d₄ in CS₂ Solution (Other conditions are the same as Figure 31.)

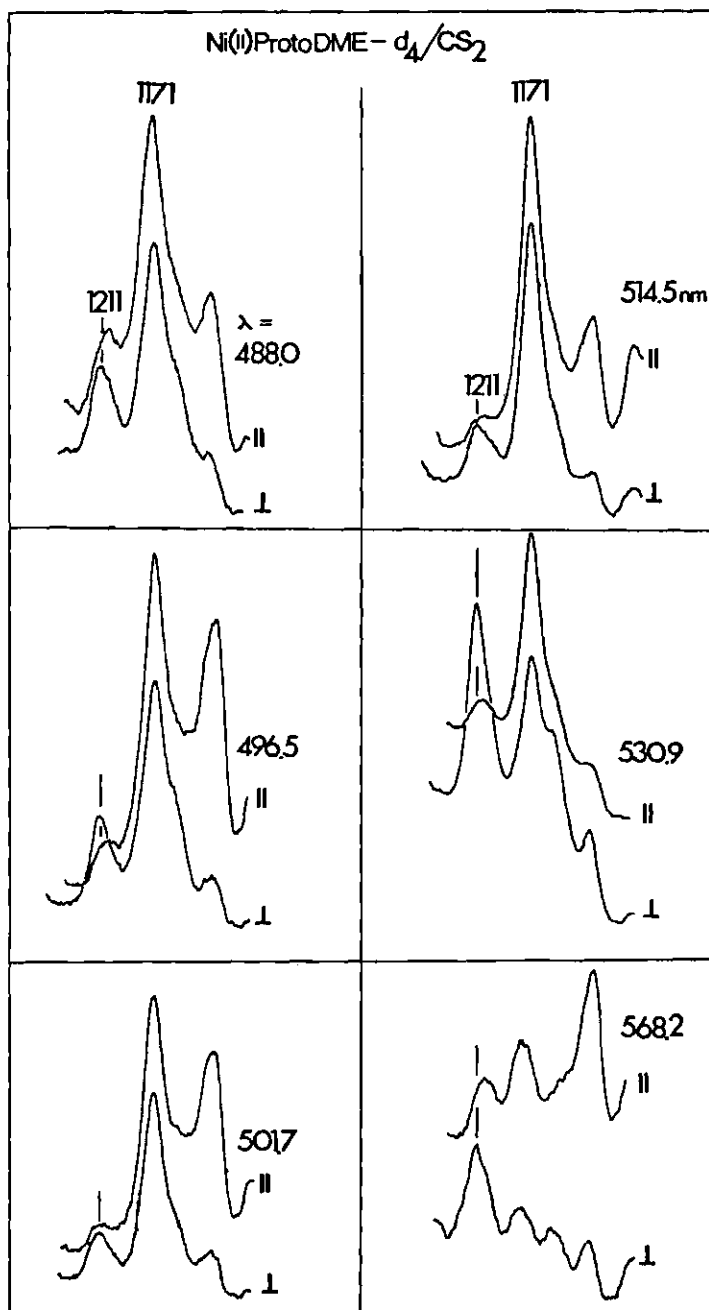


Figure 34. Resonance Raman Spectra of Ni(II)ProtoDME-meso- d_4 in CS₂ Solution (Other conditions are the same as Figure 31.)

Ni(II)Etio-meso-d₄, Ni(II)MesoDME-meso-d₄, and Ni(II)ProtoDME-meso-d₄ in parallel and perpendicular polarization at 1100-1250 cm⁻¹ region. The spectra of each sample in CS₂ solution are recorded using six to seven different exciting laser lines.

The scattering intensities of 1203 and 1206 cm⁻¹ of Ni(II)OEP-d₄ and Ni(II)Etio-d₄, respectively, are observable only in perpendicular polarization; therefore, these two lines are inversely polarized lines. However, the Raman spectra of Ni(II)MesoDME-d₄ show scattering intensity in the parallel polarization of 1207 cm⁻¹ especially those spectra recorded using 530.9 and 568.2 nm exciting lines. The Raman intensity of 1211 cm⁻¹ of Ni(II)ProtoDME-d₄ in parallel polarization is even more clearly indicated in the spectra obtained at six different exciting lines. Therefore these two lines (1207 and 1211 cm⁻¹) are anomalously polarized lines.

If the molecule has D_{4h} symmetry (Ni(II)OEP-d₄), then a_{2g} modes should have $\rho = \infty$, since their scatter tensors are strictly antisymmetric (case 5 of McClain, 1971). There are three possible explanations for a significant parallel component of anomalously polarized modes. The effective symmetry of the molecule may be less than D_{4h}, in which case the formerly a_{2g} modes may acquire symmetric as well as antisymmetric components of the scattering tensor. Alternatively, there may be accidental degeneracies between a_{2g} modes and modes of other symmetries, which are polarized (a_{1g}) or depolarized (b_{1g} or b_{2g}), giving an overall depolarization ratio which is anomalous. Third, the excited state may be slightly split (~ 100 cm⁻¹) and this will cause dispersion in depolarization ratio (Collins, et al., 1976). Since the spectra of these four

metalloporphyrins are very similar and they show no unresolved component at 1207 or 1211 cm^{-1} lines, the variations of depolarization ratio for 1207 and 1211 cm^{-1} lines are interpreted in terms of lowering of the symmetry of metalloporphyrins from D_{4h} symmetry.

Comparison of the Raman intensity of 1207 cm^{-1} line of Ni(II)MesoDME-d₄ with that of 1211 cm^{-1} line of Ni(II)ProtoDME-d₄ shows higher intensity for 1211 cm^{-1} line in parallel polarization component. This result is attributed to the influence of the two vinyl substituents at the periphery of the Ni(II)ProtoDME-d₄. These double bonds, which are saturated in Ni(II)MesoDME-d₄, are in a position to conjugate with the π system of the porphyrin ring, and indeed the electronic spectra of Ni(II)-ProtoDME-d₄ is red-shifted with respect to its saturated analog (Ni(II)-MesoDME-d₄) by ~ 10 nm. In addition, the vinyl substituents may have an effect on lowering the effective symmetry of Ni(II)ProtoDME-d₄. The effective symmetry of the Ni(II)ProtoDME-d₄, with the vinyl groups included, is C_s . Under this point group all vibrations have scattering tensors which can have both symmetric and antisymmetric components, so there are no symmetry restrictions on the depolarization ratio.

IV. Excitation Profiles of Nickel(II)etioporphyrin I

Resonance Raman spectra of nickel(II)etioporphyrin I-h₄ or -d₄ (Ni(II)Etio) in different solutions have been obtained with the excitation frequencies in the region of 17,000 to 22,000 cm^{-1} which encompass the entire Q band and the region between the Q and B bands. Figure 35 shows the visible spectrum together with the excitation profiles of Ni(II)Etio-h₄ or -d₄ in this region. The 1518 and 1654 cm^{-1} lines were obtained in 2 CDCl_3 : 1 CH_3COCH_3 mixed solvent solution with 1709 cm^{-1} as

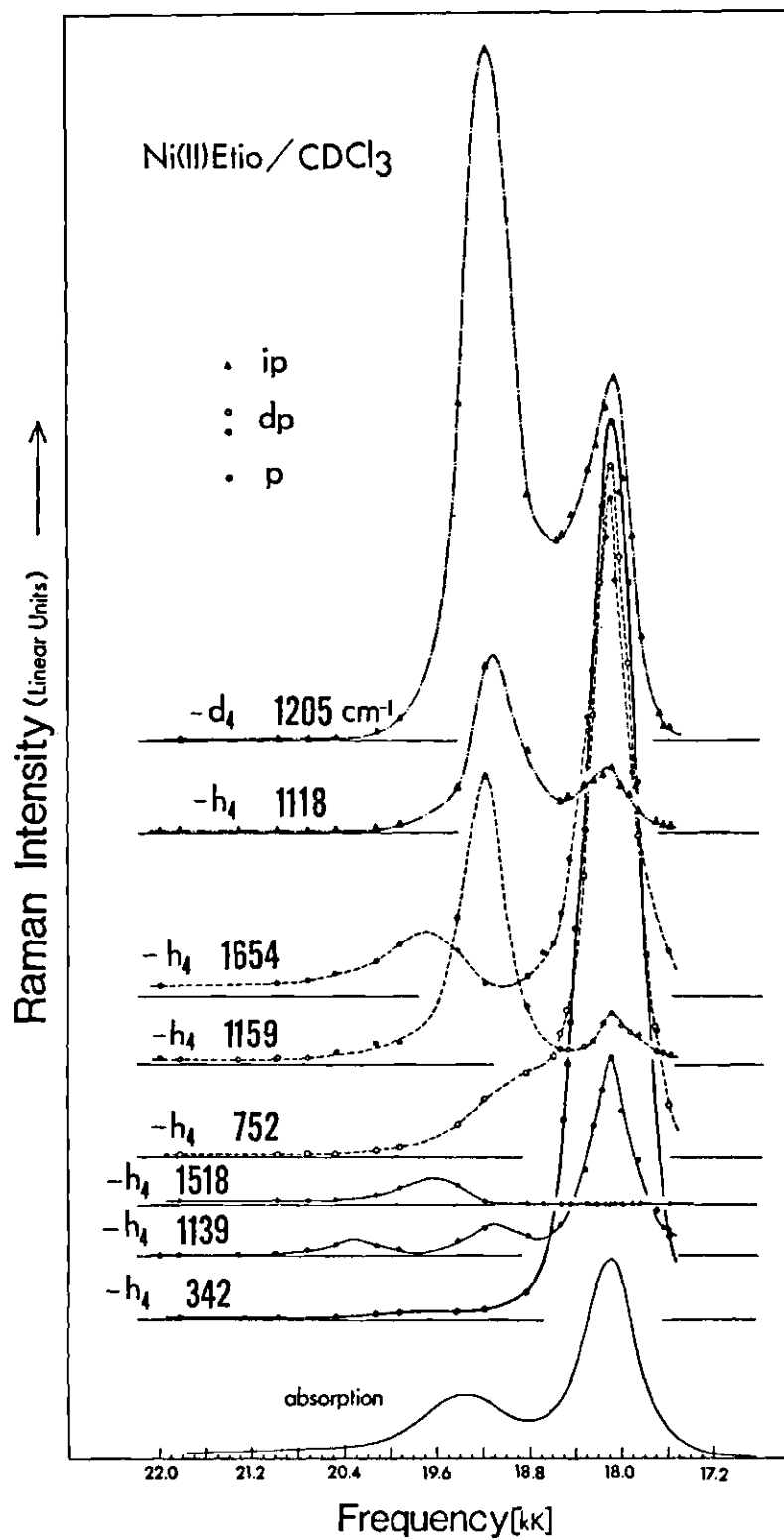


Figure 35. Excitation Profiles and Absorption Spectrum of Ni(II)Etio-meso-h₄ and -d₄ in CDCl₃

the reference line. The 342 cm^{-1} line was obtained in $3 \text{ CS}_2 : 1 \text{ CH}_2\text{Cl}_2$ mixed solvent solution with 284 cm^{-1} as the reference line. All the others were obtained in CDCl_3 solution with 907 cm^{-1} as the reference line. The reason that we used mixed solvent solution was to obtain a solvent band which is strong enough as a reference line and does not overlap with the solute bands. The relative Raman intensities of profiles have been normalized and have been corrected for chromophore absorption (Strekas, et al., 1974) and for the response of the Raman scattering apparatus.

Ni(II)Etio is a typical metalloporphyrin, but this is the first time that its excitation profiles in the Q band region have been shown to exhibit unusual behavior, especially, the excitation profiles of polarized and depolarized lines.

Based on the works of Shelnutt, et al. (unpublished), the excitation profiles can be explained qualitatively.

The 1205 and 1118 cm^{-1} are both inversely polarized lines (a_{2g} symmetry). The profiles for these two lines where the 0-0 and 0-1 maxima are resolved show greater intensity at the 0-1 frequency. This behavior can be explained by taking into account the nonadiabatic coupling contribution to the resonance Raman scattering. Near or at resonance the Herzberg-Teller B term and nonadiabatic D term contributions to the scattering tensor will be

$$(B+D)_{\rho\sigma} \sim (h_a)_{es}^o \left[\frac{M_{eg}^o M_{sg}^\sigma}{E_{e0} - E_{g0} - h\nu_0 - i\Gamma_{e0}} \left\{ 1 + \frac{h\nu_e^a}{E_{e0} - E_{s1}} \right\} \right]$$

(continued)

$$\pm \frac{M_{eg}^{\sigma} M_{sg}^{\rho}}{E_{e1} - E_{g0} - h\nu_0 - i\Gamma_{e1}} \left\{ 1 - \frac{h\nu_s^a}{E_{e1} - E_{s0}} \right\}$$

with $|e\rangle = |Q\rangle$ and $|s\rangle = |B\rangle$. The plus sign (destructive) holds for a_{1g} , b_{1g} , and b_{2g} vibrations, and the minus sign (constructive) holds for a_{2g} vibrations. Since $E_{e0} - E_{s1} < E_{e1} - E_{s0} < 0$, the nonadiabatic contribution in the curly brackets is largest for $E_{e1} - E_{s0}$ and adds to the adiabatic B term at the 0-1 transition but reduces at 0-0 transition; therefore, the intensity at 0-1 frequency is greater than that at 0-0 frequency (Shelnutt, et al., 1976).

The 1654, 1159, and 752 cm^{-1} are depolarized lines (b_{1g} or b_{2g} symmetry). The profiles of these lines show maxima at 0-0 and 0-1 transitions. For 1654 and 752 cm^{-1} lines the Raman intensity is greater at 0-0 frequency but for 1159 cm^{-1} line the Raman intensity is greater at 0-1 frequency. In a typical metalloporphyrin both low lying excited states are doubly-degenerate molecular states of E_u symmetry. In order to explain these unusual profiles, it is important to take into account the presence of electronic degeneracy of states at or near resonance in addition to the nonadiabatic contribution. In these electronically degenerate states, Jahn-Teller instability can become an important factor in determining the excitation profiles and depolarization ratios.

The Jahn-Teller effect is a kind of vibronic interaction encountered in a nonlinear molecule when the electronic state is degenerate. Jahn and Teller (1937) showed that there is always at least one non-totally symmetric mode that causes a splitting of the potential curve such that the positions of the potential minima are displaced by an amount Δ , which

is greater the larger the vibronic interaction (Figure 36). In a molecule of symmetry D_{4h} the Jahn-Teller active vibrations belong to two non-degenerate symmetry species: b_{1g} and b_{2g} (Hougen, 1964).

For the doubly degenerate Q state in D_{4h} metalloporphyrins with a Jahn-Teller effect, the shifts in the potential curves are equal but have opposite signs, which implies

$$\langle g1 | ev_+ \rangle \langle ev_+ | g0 \rangle = - \langle g1 | ev_- \rangle \langle ev_- | g0 \rangle$$

This result holds for both b_{1g} and b_{2g} Jahn-Teller active modes. For a b_{1g} mode the Raman scattering tensor pattern is

$$(\alpha_{\rho\sigma}) = \begin{pmatrix} A+B & 0 & 0 \\ 0 & -A-B & 0 \\ 0 & 0 & 0 \end{pmatrix}$$

For a b_{2g} mode the Raman scattering tensor pattern is

$$(\alpha_{\rho\sigma}) = \begin{pmatrix} 0 & A+B & 0 \\ A+B & 0 & 0 \\ 0 & 0 & 0 \end{pmatrix}$$

The tensor invariants are identical for both symmetry and $G^o = G^a = 0$, $G^s = 2(A^2 + B^2 + 2AB)$. From these results it is seen that the depolarization ratio is 3/4 and shows no dispersion; a prediction in good agreement with our experimental data. The Raman intensity is given by

$$I \sim A^2 + B^2 + 2AB$$

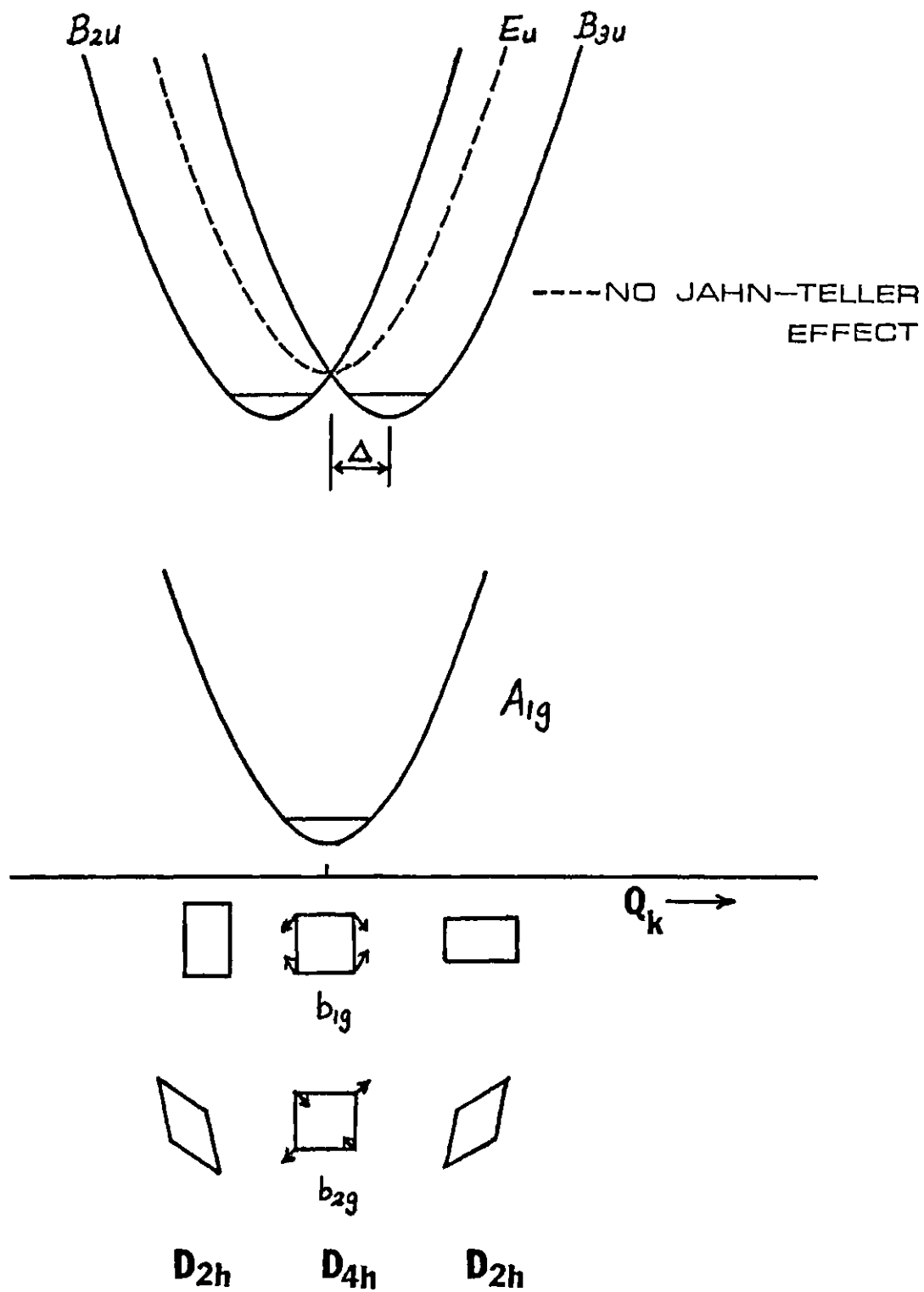


Figure 36. The Effect of Jahn-Teller Instability on a Potential Energy Curve

The presence of the cross term (AB) has a drastic effect. Depending on the relative sign between the A and B terms, the cross AB term will add or subtract from the intensity, and due to the difference in sign of the A term at the 0-0 and 0-1 frequencies, the cross term will add intensity at one frequency and subtract intensity at the other. Therefore, the excitation profiles for b_{1g} and b_{2g} modes may show greater intensity at either 0-0 or 0-1 frequency.

The 1518, 1139, and 342 cm^{-1} are polarized lines (a_{1g} symmetry). The profiles of 342 and 1518 cm^{-1} show maxima intensity at 0-0 transition and 0-1 transition, respectively. The profile of 1139 cm^{-1} shows maxima at 0-0, 0-1, and 0-2 transitions with the greatest intensity at 0-0 transition.

For a totally symmetric mode the Raman scattering tensor pattern is

$$\langle \alpha_{\rho\sigma} \rangle = \begin{pmatrix} A+B & 0 & 0 \\ 0 & A+B & 0 \\ 0 & 0 & 0 \end{pmatrix}$$

The arguments which lead to this tensor pattern are similar to those for Jahn-Teller modes except

$$\langle g1 | ev_+ \rangle \langle ev_+ | g0 \rangle = \langle g1 | ev_- \rangle \langle ev_- | g0 \rangle$$

The tensor invariants $G^o = 4/3 (A+B)^2$, $G^s = 2/3 (A+B)^2$, and $G^a = 0$ give a depolarization ratio 1/8 without dispersion. The Raman intensity is given by

$$I \sim A^2 + B^2 + 2AB$$

Again the presence of the cross term (AB) will lead to either constructive or destructive interference at either the 0-0 or 0-1 transition and thus the excitation profiles may show greater intensity at either 0-0 or 0-1 frequency.

APPENDIX I

METALLOPORPHYRIN EXCITED ELECTRONIC STATES

Figure 37 shows an electronic absorption spectrum of a typical metalloporphyrin. It displays an intense B(Soret) band ($\epsilon \sim 10^5 \text{ M}^{-1} \text{ cm}^{-1}$) at about 400 nm and a weaker Q band ($\epsilon \sim 10^3 \text{ M}^{-1} \text{ cm}^{-1}$) at about 550 nm. The Q band is composed of prominent 0-0 transition α band and 0-1 transition β band which is a vibronic side band.

Molecular orbital calculations by Gouterman, et al. (1963) indicate that under the D_{4h} molecule symmetry the highest filled molecular orbitals of the π -ring system are non-degenerate orbitals of a_{1u} and a_{2u} symmetry, the lowest unfilled orbitals are doubly-degenerate orbitals of e_g symmetry. The ground state configuration gives rise to a ground state of A_{1g} symmetry, the two excited state configurations give rise to molecular states of E_u symmetry. The two excited E_u molecular states are nearly degenerate and consequently subject to strong configuration interaction with the result that the transition dipoles add for the higher energy transition (B band) and largely cancel for the lower energy one (Q band) which can "borrow" back some of the intensity of the higher energy transition by vibronic coupling.

The symmetry of the vibrations effective in coupling B and Q bands can be determined from the direct product of the irreducible representatives to which the states B and Q belong. Since both B and Q states are E_u symmetry, reference to a character table for the D_{4h} molecular symmetry

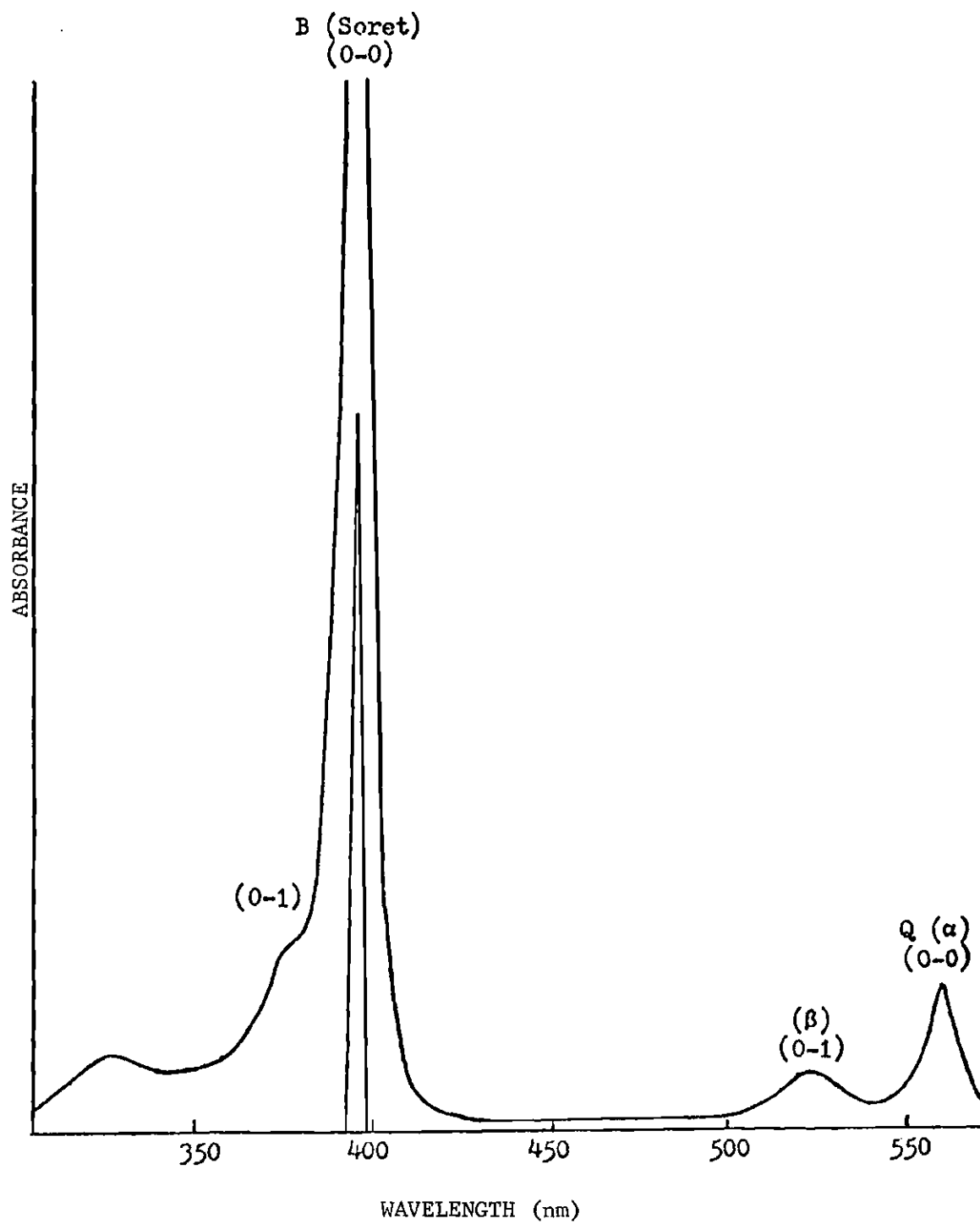


Figure 37. Absorption Spectrum of a Typical Metalloporphyrin:
Cu(II)OEP in Hexane at Room Temperature

gives

$$\Gamma_B \times \Gamma_Q = \Gamma_{E_u} \times \Gamma_{E_u} = a_{1g} + a_{2g} + b_{1g} + b_{2g}$$

that is, only vibrational modes of a_{1g} , a_{2g} , b_{1g} , and b_{2g} symmetries can couple with the states B and Q. Thus modes of these symmetries contribute to the 0-1 absorptional band of the Q band.

In the cyclic polyene model of Perrin, et al. (1969), only the nontotally symmetric vibrations of a_{2g} (ap), b_{1g} (dp), and b_{2g} (dp) symmetries are vibronically active. Although allowed group theoretically, the a_{1g} (p) vibration is inactive in this model which also discards bending modes. Consideration of porphyrin rather than a sixteen membered cyclic polyene shows that it is feasible for pyrrole ring coordinates of a_{1g} symmetry to be vibronically active.

APPENDIX II

PRESERVATION OF LENS PROTEINS

Usually biological materials are easily spoiled under improper preservation; therefore, the preservation of biological samples after the experiments is important especially for those samples which are difficult to obtain such as normal human lenses. Lyophilization is a common process of reducing protein solution to dryness. Through this process, the unbonded and loosely bonded water molecules are removed from the frozen sample. This process has been used for a long time with great success to preserve protein in the solid state without loss of its activity. Thus it is quite possible to apply this process to preserve the whole lens proteins after the lens has been used for experiments in the intact state.

Figure 38 shows the Raman spectra of the nucleus of a four year old rabbit lens in both intact and lyophilized states. For comparison, these spectra are taken from not only the same lens but the same position. The lyophilized lens is dried until its weight is constant (about two days). From the amide III region ($1220-1300\text{ cm}^{-1}$) which is the most sensitive region for protein conformation changes, it is seen that both spectra show a strong amide III band at 1240 cm^{-1} , indicating that the lens proteins whether in intact state or in lyophilized state exist predominantly in antiparallel β -pleated sheet structure and lyophilization does not change the major conformation of the lens proteins. From the

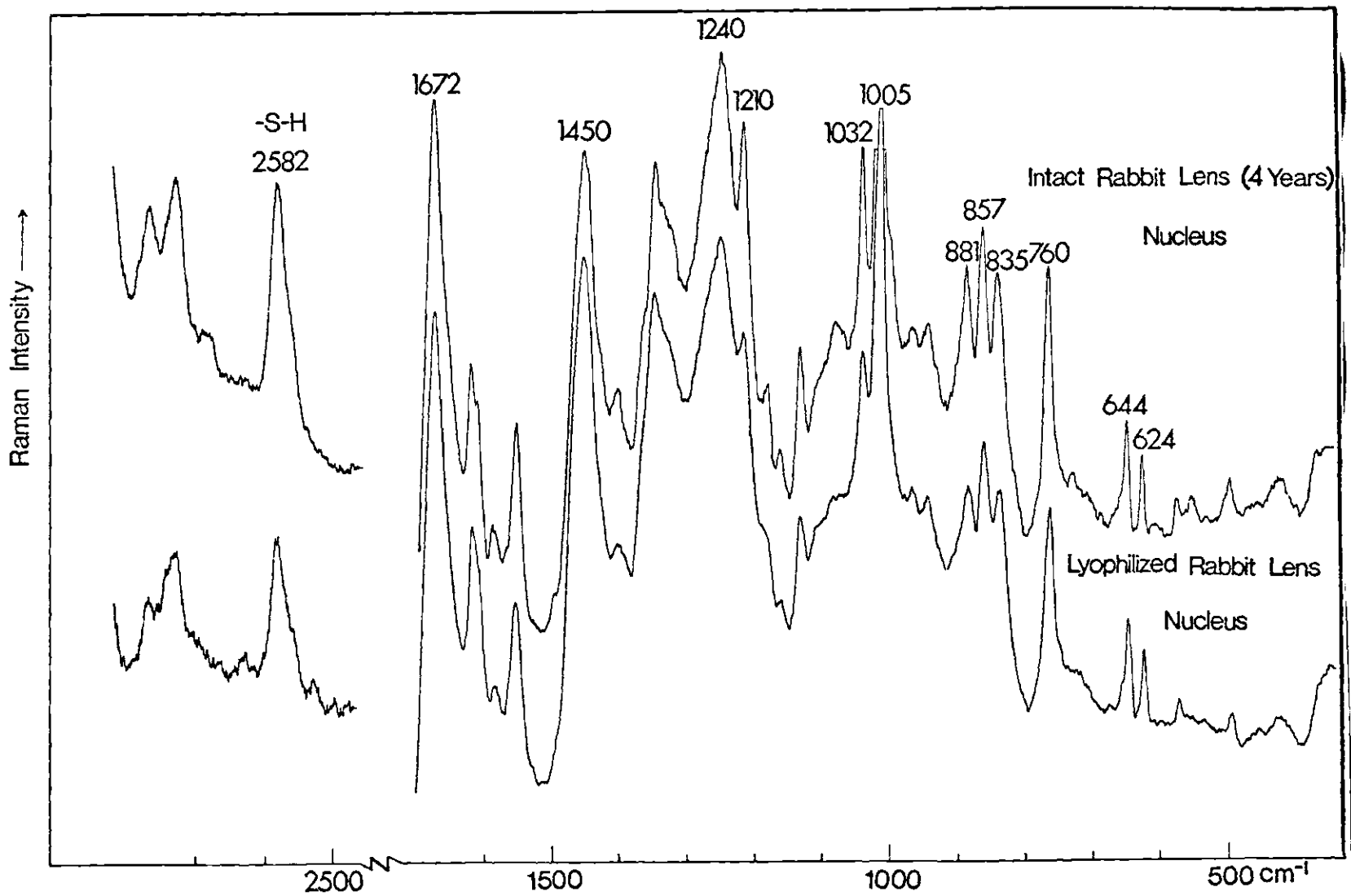


Figure 38. Raman Spectra of the Nucleus of Rabbit Lens in Both Intact and Lyophilized States

amide I region ($1630-1680\text{ cm}^{-1}$) which shows a strong and sharp peak at 1672 cm^{-1} in both spectra, it also indicates the existence of β -structure in both states of the lens proteins. Also, the peak intensity ratio of 624 cm^{-1} to 644 cm^{-1} which is proportional to the ratio of phenylalanine to tyrosine and the peak intensity ratio of 835 cm^{-1} to 857 cm^{-1} which depends on the nature of the hydrogen bonding of the phenolic hydroxyl groups in the tyrosyl residues are not changed upon lyophilization, indicating that the constituents and environments of these groups are still the same after lyophilization.

Although the amide III, amide I, and some other frequencies show no change upon lyophilization, lyophilization is a process which will induce a replacement of a certain number of protein-water interactions by protein-protein interactions; therefore, it is expected that the environments of protein molecules will show a small modification upon lyophilization. By comparing of the spectra of the lens proteins in both states at 551 , 1032 , 1076 , and 1210 cm^{-1} , it is seen that the relative peak high intensities of each pair are slightly different, indicating that the protein environments which correspond to these vibrations have been modified slightly.

For sulfhydryl groups which include mainly protein-SH and glutathione-SH, it is shown that the area intensity ratios of 2582 cm^{-1} to 2730 cm^{-1} in the intact state and in the lyophilized state are 0.97 and 0.98 , respectively. Meanwhile the intensity of the disulfide bond region does not increase upon lyophilization. Therefore, lyophilization of the intact lens can prevent air oxidation and decomposition of the sulfhydryl groups and preserve these groups as in the intact state.

Similar results are found in the cortex portion of the lens. From these results it is concluded that lyophilization can be used as a process for the preservation of the whole lens proteins. This process has the advantages of keeping the major protein conformation and the oxidation state of the sulfhydryl groups unchanged.

APPENDIX III

RESONANCE RAMAN SPECTRA AND EXCITATION PROFILES

NICKEL(II)ETIOPORPHYRIN I

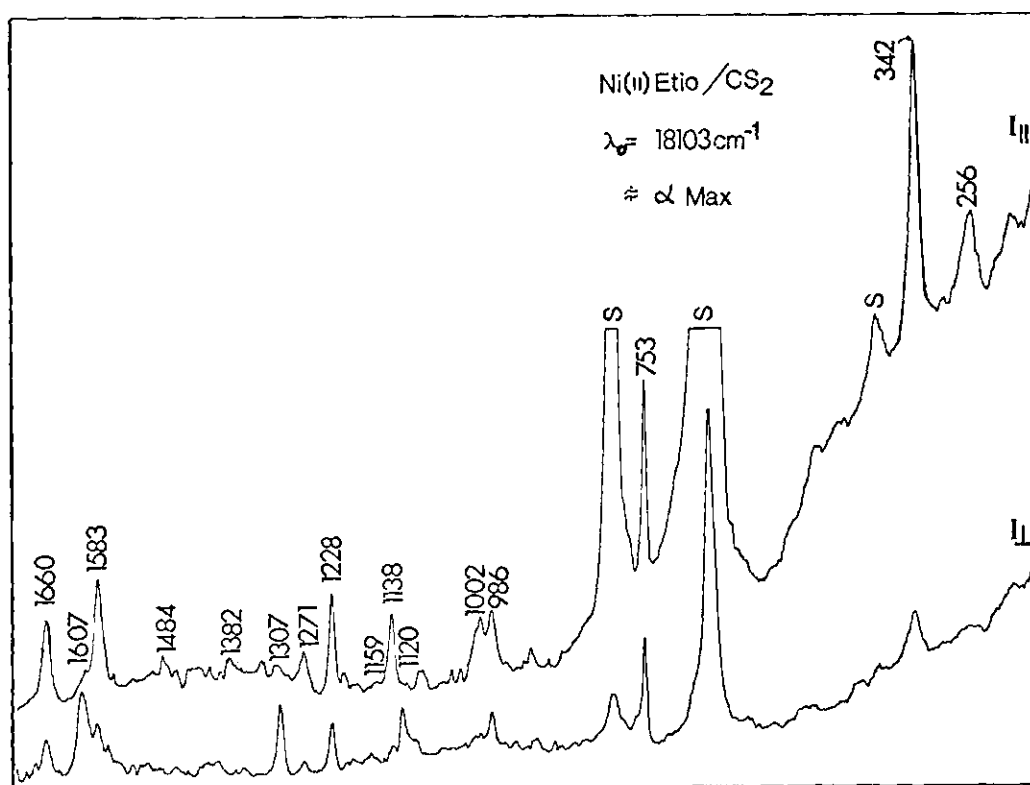


Figure 39. Resonance Raman Spectra (I_{||} and I_⊥) of Ni(II)Etio in CS₂ Solution

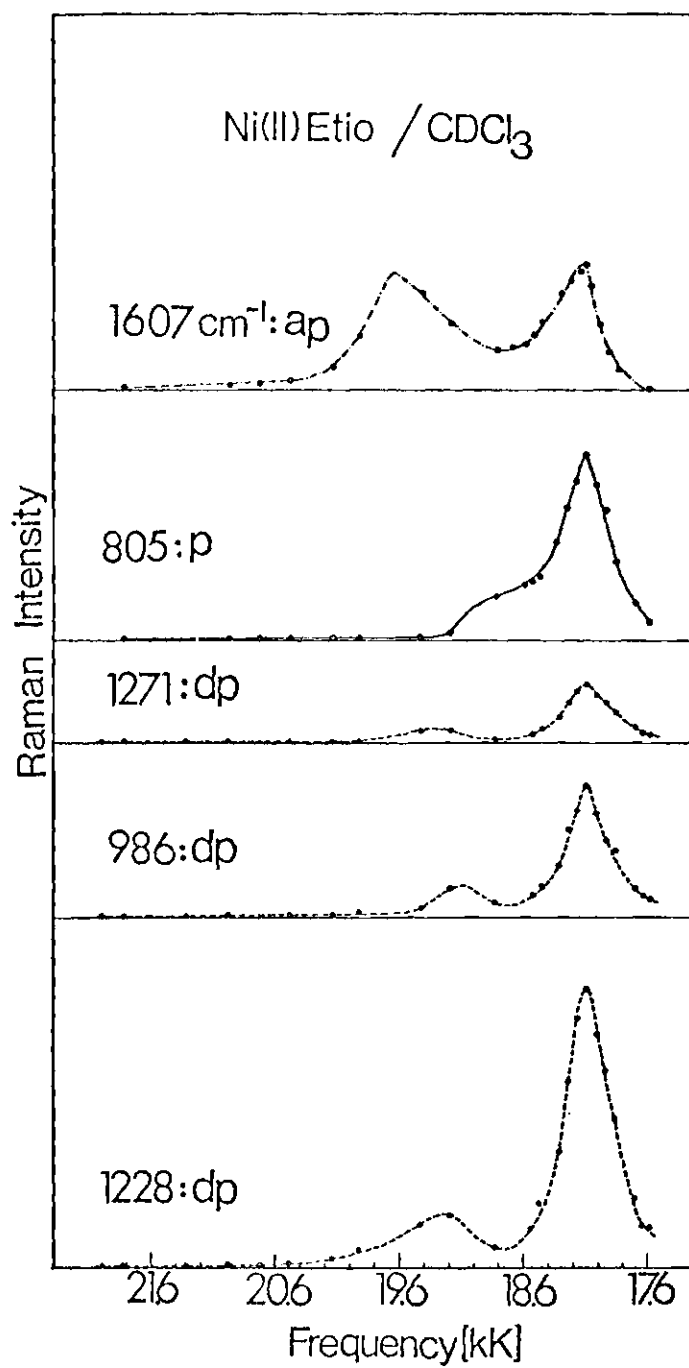


Figure 40. Excitation Profiles of Ni(II)Etio in CDCl₃

APPENDIX IV

VISIBLE ABSORPTION SPECTRA AND DEPOLARIZATION RATIOS
 OF DEUTERATED NICKEL (II)MESOPORPHYRIN IX DIMETHYL ESTER
 AND NICKEL (II)PROTOPORPHYRIN IX DIMETHYL ESTER

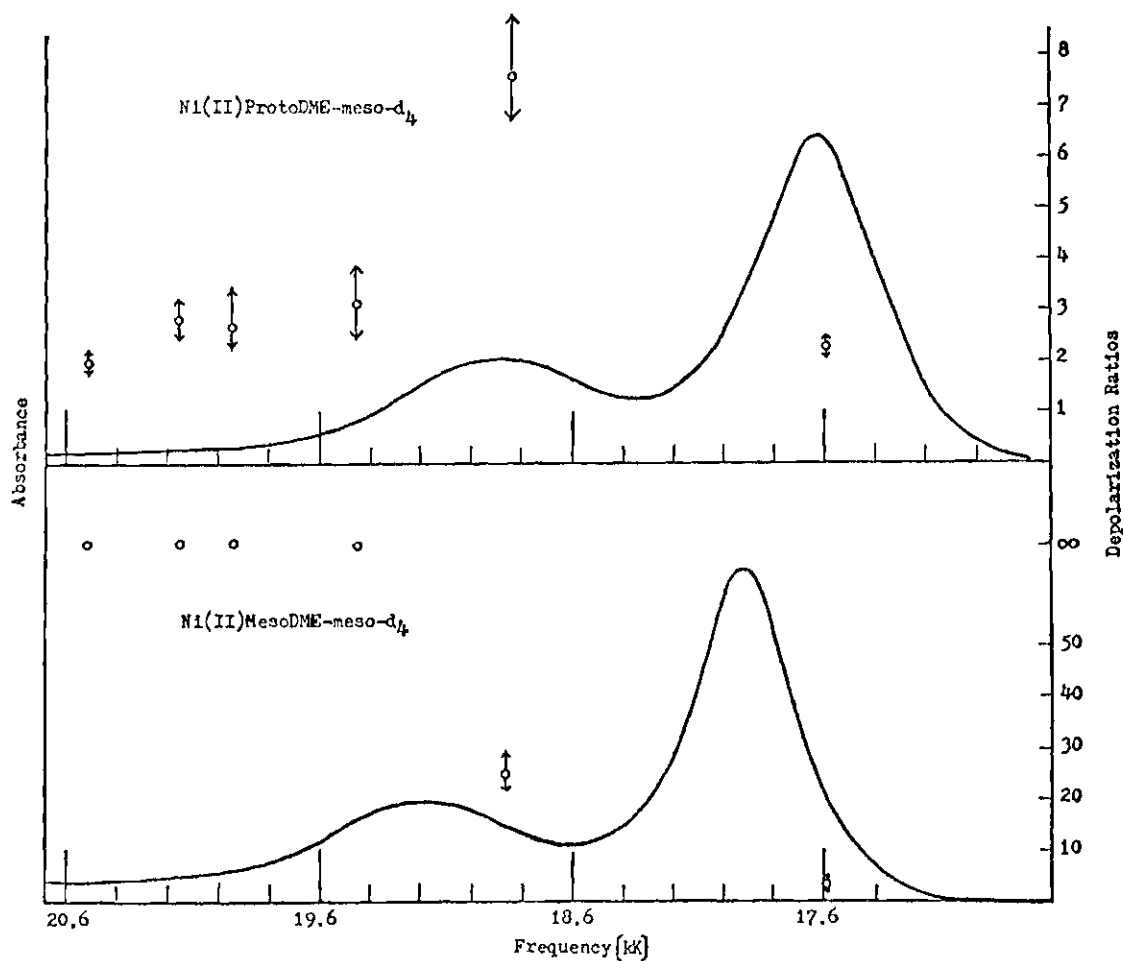


Figure 41. Visible Absorption Spectrum and Depolarization Ratios (1211 cm^{-1}) of Ni(II)ProtoDME-meso-d₄ (top), Visible Absorption Spectrum and Depolarization Ratios (1207 cm^{-1}) of Ni(II)MesoDME-meso-d₄ (bottom)

BIBLIOGRAPHY

- Abe, M., Kitagawa, T., and Kyogoku, Y., Chem. Lett., 249 (1976).
- Adler, A. D., Longo, F. R., Kampas, F., and Kim, J., J. Inorg. Nucl. Chem., 32, 2443 (1970).
- Albrecht, A. C., J. Chem. Phys., 34, 1476 (1961).
- Albrecht, A. C. and Hutley, M. C., J. Chem. Phys., 55, 4438 (1971).
- Aleksanyan, V. T. and Sterin, Kh. E., Optika i Spektroskopiya, 2, 562 (1957).
- Anfinsen, C. B., Haber, E., Sela, M., and White, F. H., Jr., Proc. Nat. Acad. Sci. USA, 47, 1309 (1961).
- Arguello, C. A., Mendes, G. F., and Leite, R. C. C., Appl. Opt., 13, 1731 (1974).
- Armand, G., Balazs, E. C., and Testa, M., Exp. Eye Res., 10, 143 (1970).
- Augusteyn, R. C., Exp. Eye Res., 19, 91 (1974).
- Augusteyn, R. C., Ophthal. Res., 7, 217 (1975).
- Bader, T. R. and Gold, A., Phys. Rev., 171, 997 (1968).
- Barber, G. W., Exp. Eye Res., 16, 85 (1973).
- Bare, G. H., Bromberg, P. A., and Alben, J. O., Fed. Proc., 33, 1302 (1974).
- Begley, R. F., Harvey, A. B., and Byer, R. L., Appl. Phys. Lett., 25, 387 (1974).
- Begley, R. F., Harvey, A. B., Byer, R. L., and Hudson, B. S., J. Chem. Phys., 61, 2466 (1974).
- Behringer, J., Z. Elektrochem., 62, 906 (1958).
- Behringer, J., in "Raman Spectroscopy-Theory and Practice," (H. A. Szymanski, ed.), Vol. 1, Chapt. 6, pp. 168-223, Plenum Press, New York, 1967.
- Behringer, J., Mol. Spectrosc., 2, 100 (1974).

BIBLIOGRAPHY (Continued)

- Behringer, J., *J. Raman Spectrosc.*, 2, 275 (1974).
- Bjork, I., *Exp. Eye Res.*, 9, 152 (1970).
- Blout, E. R., Lozé, C. De and Asadourian, A., *J. Amer. Chem. Soc.*, 83, 1895 (1961).
- Bonnett, R. and Stephenson, G. S., *Proc. Chem. Soc.*, 291 (1964).
- Bours, J. and Brahma, S. K., *Exp. Eye Res.*, 16, 131 (1973).
- Brunner, H., Mayer, A., and Sussner, H., *J. Mol. Biol.*, 70, 153 (1972).
- Brunner, H. and Sussner, H., *Biochem. Biophys. Acta*, 310, 20 (1973).
- Brunner, H., *Biochem. Biophys. Res. Commun.*, 51, 888 (1973).
- Brunner, H., Mayer, A., Gersonde, K., and Winterhalter, K., *FEBS Lett.*, 48, 141 (1974).
- Buckingham, R. H., *Exp. Eye Res.*, 14, 123 (1972).
- Burger, H., Burczyk, K., Buchler, J. W., Fuhrhop, J. H., Hofler, F., and Schrader, B., *Inorg. Nucl. Chem. Lett.*, 6, 171 (1970).
- Caughey, W. S., Barlow, C. H., O'Keefe, D. H., and O'Toole, M. C., *Ann. N. Y. Acad. Sci.*, 206, 296 (1973).
- Caughey, W. S., Barlow, C. H., Maxwell, J. C., Volpe, J. A., and Wallace, W. J., *Ann. N. Y. Acad. Sci.*, 244, 1 (1975).
- Chantry, G. W., in "The Raman Effect," (A. Anderson, ed.), Vol. 1, Chapt. 2, pp. 49-94, Marcel Dekker, Inc., New York, 1971.
- Chen, M. C. and Lord, R. C., *J. Amer. Chem. Soc.*, 96, 4750 (1974).
- Chou, P. Y. and Fasman, G. D., *Biochemistry*, 13, 211 (1974a).
- Chou, P. Y. and Fasman, G. D., *Biochemistry*, 13, 222 (1974b).
- Clayton, R. M., in "The Eye," (H. Davson and L. T. Graham, Jr., ed.), Vol. 5, Chapt. 5, pp. 399-494, Academic Press, New York, 1974.
- Collins, D. M. and Hoard, J. L., *J. Amer. Chem. Soc.*, 92, 3761 (1970).
- Collins, D. M., Countryman, R., and Hoard, J. L., *J. Amer. Chem. Soc.*, 94, 2066 (1972).

BIBLIOGRAPHY (Continued)

- Collins, D. W., Fitchen, D. B., and Lewis, A., *J. Amer. Phys.*, 59, 5714 (1973).
- Collins, D. W., Champion, P. M., and Fitchen, D. B., *Chem. Phys. Lett.*, 40, 416 (1976).
- Collman, J. P., Gagne, R. R., Reed, C. A., Robinson, W. T., and Rodley, G. A., *Proc. Nat. Acad. Sci. USA*, 71, 1326 (1974).
- Countryman, R., Collins, D. M., and Hoard, J. L., *J. Amer. Chem. Soc.*, 91, 5166 (1969).
- Croft, L. R., *Biochem. J.*, 128, 961 (1972).
- Cullen, D. L. and Meyer, E. F., Jr., *Acta Crystallogr.*, B29, 2507 (1973).
- Cullen, D. L. and Meyer, E. F., Jr., *J. Amer. Chem. Soc.*, 96, 2095 (1974).
- Davidson, B. and Fasman, G. D., *Biochemistry*, 6, 1616 (1967).
- Dillon, J., Spector, A., and Nakanishi, K., *Nature*, 259, 422 (1976).
- Dische, Z., Borenfreund, E., and Zelmenis, G., *A.M.A. Archs Ophthal.*, 55, 471 (1956).
- Dolphin, D., Forman, A., Borg, D. C., Fajer, J., and Felton, R. H., *Proc. Nat. Acad. Sci. USA*, 68, 614 (1971).
- Eicher, H., Bade, D., and Parak, F., *J. Chem. Phys.*, 64, 1446 (1976).
- Falk, J. E., in *BBA Library, "Porphyrins and Metalloporphyrins--Their General, Physical and Coordination Chemistry, and Laboratory Methods,"* Vol. 2, Elsevier Publishing Company, Amsterdam, 1964.
- Felton, R. H., Yu, N. T., O'Shea, D. C., and Shelnutt, J. A., *J. Amer. Chem. Soc.*, 96, 3675 (1974).
- Fleischer, E. B., *J. Amer. Chem. Soc.*, 85, 146 (1963).
- Fleischer, E. B., *J. Amer. Chem. Soc.*, 85, 1353 (1963).
- Fleischer, E. B., Miller, C., and Webb, L. E., *J. Amer. Chem. Soc.*, 86, 2342 (1964).
- Friedman, J. M. and Hochstrasser, R. M., *Chem. Phys.*, 1, 457 (1973).
- Friedman, J. M. and Hochstrasser, R. M., *Chem. Phys.*, 6, 155 (1974).

BIBLIOGRAPHY (Continued)

- Friedman, J. M. and Hochstrasser, R. M., Chem. Phys. Lett., 32, 414 (1975a).
- Friedman, J. M. and Hochstrasser, R. M., Chem. Phys. Lett., 33, 225 (1975b).
- Frushour, B. G. and Koenig, J. L., Biopolymers, 13, 455 (1974).
- Fuhrhop, J. -H. and Mauzerall, D., J. Amer. Chem. Soc., 91, 4174 (1969).
- Genis-Galvez, J. M., Maisel, H., and Castro, J., Exp. Eye Res., 7, 593 (1968).
- Gouterman, M., Wagniere, H., and Snyder, L. C., J. Mol. Spectrosc., 11, 108 (1963).
- Gouterman, M., Ann. N. Y. Acad. Sci., 206, 70 (1973).
- Gouterman, M., Schwartz, F. P., Smith, P. D., and Dolphin, D., J. Chem. Phys., 59, 676 (1973).
- Greenfield, N. and Fasman, G. D., Biochemistry, 8, 4108 (1969).
- Hamaguchi, H., Harada, I., and Shimanouchi, T., Chem. Lett., 1405 (1974).
- Hamor, M. J., Hamor, T. A., and Hoard, J. L., J. Amer. Chem. Soc., 86, 1938 (1964).
- Hanson, L. K., Gouterman, M., and Hanson, J. C., J. Amer. Chem. Soc., 95, 4822 (1973).
- Hoard, J. L., Hamor, M. J., Hamor, T. A., and Caughey, W. S., J. Amer. Chem. Soc., 87, 2312 (1965).
- Hoard, J. L., Science, 174, 1295 (1971).
- Hoard, J. L., Ann. N. Y. Acad. Sci., 206, 18 (1973).
- Hoard, J. L. and Scheidt, W. R., Proc. Nat. Acad. Sci. USA, 70, 3919 (1973).
- Hockwin, O., Exp. Eye Res., 15, 235 (1973).
- Hoffman, A. B., Collins, D. M., Day, V. W., Fleischer, E. B., Srivastava, T. S., and Hoard, J. L., J. Amer. Chem. Soc., 94, 3620 (1972).
- Hougen, J. T., J. Mol. Spectrosc., 13, 149 (1964).

BIBLIOGRAPHY (Continued)

- Jahn, H. A. and Teller, E., Proc. Roy. Soc., A161, 220 (1937).
- Jones, H. A. and Lerman, S., Can. J. Biochem., 49, 426 (1971).
- Hsu, S. L., Moore, W. H., and Krimm, S., Biopolymers, in press.
- Kamei, T., Acta Soc. Ophthal. Jap., 62, 1430 (1958).
- Kenner, G. W., Smith, K. M., and Sutton, M. J., Tetrahedron Letters, 16, 1303 (1973).
- Kiefer, W. and Bernstein, H. J., Appl. Spectrosc., 25, 500 (1971).
- Kitagawa, T., Ogoshi, H., Watanabe, E., and Yoshida, Z., Chem. Phys. Lett., 30, 451 (1975).
- Kitagawa, T., Abe, M., Kyogoku, Y., Ogoshi, H., Watanabe, E., and Yoshida, Z., J. Phys. Chem., 80, 1181 (1976).
- Kobayashi, H. and Yanagawa, Y., Bull. Chem. Soc. Jpn., 45, 450 (1972).
- Koenig, D. F., Acta Crystallogr., 18, 663 (1965).
- Koenig, J. L., J. Polym. Sci., Part D., 6, 59 (1972).
- Krimm, S. and Abe, Y., Proc. Nat. Acad. Sci. USA, 69, 2788 (1972).
- Kuck, J. F. R., Jr., in "Biochemistry of the Eye," (C. N. Graymore, ed.), Chapt. 5, pp. 319-371, Academic Press, New York, 1970.
- Kuck, J. F. R., Jr., in "Cataract and Abnormalities of the Lens," (J. G. Bellows, ed.), Chapt. 3, pp. 69-96, Grune and Stratton, Inc., New York, 1974.
- Kuck, J. F. R., Jr., East, E. J., and Yu, N. T., Exp. Eye Res., 23, 9 (1976).
- Kurzel, R. B., Wolbarsht, M. L., and Yamanashi, B. S., Exp. Eye Res., 17, 65 (1973).
- Lerman, S. and Zigman, S., Acta Ophthalmol., 45, 193 (1967).
- Lerman, S., Ann. Ophthalmol., 1, 73 (1969).
- Lerman, S., Isr. J. Med. Sci., 8, 1583 (1972).
- Lerman, S., Kuck, J. F. R., Jr., Borkman, R. F., and Saker, E., Ophthal. Res., in press.

BIBLIOGRAPHY (Continued)

- Li, L. -K. and Spector, A., *Exp. Eye Res.*, 19, 49 (1974).
- Little, R. G. and Ibers, J. A., *J. Amer. Chem. Soc.*, 96, 4440 (1974a).
- Little, R. G. and Ibers, J. A., *J. Amer. Chem. Soc.*, 96, 4452 (1974b).
- Loehr, T. M. and Loehr, J. S., *Biochem. Biophys. Res. Commun.*, 55, 218 (1973).
- Lord, R. C. and Yu, N. T., *J. Mol. Biol.*, 50, 509 (1970a).
- Lord, R. C. and Yu, N. T., *J. Mol. Biol.*, 51, 203 (1970b).
- McClain, W. M., *J. Chem. Phys.*, 55, 2789 (1971).
- McLees, B. D. and Caughey, W. S., *Biochemistry*, 68, 642 (1968).
- Mendelsohn, R., Sunder, S., Verma, A. L., and Bernstein, H. J., *J. Chem. Phys.*, 62, 37 (1975).
- Mendelsohn, R., Sunder, S., and Bernstein, H. J., *J. Raman Spectrosc.*, 3, 303 (1975).
- Meyer, E. F., Jr., *Acta Crystallogr.*, B28, 2162 (1972).
- Mingardi, M., Siebrand, W., Van Laeke, D., and Jacon, M., *Chem. Phys. Lett.*, 31, 208 (1975).
- Mingardi, M. and Siebrand, W., *J. Chem. Phys.*, 62, 1074 (1975).
- Miyazawa, T., Shimanouchi, T., and Mizushima, S., *J. Chem. Phys.*, 24, 408 (1956).
- Miyazawa, T., Shimanouchi, T., and Mizushima, S., *J. Chem. Phys.*, 29, 611 (1958).
- Miyazawa, T., *J. Chem. Phys.*, 32, 1647 (1960).
- Miyazawa, T. and Blout, E. R., *J. Amer. Chem. Soc.*, 83, 712 (1961).
- Moustakali, I. and Tulinsky, A., *J. Amer. Chem. Soc.*, 95, 6811 (1973).
- Nafie, L. A., Pézolet, M., and Peticolas, W. L., *Chem. Phys. Lett.*, 20, 563 (1973).
- Nogami, N., Sugeta, H., and Miyazawa, T., *Chem. Lett.*, 147 (1975).

BIBLIOGRAPHY (Continued)

- Ogoshi, H., Saito, Y., and Nakamoto, K., *J. Chem. Phys.*, 57, 4194 (1972).
- Perrin, M. H., Gouterman, M., Perrin, C. L., *J. Chem. Phys.*, 50, 4137 (1969).
- Perutz, M. F., *Nature*, 228, 726 (1970a).
- Perutz, M. F., *Nature*, 228, 734 (1970b).
- Perutz, M. F., *Nature*, 237, 495 (1972).
- Perutz, M. F. and Fermi, G. (unpublished results).
- Petersen, R. C., *Acta Crystallogr.*, B25, 2527 (1969).
- Peticolas, W. L., Nafie, L., Stein, P., and Fanconi, B., *J. Chem. Phys.*, 52, 1576 (1970).
- Pézolet, M., Nafie, L. A., and Peticolas, W. L., *J. Raman Spectrosc.*, 1, 455 (1973).
- Piatigorsky, J., Zelenka, P., and Simpson, R. T., *Exp. Eye Res.*, 18, 435 (1974).
- Pirie, A., *Isr. J. Med. Sci.*, 8, 1567 (1972).
- Placzek, G. in "The Rayleigh and Raman Scattering," UCRL Trans. No. 526 (L), from "Handbush der Radiologie," (E. Marx, ed.), VI. 2, pp. 209-374, Akademische Verlagsgesellschaft, Leipzig, 1934.
- Rabaey, M., *Exp. Eye Res.*, 1, 310 (1962).
- Rabaey, M., *Nature*, 198, 206 (1963).
- Rabaey, M., Rikkers, I., and De Mets, M., *Exp. Eye Res.*, 14, 208 (1972).
- Radonovich, L. J., Bloom, A., and Hoard, J. L., *J. Amer. Chem. Soc.*, 94, 2073 (1972).
- Rakshit, G. and Spiro, T. G., *Biochemistry*, 13, 5317 (1974).
- Satoh, K., Bando, M., and Nakajima, A., *Exp. Eye Res.*, 15, 167 (1975).
- Schachar, R. A. and Solin, S. A., *Invest. Ophthal.*, 14, 380 (1975).
- Scheidt, W. R. and Hoard, J. L., *J. Amer. Chem. Soc.*, 95, 8281 (1973).

BIBLIOGRAPHY (Continued)

- Scheidt, W. R. and Frisse, M. E., *J. Amer. Chem. Soc.*, 97, 17 (1975).
- Scharf, B., *J. Chem. Phys.*, 55, 1379 (1971).
- Shelnutt, J. A., O'Shea, D. C., Yu, N. T., Cheung, L. D., and Felton, R. H., *J. Chem. Phys.*, 64, 1156 (1976).
- Shimanouchi, T., Koyama, Y., and Itoh, K., *Poly. Sci., Japan*, Vol. III, 273, 1973.
- Siamwiza, M. N., Lord, R. C., Chen, M. C., Takamatsu, T., Harada, I., Matsuura, H., and Shimanouchi, T., *Biochemistry*, 14, 4870 (1975).
- Silvers, S. J. and Tulinsky, A., *J. Amer. Chem. Soc.*, 89, 3331 (1967).
- Solovyov, K. N., Ksenofontova, N. M., Shkirman, S. F., Kachura, T. F., *Spectrosc., Lett.*, 6, 455 (1973).
- Spaulding, L. D., Chang, C. C., Yu, N. T., and Felton, R. H., *J. Amer. Chem. Soc.*, 97, 2517 (1975).
- Spector, A., *Exp. Eye Res.*, 11, 376 (1971).
- Spector, A., Li, L. -K., Augusteyn, R. C., Schneider, A., and Freund, T., *Biochem. J.*, 124, 337 (1971).
- Spector, A., Roy, D., and Stauffer, J., *Exp. Eye Res.*, 21, 9 (1975).
- Spiro, T. G. and Strekas, T. C., *Proc. Nat. Acad. Sci. USA*, 69, 2622 (1972).
- Spiro, T. G. and Strekas, T. C., *J. Amer. Chem. Soc.*, 96, 338 (1974).
- Spiro, T. G., *Acc. Chem. Res.*, 7, 339 (1974).
- Spiro, T. G., in "Chemical and Biochemical Applications of Lasers," (C. B. Moore, ed.), Vol. 1, Chapt. 2, pp. 29-70, Academic Press, New York, 1974.
- Stein, P., Burke, J. M., and Spiro, T. G., *J. Amer. Chem. Soc.*, 97, 2304 (1975).
- Strekas, T. C. and Spiro, T. G., *Biochem. Biophys. Acta*, 263, 830 (1972a).
- Strekas, T. C. and Spiro, T. G., *Biochem. Biophys. Acta*, 278, 188 (1972b).

BIBLIOGRAPHY (Continued)

- Strekas, T. C., Packer, A. J., and Spiro, T. G., *J. Raman Spectrosc.*, 1, 197 (1973).
- Strekas, T. C. and Spiro, T. G., *J. Raman Spectrosc.*, 1, 387 (1973).
- Strekas, T. C. and Spiro, T. G., *Biochem. Biophys. Acta*, 351, 237 (1974).
- Strekas, T. C., Adams, D. H., Packer, A., and Spiro, T. G., *Appl. Spectrosc.*, 28, 324 (1974).
- Sugeta, H., Go, A., and Miyazawa, T., *Chem. Lett.*, 83 (1972).
- Sugeta, H., Go, A., and Miyazawa, T., *Bull. Chem. Soc.*, 46, 3407 (1973).
- Sunder, S. and Bernstein, H. J., *Can. J. Chem.*, 52, 2851 (1974).
- Sunder, S., Mendelsohn, R., and Bernstein, H. J., *Biochem. Biophys. Res. Commun.*, 62, 12 (1975).
- Sussmer, H., Mayer, A., Brunner, H., and Fasold, H., *Eur. J. Biochem.*, 41, 465 (1974).
- Tang, J. and Albrecht, A. C., *J. Chem. Phys.*, 49, 1144 (1968).
- Tang, J. and Albrecht, A. C., in "Raman Spectroscopy-Theory and Practice," (H. A. Szymanski, ed.), Vol. 2, Chapt. 2, pp. 33-68, Plenum Press, New York, 1970.
- Tang, S-P. W., Spiro, T. G., Antanaitis, C., Moss, T. H., Holm, R. H., Herskovitz, T., and Mortensen, L. E., *Biochem. Biophys. Res. Commun.*, 62, 1 (1975).
- Thoft, R. A. and Kinoshita, J. H., *Invest. Ophthal.*, 4, 122 (1965).
- Timkovich, R. and Tulinsky, A., *J. Amer. Chem. Soc.*, 91, 4430 (1969).
- Tulinsky, A., *Ann. N. Y. Acad. Sci.*, 206, 47 (1973).
- Tsuboi, M., Hirakawa, A. Y., and Muraishi, S., *J. Mol. Spectrosc.*, 56, 146 (1975).
- van Dam, A. F. and Cate, G. T., *Biochem. Biophys. Acta*, 121, 183 (1966).
- van Heyningen, R., *Sci. Amer.*, 233, No. 6, 70 (1975).
- van Labeke, D., Jacon, M., and Bernard, L., *Chem. Phys. Lett.*, 27, 123 (1974).

BIBLIOGRAPHY (Continued)

- van Vleck, J. H., Proc. Nat. Acad. Sci. USA, 15, 754 (1929).
- Verma, A. L. and Bernstein, H. J., J. Raman Spectrosc., 2, 163 (1974).
- Verma, A. L. and Bernstein, H. J., Biochem. Biophys. Res. Commun., 57, 255 (1974).
- Verma, A. L., Mendelsohn, R., and Bernstein, H. J., J. Chem. Phys., 61, 383 (1974).
- Verma, A. L. and Bernstein, H. J., J. Chem. Phys., 61, 2560 (1974).
- Waley, S. G., in "The Eye," (H. Davson, ed.), Vol. 1, 2nd Ed., Chapt. 5, pp. 299-379, Academic Press, New York, 1969.
- Watanabe, H. and Kawakami, I., Exp. Eye Res., 17, 205 (1973).
- Wilser, W. T. and Fitchen, D. B., J. Chem. Phys., 62, 720 (1975).
- Woodruff, W. H., Spiro, T. G., and Yonetani, T., Proc. Nat. Acad. Sci. USA, 71, 1065 (1974).
- Woodruff, W. H. and Spiro, T. G., Appl. Spectrosc., 28, 576 (1974).
- Woodruff, W. H., Adams, D. H., Spiro, T. G., and Yonetani, T. J., J. Amer. Chem. Soc., 97, 1695 (1975).
- Yamamoto, T., Palmer, G., Gill, D., Salmeen, I. T., and Riami, L., J. Biol. Chem., 248, 5211 (1973).
- Yu, N. T. and Liu, C. S., J. Amer. Chem. Soc., 94, 5127 (1972).
- Yu, N. T., Jo, B. H., and Liu, C. S., J. Amer. Chem. Soc., 94, 7572 (1972).
- Yu, N. T., Liu, C. S., and O'Shea, D. C., J. Mol. Biol., 70, 117 (1972).
- Yu, N. T. and Jo, B. H., J. Amer. Chem. Soc., 95, 5033 (1973).
- Yu, N. T., Jo, B. H., and O'Shea, D. C., Arch. Biochem. Biophys., 156, 71 (1973).
- Yu, N. T., Jo, B. H., Chang, R. C. C., and Huber, J. D., Arch. Biochem. Biophys., 160, 614 (1974).
- Yu, N. T. and East, E. J., J. Biol. Chem., 250, 2196 (1975).

BIBLIOGRAPHY (Concluded)

- Yu, T. J., Lippert, J. L., and Peticolas, W. L., *Biopolymers*, 12, 2161 (1973).
- Zigman, S., Schultz, J., and Yulo, T., *Exp. Eye Res.*, 15, 201 (1973).
- Zigman, S., Griess, G., Yulo, T., Schultz, J., *Exp. Eye Res.*, 15, 255 (1973).
- Zigman, S., Schultz, J., Yulo, T., Griess, G., *Exp. Eye Res.*, 15, 209 (1973).
- Zwaan, J., *Exp. Eye Res.*, 5, 267 (1966).

VITA

Robert Cheng Chi Chang was born October 2, 1947, in Taichung, Taiwan, the son of T'san-Ti and T'sai-Ping Chang. Upon graduation from Provincial Taichung First High School in 1966, he entered National Taiwan University and received the Bachelor of Science degree in Agricultural Chemistry in 1970. During the next year, he was a Second Lieutenant platoon leader in an army recruit training camp. In September 1971, he entered the graduate program of National Taiwan University. In September 1972, he came to the United States to enroll in the Graduate Division of the Georgia Institute of Technology to work for the Doctor of Philosophy in the School of Chemistry. During this time at Georgia Tech, he was supported by teaching and research assistantships.

Mr. Chang married Yi-Huei Wu in Taichung, Taiwan in December, 1973.